2014

Effect of a Dual Loop Thermal Management Arrangement with a Single Module Radiator on Vehicle Power Consumption

Timothy Reaburn
University of Windsor

EFFECT OF A DUAL LOOP THERMAL MANAGEMENT ARRANGEMENT WITH A SINGLE MODULE RADIATOR ON VEHICLE POWER CONSUMPTION

by

Timothy Reaburn

A Thesis
Submitted to the Faculty of Graduate Studies
through the Department of Mechanical, Automotive, and Materials Engineering
in Partial Fulfillment of the Requirements for
the Degree of Master of Applied Science at the
University of Windsor

Windsor, Ontario, Canada

2014

Effect of a Dual Loop Thermal Management Arrangement with a Single Module Radiator on Vehicle Power Consumption

by

Timothy Reaburn

APPROVED BY:

_____

X. Xu
Department of Civil and Environmental Engineering

_____

G. Reader
Department of Mechanical, Automotive, and Materials Engineering

_____

M. Zheng, Advisor
Department of Mechanical, Automotive, and Materials Engineering

5 March, 2014

DECLARATION OF ORIGINALITY

I hereby certify that I am the sole author of this thesis and that no part of this thesis has been published or submitted for publication.

I certify that, to the best of my knowledge, my thesis does not infringe upon anyone's copyright nor violate any proprietary rights and that any ideas, techniques, quotations, or any other material from the work of other people included in my thesis, published or otherwise, are fully acknowledged in accordance with the standard referencing practices. Furthermore, to the extent that I have included copyrighted material that surpasses the bounds of fair dealing within the meaning of the Canada Copyright Act, I certify that I have obtained a written permission from the copyright owner(s) to include such material(s) in my thesis and have included copies of such copyright clearances to my appendix.

I declare that this is a true copy of my thesis, including any final revisions, as approved by my thesis committee and the Graduate Studies office, and that this thesis has not been submitted for a higher degree to any other University or Institution.

ABSTRACT

A single module radiator within a dual loop vehicle thermal management setup was investigated as a method for reducing the vehicle power consumption when the air conditioner was operating. The cooling fan and the air conditioning compressor consume the most vehicle power within the vehicle thermal management system. The simulation results indicated that the single module radiator decreased the fan power consumption by 31% compared to the dual loop setup while the power consumption of the air conditioning compressor did not change. The total vehicle power consumption improved by 3% compared to the dual loop setup when the air conditioner was operating and by 7% compared to the standard vehicle thermal management setup. The simulations revealed that this was due to an improvement in the underhood cooling airflow rates and an increase in the initial temperature difference between the coolant and air entering the radiator.

DEDICATION

I would like to dedicate my thesis to my parents for all their support and encouragement throughout my education.

ACKNOWLEDGEMENTS

I would like to thank all the people at Chrysler and Fiat for the opportunity to work within their research centers during the course of my thesis. I would like to especially thank my industrial advisers, Sadek Rahman, Matteo Rostagno and Carloandrea Malvicino for their knowledge and guidance through the entire process of my thesis.

I would like to recognize Francesco Lovuolo for teaching me how to use the simulation software and for his assistance helping me troubleshoot any simulation problems I had while at Fiat. I would also like to recognize Larry Chen for his help and guidance in trouble shooting my simulation problems while at Chrysler.

I would also like to thank Dr. Peter Frise, Jan Stewart, Mr. Mohammed Malik, Dr. Ming Zheng, Dr. Ezio Spessa and Dr. Giovanni Bellingardi for allowing me to have the unique opportunity to be a part of this program. Without their efforts this program and opportunity would not be possible.

TABLE OF CONTENTS

LIST OF TABLES

LIST OF FIGURES

LIST OF NOMENCLATURE

Abbreviations

A/C	air conditioning
ATB	air to boil
CAC	charge air cooler
CAFE	corporate average fuel economy
CFD	computational fluid dynamics
HT	high temperature
HTR	high temperature radiator
LT	low temperature
LTR	low temperature radiator
NEDC	new European driving cycle
TSTAT	thermostat
VTMS	vehicle thermal management system

Uppercase

A_{LTR}	frontal area of the low temperature radiator	[m^2]
A_{SM}	frontal area of the single module area	[m^2]
A_{tube}	tube side convection area	[m^2]
A_{air}	air side fin convection area	[m^2]
C_{min}	lowest heat capacity flow between the air and the coolant	[W/K]
C_{press}	constant fan pressure coefficient	[-]
D_{fan}	fan diameter	[m]
G_{wall}	tube wall and fin resistance	[W/K]

H	enthalpy of the coolant volume in a heat exchanger	[J]
K_{eng}	engine pressure drop coefficient	[-]
K_{grill}	front grill pressure increase coefficient	[-]
L_{cool}	condenser coolant side characteristic length	[m]
L_{ref}	condenser refrigerant side characteristic length	[m]
N_{fan}	fan speed	[rpm]
N_{pump}	pump speed	[rpm]
Nu	Nusselt number	[-]
Nu_{turb}	turbulent Nusselt number	[-]
NTU	number of transfer units	[-]
Pr	Prandlt number	[-]
Pr_l	Prandlt number of liquid state refrigerant	[-]
$\dot{Q}_{act}$	actual heat transfer	[W]
$\dot{Q}_{LTR}$	low temperature radiator heat transfer	[W]
$\dot{Q}_{SM}$	single module radiator heat transfer	[W]
Re	Reynolds number	[-]
Re_l	Reynolds number of liquid state refrigerant	[-]
T_{airamb}	ambient air temperature	[^oC]
$T_{AirToBoil}$	air to boil temperature	[^oC]
$T_{coolboil}$	coolant boiling temperature	[^oC]
$T_{engcool}$	engine outlet coolant temperature	[^oC]
T_{incool}	coolant inlet temperature	[^oC]
T_{inair}	air inlet temperature	[^oC]

T_{wall}	heat exchanger tube wall temperature	[^{o}C]
UA_s	total system resistance	[W/K]
V_{veh}	vehicle velocity	[m/s]
V_{uh}	underhood air velocity	[m/s]

Lowercase

a	Nusselt number coefficient from heat exchanger performance data	[-]
b	Nusselt number coefficient from heat exchanger performance data	[-]
c	ratio between the minimum and the maximum heat capacity flows	[-]
d_{hcool}	condenser coolant side hydraulic diameter	[m]
d_{href}	condenser refrigerant side hydraulic diameter	[m]
dp_{fan}	pressure increase of the air travelling through the fan	[Pa]
dm	mass differential	[kg]
dt	time differential	[s]
h	specific coolant enthalpy	[J/kg]
h_{2phase}	refrigerant convection coefficient during 2-phase flow	[W/m^2·K]
h_{cool}	coolant convection coefficient	[W/m^2·K]
h_{air}	air convection coefficient	[W/m^2·K]
$\dot{m}_{flow}$	coolant mass flow rate through parallel pipe	[kg/s]
$\dot{m}_{tot}$	total coolant mass flow rate	[kg/s]
p_{red}	ratio between the saturation pressure and critical pressure	[-]
x	gas mass fraction	[-]

Greek

Δp_{grill}	air pressure difference across the front grill	[Pa]

Δp_{eng}	air pressure difference across the engine	[Pa]
Δp_{flow}	pressure difference through paraellel pipe	[Pa]
Δp_{pipe}	coolant pressure difference through the hoses	[Pa]
Δp_{hx}	coolant pressure difference through the heat exchangers	[Pa]
Δp_{sys}	coolant pressure difference through the system	[Pa]
ϵ	heat exchanger effectiveness	[-]
λ	thermal conductivity	[W/m·K]
ρ_{air}	coolant density	[kg/m^3]
$\dot{\forall}_{cool}$	coolant flow rate	[m^3/s]

CHAPTER 1: INTRODUCTION

1.1 Background

In the current automotive industry, many companies are focusing on improving the vehicle fuel economy to meet consumer demands and stricter government standards in both Europe and North America. The North American governments' vehicle fuel economy standard, the Corporate Average Fuel Economy (CAFE) standard, is currently set at 26 mpg. The CAFE standard is set to increase to 35.5 mpg in 2016 and will increase further to 54.5 mpg in 2025 [1]. The CAFE standard measures the vehicle fuel economy based on the average fuel economy of an automotive company's entire line of vehicles. If these standards are not met, then the vehicle manufacturer will receive a fine of $5.50 in the United States per vehicle produced for every 0.1 mpg below the limit [2].

In Europe, a mandatory company average fuel economy regulation will come into effect for the first time in 2015 and will be set at 130 g of CO_2/km (42 mpg). This standard will tighten further to 95 g of CO_2/km (57.5 mpg) in 2020 [3]. The current average vehicle fuel economy in Europe is around 150 CO_2/km (36.4 mpg) [4].

In order to meet these demands, Fiat and Chrysler are working to improve the vehicle fuel economy while maintaining passenger comfort and the performance of vehicle systems. This is accomplished by developing lighter materials, improving vehicle aerodynamics and by improving the efficiency of the power consuming vehicle systems. The vehicle thermal management system (VTMS) is one of the systems that can be improved to increase the overall vehicle fuel efficiency.

The vehicle fuel economy can be improved by reducing the total power consumption of the various system components within the VTMS, such as the cooling fan, compressor, blower and coolant pump. The cooling system also affects the vehicle aerodynamic drag because of the cooling airflow through the underhood compartment. By decreasing the pressure drop across the front-end heat exchangers, the cooling drag decreases, provides better underhood airflow and reduces vehicle aerodynamic drag.

Currently one of the ways the VTMS is being improved to consume less vehicle power is by re-arranging its layout. The new arrangement, the dual loop cooling arrangement, has had two main benefits. The first is that the demand on the cooling fan has been reduced, which decreases the power consumed by the system. The second is that the pressure drop across the front-end heat exchangers has been reduced, which provides better airflow across the front-end heat exchangers.

1.2 Dual Loop Cooling Arrangement

The VTMS has a standard underhood arrangement of the front-end heat exchangers that most production vehicles currently use. The standard arrangement has several air cooled heat exchangers in front of the engine, including a radiator to cool the engine, a condenser to cool the air conditioning system refrigerant, and a charge air cooler (CAC) to cool the air from the turbocharger. The standard underhood heat exchanger arrangement is shown in Figure 1.1. Each subsystem (e.g. CAC, condenser, engine) has its own fluid to be cooled, which is brought to the front of the vehicle and then back to the engine compartment.

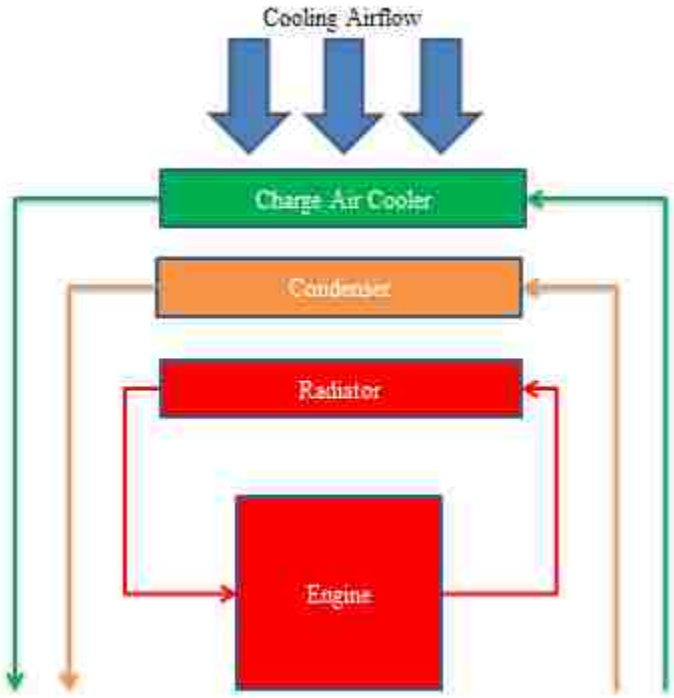

Figure 1.1: Standard Vehicle Thermal Management Setup

A newer way to arrange the VTMS is the dual loop cooling arrangement. The dual loop system only has two air cooled heat exchangers in front of the engine, i.e. the high temperature radiator (HTR) and the low temperature radiator (LTR). The HTR cools the engine coolant. The condenser and CAC are moved back into the engine compartment closer to their respective subsystems, sharing the same coolant loop. The LTR cools the coolant that is used to cool the other subsystems in the system (e.g. condenser, CAC). The dual loop cooling arrangement is shown in Figure 1.2.

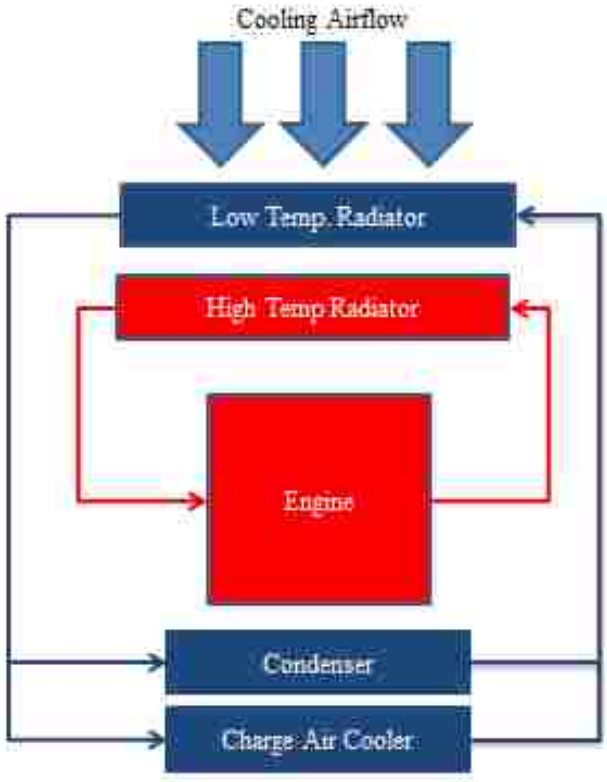

Figure 1.2: Dual Loop Cooling System Arrangement

The dual loop arrangement was first developed by Modine Manufacturing [5]. The dual loop system improved the vehicle fuel economy when compared to the standard setup. The improvement in fuel economy was attributed to the reduced number of front-end heat exchangers which decreased the air side pressure drop [5]. The airflow rate through the cooling system increased due to the reduction of the air side pressure drop. The greater airflow rate reduced the temperature of the air exiting the LTR and entering the HTR, which increased the cooling potential of the HTR. The greater airflow rate also decreased the amount of power the fan consumed because the fan had a smaller pressure drop to overcome [5].

The dual loop cooling arrangement was later developed by Valeo, an automotive components manufacturer, which modified the system to control the coolant flow to the

high temperature and the low temperature radiators [6]. When the engine is operating at low and medium loads, a valve opens allowing coolant from the LTR to also flow through half of the HTR. When the engine is operating at high loads, the valve is closed and only the high temperature loop coolant can flow through the HTR.

A prototype of this setup was created by Valeo on a 2006 Mercedes with a 2.2L diesel engine. The dual loop arrangement prototype was capable of reducing the vehicle's urban driving fuel consumption by 8%, with comparable engine cooling and A/C system performance to the standard system arrangement [6]. The charge air was cooled to a lower temperature in the dual loop setup because the CAC was liquid cooled. The total front-end space, both the depth and volume occupied by the heat exchangers, was reduced. The front-end depth was reduced by 49% and the underhood volume was reduced by 40%. The reduction in heat exchanger depth is shown in Figure 1.3.

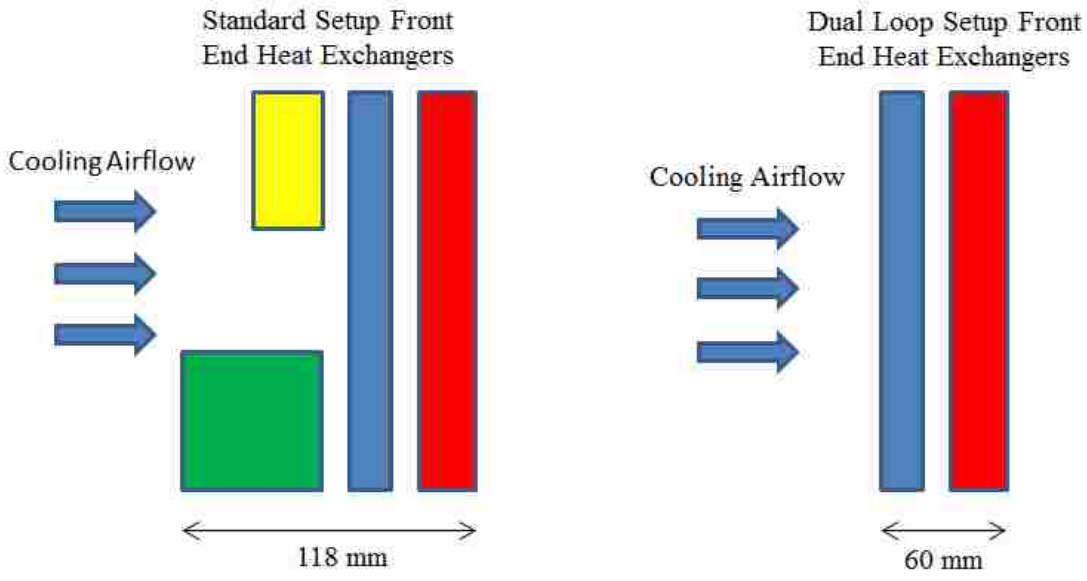

Figure 1.3: Dual Loop Heat Exchanger Depth Reduction

Fiat developed a dual loop arrangement prototype for a 2012 Fiat Punto with a 1.2L diesel engine. It was a simplified version of the Valeo dual loop system, using no valves to control the coolant flow. This reduced the number of extra components and additional system controls. The dual loop system was capable of improving the fuel economy by 4% with the A/C on [7,8]. The improvement in fuel economy was attributed to decreased fan activation. The fan was only activated based on the average cooling needs of each component in the low temperature loop (condenser and CAC) because they share the same cooling circuit [7,8]. In the standard setup, the fan is activated based on the cooling needs of the individual components because they have separate cooling circuits.

1.3 VTMS Component Power Consumption

The VTMS has various components such as the cooling fan, coolant pump and A/C compressor, which all consume vehicle power to operate, either mechanically driven by the engine or by electrical power from the alternator. If the power consumption of these components is reduced, then the fuel efficiency of the entire vehicle will improve. The greatest power consumption of the VTMS is when the A/C is in operation. In general, the vehicle fuel efficiency decreases 5-25% when the air conditioning is operating [9].

The fuel efficiency of the vehicle decreases when the A/C is operating because the A/C compressor is operating and the cooling fan is operating more frequently to meet the additional condenser cooling needs. Reducing the amount of power consumed by both the compressor and the cooling fan during the A/C operation will have a large effect on vehicle fuel economy compared to the other components in the VTMS. The power

consumption of the cooling fan and the A/C compressor of a Fiat Punto with a dual loop cooling setup during the NEDC test with the A/C operating are shown in Table 1.1 [10].

Table 1.1: Fiat Punto VTMS Component Power Consumption

Component	Power Consumed (W)	Alternator Power (Efficiency 60%) (W)
Cooling Fan	340	570
A/C Compressor	2490	2490

The compressor power can be reduced by increasing the cooling capacity of the condenser. If the condenser has a larger cooling capacity, the refrigerant can be at a lower temperature and still maintain enough heat transfer for the condensation of the refrigerant to occur. The compressor outlet refrigerant pressure is lowered to achieve a lower temperature, which reduces the power the compressor consumes [11].

The power the cooling fan uses can be reduced by decreasing the airflow resistance across the front-end heat exchangers. The smaller the resistance, the less power the fan will consume to provide an adequate cooling airflow rate. The lower airflow resistance will also increase the airflow rate when the fan is not activated, which reduces the need to increase the airflow rate by using the fan [12].

1.4 VTMS Effect on Vehicle Aerodynamics

The airflow over the vehicle has three separate flow paths: macro (around the outsides of the vehicle), underneath the vehicle, and through the underhood compartment. The VTMS has an effect on the vehicle drag due to the airflow through the underhood compartment. The drag due to the airflow through the underhood compartment is called

the cooling drag. The cooling drag is the difference between the vehicle drag when the front grill air inlets are open and the vehicle drag when the front grill air inlets are closed. The cooling drag contributes 5 to 10% of the total vehicle drag depending on the vehicle type [13].

The cooling drag is a function of the air inlet and outlet geometry, the underhood arrangement geometry and the air inlet and outlet pressures and velocities. The change of the arrangement of the underhood components will have an effect of the total cooling drag. In particular, increasing the space between the engine block and the radiator has been shown to reduce the cooling drag [14]. Cooling drag tests, on a simplified vehicle body representing an actual vehicle, showed that increasing the distance between the engine block and radiator from 6 cm to 20 cm decreased the overall vehicle drag coefficient by 1.4% and the cooling drag coefficient by 17.4%. The vehicle lift coefficient also decreases with increased spacing between the engine block and the radiator [14]. The more underhood compartment space available by reducing the amount of space occupied by the VTMS, the easier it is to arrange the components to decrease the cooling drag.

1.5 Single Module Radiator

The dual loop setup can potentially be improved further by combining the two front-end radiators, the low temperature and high temperature radiators into a single module. In the single module setup, there are two separate cooling loops just like in the standard dual loop setup however the radiators will be placed within a single component as shown in Figure 1.4. In the standard dual loop setup, the high temperature and low temperature radiators are two separate components as previously shown in Figure 1.2.

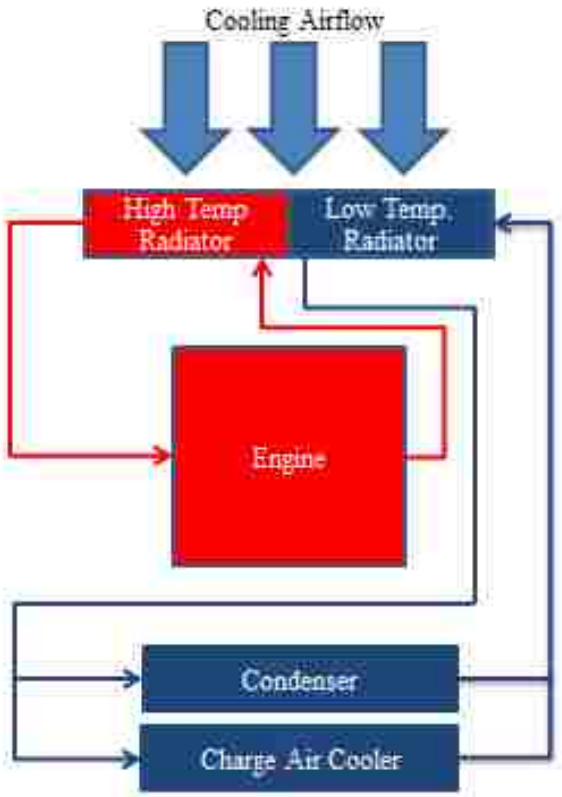

Figure 1.4: Single Module Setup

The potential advantages of combining the two front-end radiators into a single module are that the front-end airflow resistance and the incoming temperature into the HTR should be lower. In the standard dual loop setup, the incoming cooling air must flow through the LTR before flowing through the HTR. As the air flows through the LTR, it increases in temperature due to the heat transfer from the LTR and decreases in pressure due to the airflow resistance of the LTR. In the single module setup, the cooling air is not heated by the LTR before entering the HTR which increases the cooling potential of the HTR. The cooling air in the single module setup only flows through a single layer of heat exchangers, as shown in Figure 1.5, which decreases the system

resistance. The cooling fan will require less power to overcome a smaller airflow resistance.

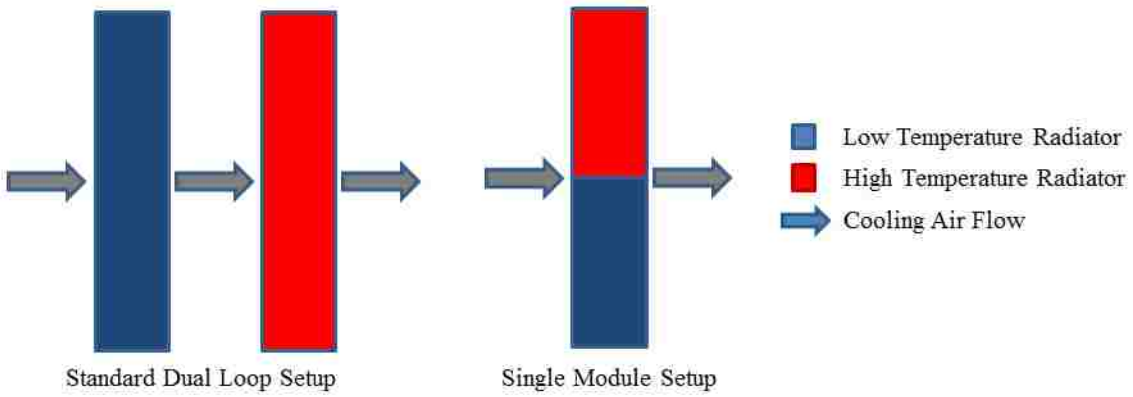

Figure 1.5: Standard Dual Loop Setup (Left) and Single Module Setup (Right)

The Denso Corporation designed a single module heat exchanger, combining the condenser and the radiator [15]. When compared to the standard condenser and radiator setup, there was a 10% increase in the overall heat transfer of both the condenser and the radiator [15]. This increase was attributed to the decrease in the system resistance which increased the airflow rate across the heat exchangers.

The Calsonic Kansei Corporation developed a system where some front-end heat exchangers were combined into a single module in an effort to decrease the front-end space occupied by the heat exchangers [16]. The condenser and sub-radiator (which cooled the coolant from a water cooled CAC) were combined into a single module. The single module system layout improved the fuel economy by 3-5% and reduced the space occupied by the front-end heat exchangers by 40% [16]. The improved fuel economy was attributed to a reduction of airflow resistance through the heat exchangers which reduced the fan power consumption 30-40% [16].

1.6 One Dimensional Simulation

One-dimensional simulation tools are currently used within Chrysler and Fiat to model the VTMS and have become an essential part of the design process. They are used to predict the performance of the VTMS under various vehicle operating conditions. They provide a simple simulation that can be used to size components within the system and ensure that the entire system operates effectively. One-dimensional simulation is used to speed up the design process of a new system which saves time and lowers costs when compared to CFD simulation or full vehicle testing.

AMESim is a one-dimensional simulation program used to model thermal, mechanical, hydraulic and pneumatic systems. The AMESim libraries that were used in this thesis to represent the VTMS were the thermal, the thermal-hydraulic, the pneumatic flow, the 2-phase flow, the heat and the thermal mass libraries. The different components of a VTMS such as heat exchangers, coolant pumps and the thermostat (TSTAT) are represented within these libraries. The components can be arranged and connected in any way to best represent the system to be simulated.

1.7 External Airflow Modelling

The underhood cooling airflow experiences a pressure drop as it moves through the system because of the system resistance of the various components, such as the front grill, heat exchangers and engine. The total system resistance of the underhood cooling airflow changes when the heat exchangers are removed or the arrangement is changed which also changes the underhood airflow rates. The system resistance for the dual loop setup will be different than the single module setup.

The single module radiator system had no prototype to use to measure the airflow by experimental testing. To predict the underhood cooling airflow, the one-dimensional simulation tools were used. Such simulation tools have been used to predict the airflow rates across front-end heat exchangers using the individual component performance evaluation data (bench test data) [17]. The pressure drop across each heat exchanger was used to ensure that the flow was divided correctly among each flow path to accurately predict the performance of each heat exchanger. A similar method was used to predict the total airflow rate when changing the resistances of the front-end heat exchangers.

CHAPTER 2: TESTING AND SIMULATION

2.1 Project Description

The investigation in this thesis was to determine the effect on vehicle fuel economy of incorporating a single module radiator into the dual loop VTMS currently in development by Fiat on a Fiat Punto with a 1.4L 4 cylinder spark ignition engine. The single module radiator included both the HTR and LTR in the same module, as previously shown in Figure 1.4. The purpose of including a single module radiator into the dual loop setup was to attempt to reduce the fan and compressor power consumption and consequently improve the vehicle fuel economy. The single module radiator however has a reduced total frontal area compared to the dual loop setup which may not have been great enough to meet the system cooling needs.

The combination of the HTR and LTR into a single module removes an entire heat exchanger module from the dual loop system. This will improve the initial inlet temperature difference between the HTR coolant and the incoming airflow. The cooling airflow will be at the ambient air temperature when entering the HTR in the single module setup because the air no longer flows through the LTR before entering the HTR. The heat transfer potential of the HTR increases with a larger initial temperature difference which allows the cooling airflow rate provided by the fan to be decreased.

The system resistance to the cooling airflow is also decreased by removing a heat exchanger. As the cooling air flows through a heat exchanger it decreases in pressure due to the airflow resistance of the heat exchanger. The system resistance in the single module setup should be smaller than the dual loop setup which will increase the cooling

airflow rate across the heat exchangers. This will decrease the fan power demand needed to increase the cooling airflow rate to the desired level.

If the cooling airflow rate is greater, the cooling capacity of the LTR will be greater, which will decrease the coolant temperature in the low temperature cooling loop. If the inlet coolant temperature in the condenser is lower, the inlet refrigerant temperature can be lowered, and still achieve the same amount of condenser heat transfer. To lower the refrigerant inlet temperature, the compressor's refrigerant outlet pressure can be lowered which decreases the amount of power the compressor consumes.

The goal of the project was to determine if the dual loop setup with a single module radiator would reduce the power consumption of the VTMS when the A/C system was activated while maintaining the same system performance as the dual loop setup. The success of the single module radiator was determined from the simulation results.

A model of the dual loop setup was constructed using the supplier component data and was calibrated using the experimental data from Air-to-Boil (ATB) and New European Driving Cycle (NEDC) tests conducted on a Fiat Punto with a prototype of the dual loop setup. Once the simulation model was calibrated, it was used to construct a model of the dual loop setup with a single module radiator. The ATB and NEDC tests were simulated on the single module radiator model. The simulation results of the ATB and NEDC tests from the dual loop model and the single module radiator model were compared to determine the improvement in system performance and power consumption.

2.2 Dual Loop System

The simulation model of the dual loop setup was created based on the actual system arrangement. The complete dual loop system arrangement is shown in Figure 2.1. The system contains five heat exchangers, two coolant pumps (one for the high temperature loop and one for the low temperature loop) and a TSTAT in the high temperature loop, which controls the coolant flow to the radiator. The low temperature loop contains the A/C condenser and the CAC (intercooler) for the charge air from the turbocharger.

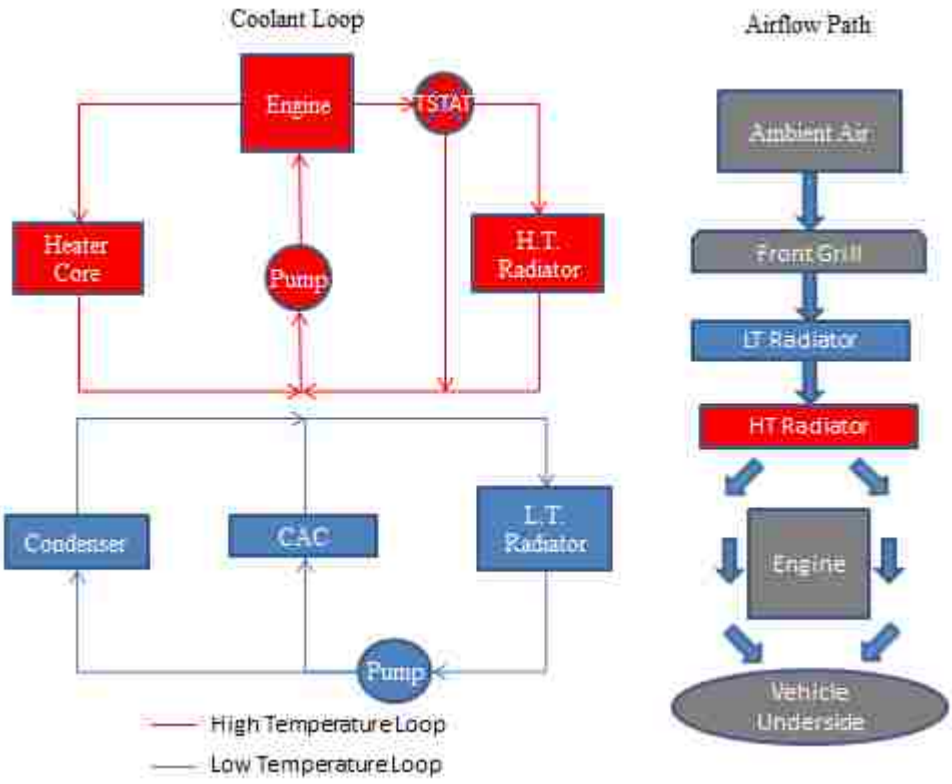

Figure 2.1: Dual Loop Model Basic System Layout

2.3 Component Experimental Data

The individual components within the simulation model were first calibrated to match the performance of the actual components. The individual components such as the

heat exchangers and pumps were calibrated based on the bench testing data which was provided by the supplier of each component.

The bench testing data included the heat transfer performance, and the coolant and air pressure drop through the heat exchanger. The heat transfer bench test was performed by the supplier of each heat exchanger in a calorimetric wind tunnel [18]. The total heat transfer was monitored by measuring the temperature of the coolant and the air, at the inlet and outlet locations. The airflow and coolant flow rates were varied to measure the heat transfer at various flow rates. The supplier of each heat exchanger performed the bench test and provided data similar to that shown in Table 2.1 [19], which only contains one coolant flow rate. The full set of data, not shown here, includes multiple coolant flow rates. The heat transfer data was used to calibrate the heat transfer characteristics of the heat exchanger in the simulation model.

Table 2.1: Sample Bench Test Data Sheet for High Temperature Radiator [19]

Inlet Temperature Difference between Coolant and Air: 65^{o}C			
Air Speed (m/s)	Coolant Flow Rate (kg/s)	Effectiveness (%)	Heat Transfer (kW)
1	1.11	91	17.37
2	1.11	74	28.30
3	1.11	64	36.81
4	1.11	57	43.34
5	1.11	51	48.35
6	1.11	46	52.28
7	1.11	42	55.58
8	1.11	39	58.69
9	1.11	36	62.05

The bench test to measure the pressure drops of the air and coolant was performed by varying the air and coolant flow rates through the heat exchanger. The pressure at the inlet and outlet were measured by taking the average pressure using an array of pressure probes [18]. The difference between the inlet and outlet pressure is the pressure head loss through the pipe. A sample of the pressure loss data provided by the supplier is shown in Table 2.2 [19]. The pressure head loss data was used to calibrate the system resistance of the heat exchanger to the air and coolant flows. Both the air and coolant flows were important in the model to ensure the proper amount of heat transfer.

Table 2.2: Sample Bench Test Pressure Drop Data [19]

Coolant Flow Rate (kg/s)	Coolant Pressure Drop (Pa)	Airflow Speed (m/s)	Air Pressure Drop (Pa)
0.30	10.89	1	11
0.56	38.12	2	38
0.87	70.33	3	70
1.16	107.5	4	108
1.45	149.7	5	150
1.73	196.9	6	197
2.02	249.1	7	249
2.31	306.3	8	306
2.60	368.5	9	369

The pump bench test was conducted by varying the flow resistance of the coolant through the pump. The coolant flow rate and the pressure at the inlet and outlet of the pump were measured. The test began with no flow resistance (free delivery), as the flow resistance was increased, the flow rate decreased and the pressure head increased until the shutoff head was reached (the pressure when there is no coolant flow through the pump). The pump speed was then increased and the test repeated to determine the pump curves at several pump speeds [20]. A sample of the bench test pump curves for the HT loop coolant pump is shown in Figure 2.2 [19]. The pump pressure increase, the difference in coolant pressure at the inlet and outlet, was measured across the pump, in the HT loop shown in Figure 2.1. The complete bench test pump curves for both the HT loop and LT loop coolant pumps are shown in Appendix A.

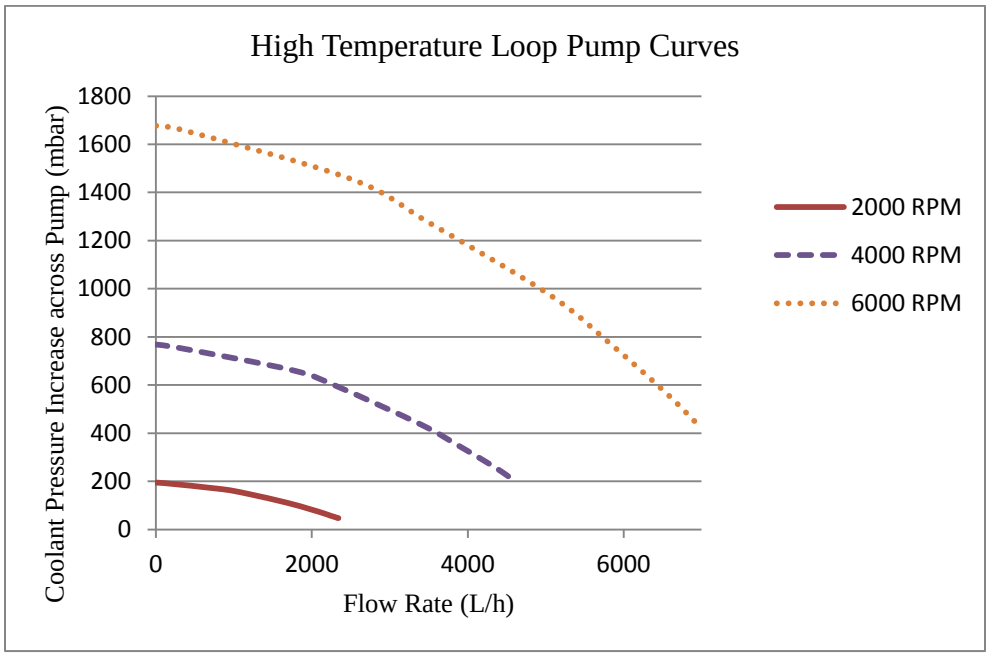

Figure 2.2: Sample Pump Curves of the HT Loop Coolant Pump [19]

The fan performance curves were determined by using a fan wind tunnel. The fan curve supplied was only at the fan's maximum activation level which corresponds to the maximum fan speed. As the airflow resistance in front of the fan was increased, the airflow rate and pressure in front and behind the fan were measured [18]. The fan affinity laws were used to determine the fan performance curves at other activation levels [18]. The bench test fan curve at 100% fan activation is shown in Figure 2.3 [19]. The air pressure increase was measured across the cooling fan, the difference in air pressure between the inlet and outlet, shown in Figure 2.1.

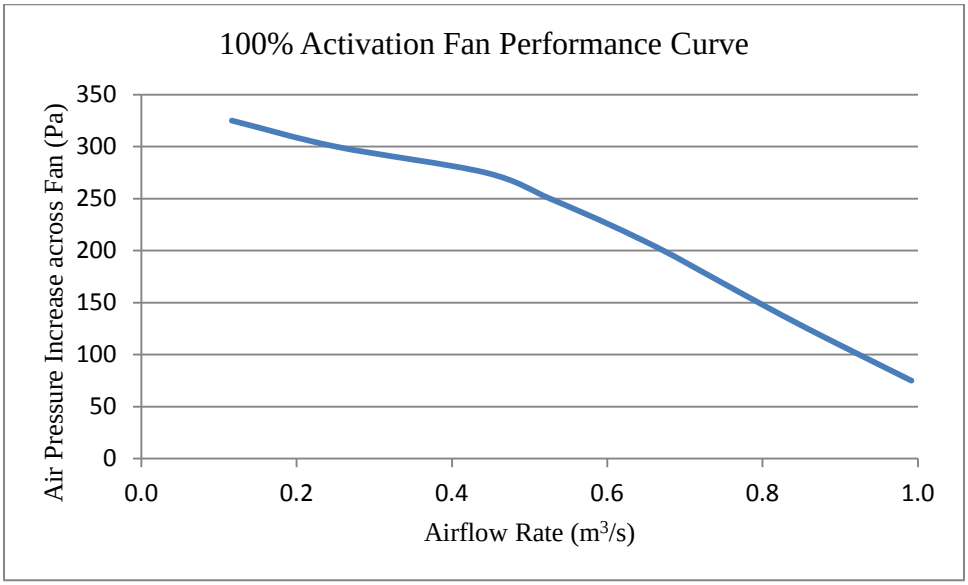

Figure 2.3: Bench Test 100% Activation Fan Performance Curve [19]

2.4 Complete System Experimental Data

Once each of the individual components were calibrated using the bench testing data, they were integrated into the model to form the complete system. The complete system was calibrated using experimental testing data from experimental tests conducted on a Fiat Punto with a dual loop cooling system prototype. The two tests conducted on the vehicle were the ATB test and the NEDC test. In each of the tests, there were several measurements recorded such as the engine speed, engine pressure and the temperature at the inlet and outlet of the coolant for each heat exchanger. The complete list of all the measurement parameters recorded is shown in Table 2.3.

Table 2.3: Experimental Tests Measurement Parameters

LT Loop Measurement Parameters	HT Loop Measurement Parameters	A/C Loop Measurement Parameters	Engine Measurement Parameters	Miscellaneous Measurement Parameters
LTR Inlet Temperature	HTR Inlet	Condenser Inlet Pressure	Engine Speed	Fan Activation
LTR Outlet Temperature	HTR Outlet Temperature	Condenser Outlet Pressure	Engine Torque	Ambient Air Temperature
Condenser Inlet Temperature	Engine Outlet Temperature	TXV Inlet Area	Engine Oil Temperature	Vehicle Speed
Condenser Outlet Temperature		Compressor Inlet Pressure		
CAC Inlet Temperature		Compressor Outlet Pressure		
CAC Outlet Temperature				
LT Pump Activation Level				

The NEDC test is the standardized vehicle test used in Europe to determine vehicle fuel economy. Its purpose is to represent the everyday driving conditions of a vehicle used in Europe. The NEDC test includes two different driving cycles, an *urban driving (city driving)* cycle and an *extra-urban (highway driving)* cycle [21]. The *urban driving* cycle includes various stops-and-starts to replicate city driving and the *extra-urban* cycle has continuous high vehicle speeds to replicate highway driving. A

comparison of the *urban driving* cycle and the *extra-urban* driving cycle is shown in Table 2.4 [21].

Table 2.4: Comparison between NEDC *Urban* and *Extra-Urban* Driving Cycles [21]

	Urban Driving Cycle	Extra-Urban Driving Cycle
Average Speed (km/h)	30 km/h	62.6 km/h
Maximum Speed (km/h)	50 km/h	120 km/h
Total Time Stopped	65 s	0 s
Total Cycle Time	195 s	400 s

At first, the *urban driving cycle* is repeated four times (0 to 780s) which is immediately followed by one *extra urban driving cycle* (780s to 1180s). The vehicle speed over the complete NEDC test is shown in Figure 2.4 [21]. The NEDC test is started from a warm start. The A/C system is not operating during the actual test, however in the experimental tests and simulations in this thesis the A/C was operating because the main objective was to decrease vehicle power consumption with the air conditioning system operating.

There are several other vehicle fuel economy tests that are used to determine vehicle fuel economy. The NEDC test has been criticized for not being an accurate driving cycle at replicating vehicle usage and fuel economy [22]. Other driving cycles which may be more accurate for predicting vehicle fuel economy such as the Federal Test Procedure 75 (FTP-75) and the Highway Fuel Economy Driving Schedule (HWFET), which are used in North America, were not used in this thesis because the Fiat Punto is

strictly a European vehicle and NEDC test data was readily available for the calibration of the simulation models.

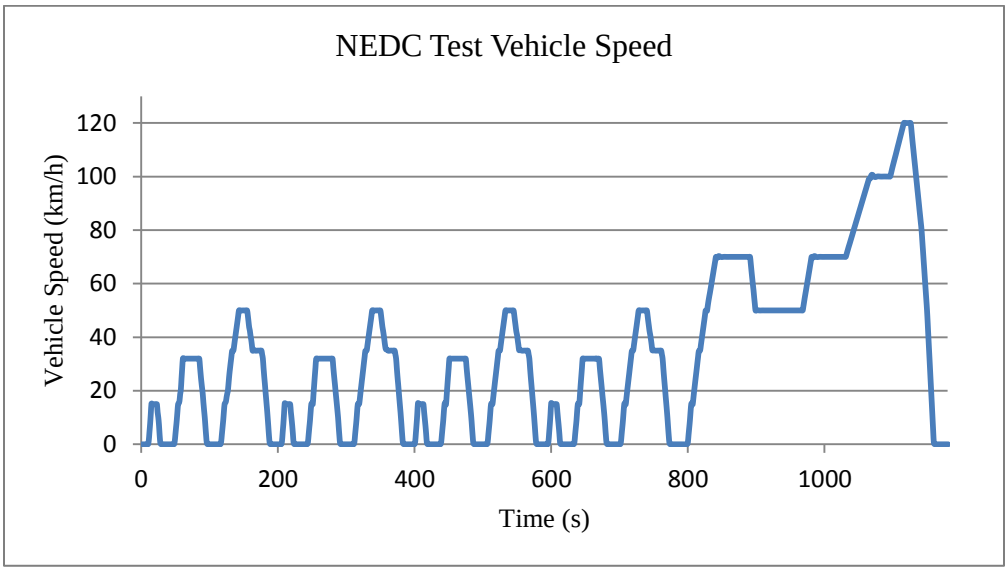

Figure 2.4: NEDC Cycle Vehicle Speed Over Complete Test

The ATB test is a steady state VTMS test designed to determine the engine cooling system (the radiator) capacity at various engine operating conditions [23]. The various vehicle operating conditions include different grades of the slope of the road, transmission gears, engine speeds, vehicle speeds and with the A/C active or inactive. The various vehicle operating test conditions used in the ATB test of the Fiat Punto are shown in Table 2.5 [24].

The ATB temperature is the ambient air temperature that will cause the engine coolant to boil when the vehicle is operating under the specified test condition. The system cooling capacity of the radiator is greater if the ATB temperature is higher. If the ATB temperature is too low, around 50^{o}C, the cooling capacity would be insufficient and

should be increased to meet the system cooling needs at the specified operating condition. The ATB temperature is calculated for each test condition using Equation 2.1:

$$T_{AirToBoil} = (T_{coolboil} - T_{cooleng}) + T_{airamb} \quad (2.1)$$

Table 2.5: Air-to-Boil Test Engine Operating Conditions

Ambient Air Temperature: 30°C				
Condition	Engine Speed (RPM)	Power at Wheels (Nomalized)	Vehicle Speed (km/h)	A/C Active (ON or OFF)
1	3255	0.38	67.9	OFF
2	3258	0.38	67.8	OFF
3	3265	0.26	44	ON
4	3449	0.18	25	OFF
5	3878	0.38	139.9	OFF
6	3888	0.92	139.9	OFF
7	3890	0.9	139.9	ON
8	5002	1	103.8	OFF
9	780	0	0	ON

2.5 Model Heat Transfer Theory

AMESim uses standard heat transfer equations to represent the heat exchanger components within the model. The NTU-effectiveness method was used to model all the heat exchangers in the model with the exception of the condenser because the condenser

contains two-phase flow, as the refrigerant undergoes a phase change from a gas to a liquid state. The heat transfer was calculated using Equation 2.2:

$$\dot{Q}_{act} = \varepsilon C_{min}(T_{incool} - T_{inair}) \tag{2.2}$$

The equation to calculate the effectiveness of a heat exchanger varies depending on the type of heat exchanger. For a cross flow heat exchanger, where the air flows over a set of tubes like the heat exchangers used in the VTMS, the effectiveness was calculated using Equation 2.3 [25]:

$$\varepsilon = 1 - (\exp\left\{\frac{NTU^{0.22}}{c}[\exp(-c\,NTU^{0.78}) - 1]\right\} \tag{2.3}$$

The Number of Transfer Units (NTU) is a dimensionless parameter of the heat exchanger that quantifies the geometrical dimensions of the heat exchanger in relation to the heat transfer. The NTU's for a heat exchanger were calculated using Equation 2.4:

$$NTU = \frac{UA_s}{C_{min}} \tag{2.4}$$

The total system resistance (UA_s) is the heat exchanger resistance to heat transfer from the coolant to the air. The total system resistance includes a convection resistance from the coolant to the tube wall of the heat exchanger, a conduction resistance through the tube structure to fins, and another convection resistance from the fins to the air flowing through the heat exchanger. The resistances are shown below in Figure 2.5. The total system resistance was calculated using Equation 2.5 [25]:

$$\frac{1}{\{UA_s\}} = \frac{1}{(h_{cool})(A_{tube})} + \frac{1}{G_{wall}} + \frac{1}{(h_{air})(A_{air})} \tag{2.5}$$

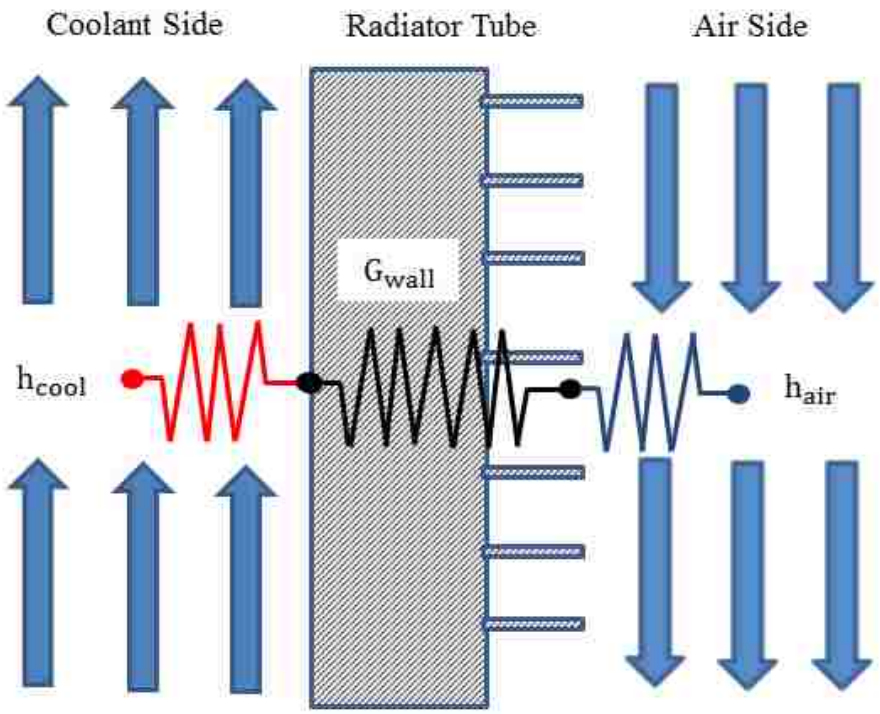

Figure 2.5: Heat Exchanger Heat Transfer Resistances

The coolant and the air side convection coefficients were determined using the Nusselt number relationship for heat exchangers. The Nusselt number relationship used for each heat exchanger is Equation 2.6:

$$\mathrm{Nu} = \mathrm{a}\left(\mathrm{Re}^{\mathrm{b}}\right)\left(\mathrm{Pr}^{\frac{1}{3}}\right) \tag{2.6}$$

The NTU-effectiveness method calculates the heat transfer using only the inlet temperature and flow rates of the coolant and air. The outlet temperatures of the coolant and air in a heat exchanger were calculated using a transient enthalpy balance because of the varying inlet temperatures and flow rates. The heat exchanger was considered a lumped mass with a constant temperature throughout the entire boundary with the

enthalpy flow entering and leaving as shown in Figure 2.6. The outlet temperature of the coolant was found using Equation 2.7 [25]:

$$\frac{dH}{dt} = \frac{dmh_1}{dt} + \frac{dmh_2}{dt} + \dot{Q}_{act} \tag{2.7}$$

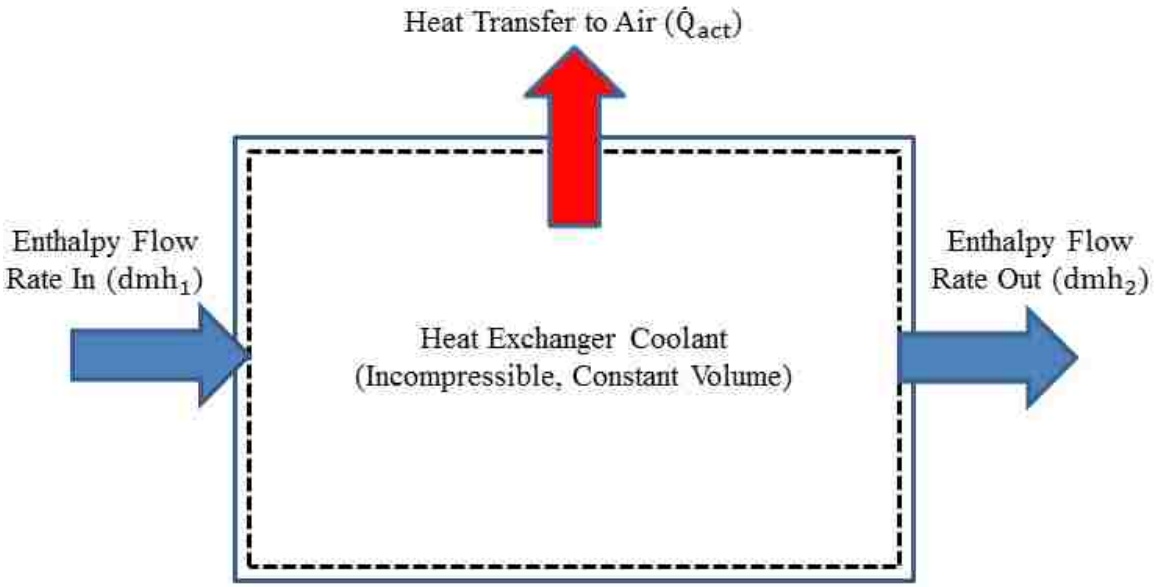

Figure 2.6: Enthalpy Flow Diagram

The condenser was not modelled using the NTU-effectiveness method because it had two phase heat transfer when the refrigerant changes phases from a gas to a liquid. The heat transfer for the condenser was modelled using Newton's law of cooling and the Shah correlation to calculate the two-phase convection heat transfer coefficient of the refrigerant. The Shah correlation is shown in Equation 2.8 [26]:

$$h_{2phase} = \left[0.023 {Re_l}^{0.8} {Pr_l}^{0.4} \left(\frac{\lambda}{d_{href}}\right)\right]\left[(1-x)^{0.8} + 3.8\,\frac{x^{0.76}(1-x)^{0.04}}{(p_{red})^{0.38}}\right] \tag{2.8}$$

The temperature difference was considered to be the difference between the refrigerant temperature at the inlet of the condenser and the temperature of the condenser tube wall. The tube wall was considered to be a lumped mass with a constant temperature. To increase the accuracy of the heat transfer in the condenser, several two-phase heat transfer components were used to represent the condenser to accurately model the temperature difference across the condenser as the coolant temperature increases.

The coolant flow through the condenser was assumed to be turbulent because of the presence of ridges on the coolant side tubes through the condenser which force the coolant into turbulence and increases the heat transfer rate. The coolant side of the condenser heat transfer was modelled using the Nusselt number equation shown in Equation 2.9 [27]:

$$\mathrm{Nu_{Turb}} = \mathrm{a}\left(\mathrm{Re^{b}}\right)\left(\mathrm{Pr^{0.8}}\right) \tag{2.9}$$

The convection heat transfer to the coolant was calculated by using the temperature difference between the coolant temperature entering the pipe and the wall temperature. The heat transfer to the coolant was calculated by using Equation 2.10 [27]:

$$\mathrm{Q} = \mathrm{h_{cool}A_{tube}}(\mathrm{T_{incool}} - \mathrm{T_{wall}}) \tag{2.10}$$

2.6 Heat Exchanger Calibration

The bench test data and the geometrical dimensions (frontal area, tube geometry, fin geometry) of each heat exchanger were used to determine the heat exchanger metallic resistance ($\mathrm{G_{wall}}$ from Equation 5) and the Nusselt number coefficients (a and b from Equation 6) for both the coolant and air sides. The values which result in the best correlation between the simulation data to the bench test data were used in the overall

VTMS model. A calibration error of 5% or less was considered acceptable for this application within Fiat and Chrysler. The calibration results for all the heat exchangers (excluding the condenser) are shown in Table 2.6. The complete calibration results are shown in Appendix A.

Table 2.6: Calibration Results for all Single Phase Heat Exchangers

Heat Exchanger	a Coolant	b Coolant	a Air	b Air	Metallic Resistance	Average Error	Max Error
HTR	4.64	1.39	1.15	0.92	13.20	0.7%	1.6%
LTR	9.51	0.42	1.06	1.10	16080	1.2%	4.0%
Heater Core	0.13	0.67	1.10	0.63	800	5.3%	11.6%
CAC	1.00	0.52	0.75	0.85	1000000	0.8%	1.2%

The metallic resistances of each heat exchanger vary greatly because the metallic resistance also includes a characteristic length which includes the fin and tube geometry as a conduction resistance. Each heat exchanger with the exception of the HTR and LTR vary from each other in terms of their geometry and setup which could be why the metallic resistance values have such a large difference between each other.

The heater core calibration had an average error of 5.3% and a maximum error of 11.6% which are both greater than the 5% error limit. The heat transfer from the heater core was negligible in all the simulations because the heater core was not active during the NEDC and ATB tests. If the simulation model were to be used to simulate a cabin warm up cycle then a different method to model the heater core would be needed. The heater core was still included in the model even though the heat transfer was negligible

because the coolant pressure drop through the heater core affected the total system resistance and the total coolant flow rate that could be provided by the coolant pump.

The calibration of the condenser was different from the other heat exchangers because the condenser is a liquid to liquid heat exchanger with two-phase flow in the refrigerant side. The hydraulic diameter and length of the refrigerant and coolant sides were needed to calibrate the condenser, which were not needed to calibrate the other heat exchangers. The calibration results for the condenser are shown in Table 2.7 and Figure 2.7.

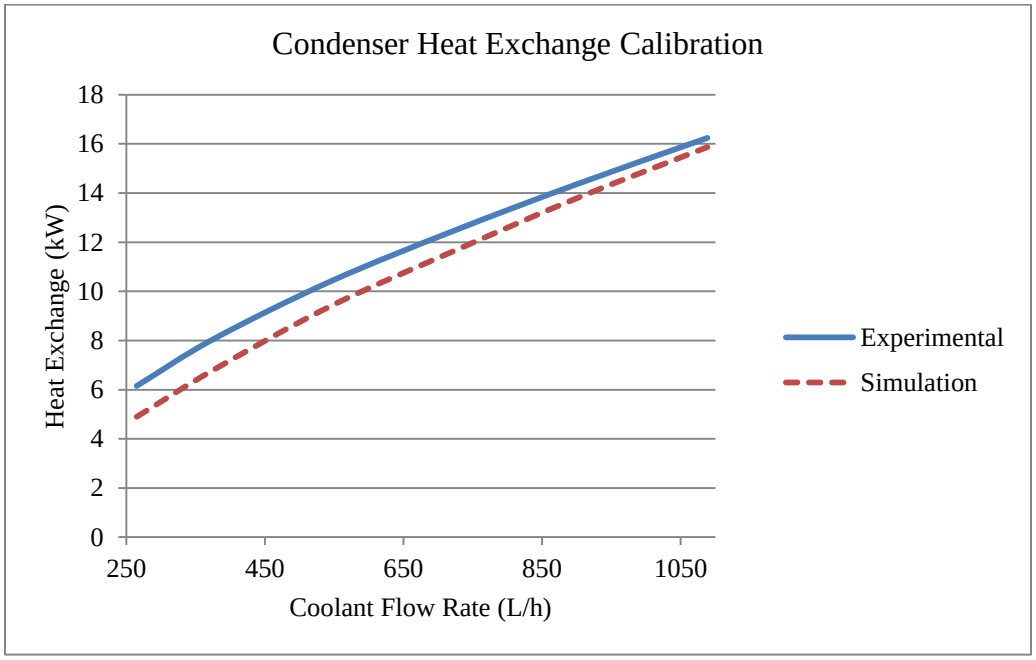

Figure 2.7: Condenser Heat Transfer Calibration

Table 2.7: Condenser Calibration Results

d_{hcool}	10.8 mm
L_{cool}	0.35 m
d_{href}	10.2 mm
L_{ref}	7.2 m
A	0.31
B	1

2.7 Model Construction

Once the individual components were calibrated for heat transfer, they were inputted into the complete model. The complete model construction is shown in Figure 2.8 for the HT coolant flow loop and in Figure 2.9 for the LT coolant flow loop. Each figure shows the different inputs and look-up tables within the model.

In the HT loop, the engine was assumed to be a lumped mass of aluminum with a constant temperature throughout the mass. The coolant within the engine was assumed to be a controlled volume with a constant temperature throughout the volume. The heat rejection from the engine to the coolant due to combustion was known from experimental data at various engine speeds and pressures. The experimental data was collected by Fiat from an engine test performed on the Fiat Punto's 1.4L 4 cylinder engine. The engine was run at several different operating conditions with a known coolant flow rate through the engine.

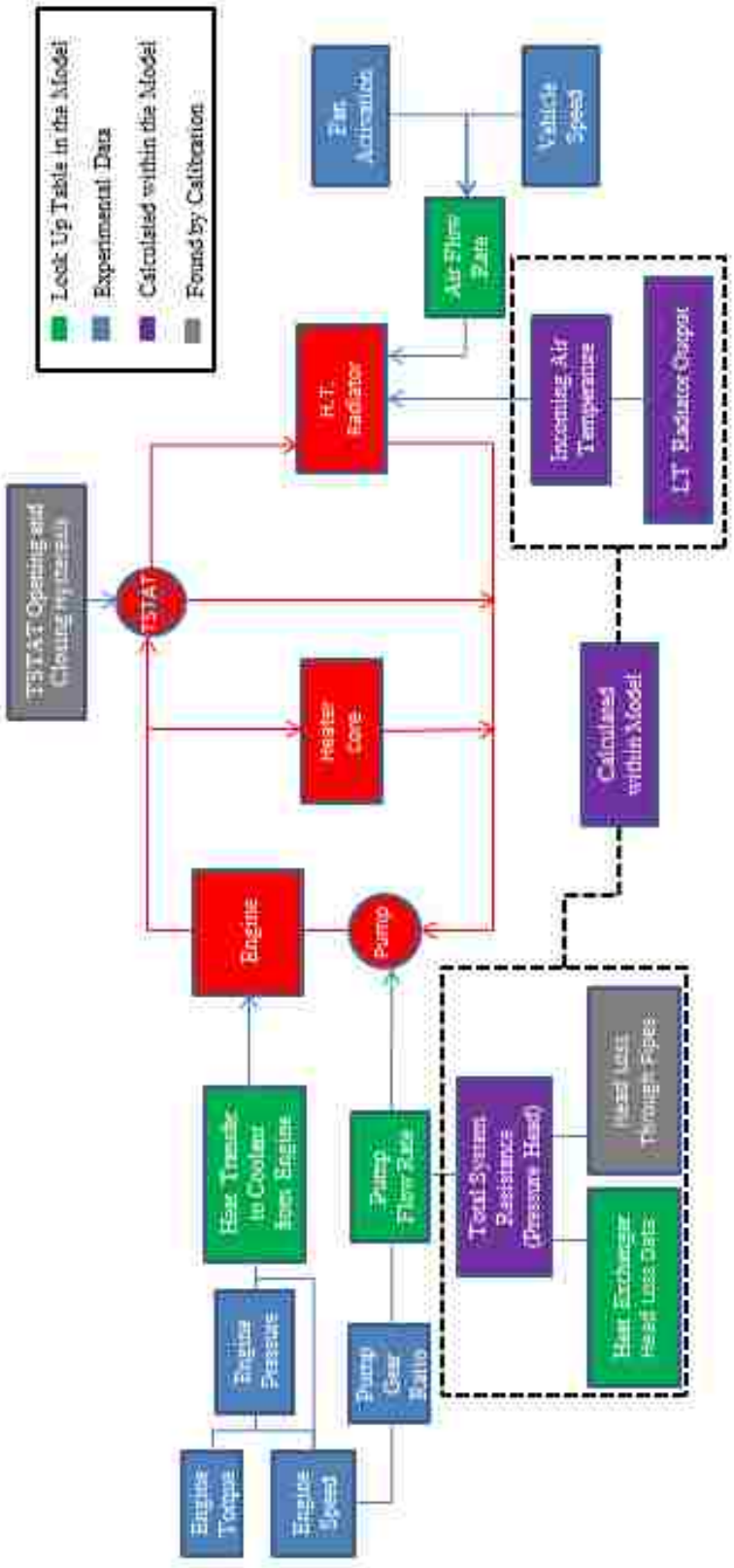

Figure 2.8: HT Loop Model Arrangement

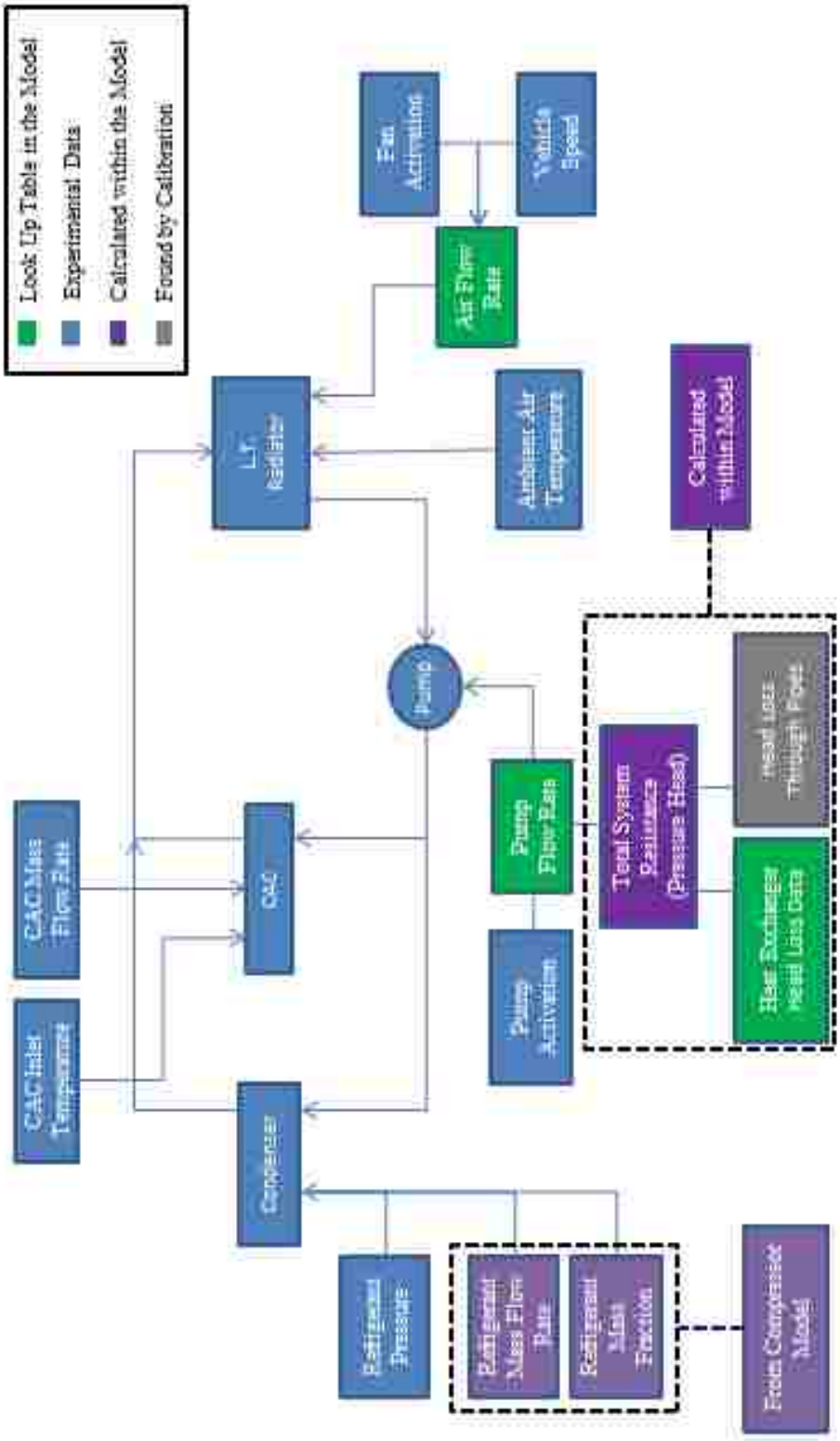

Figure 2.9: LT Loop Model Arrangement

The engine pressure and engine speed as well as the engine coolant inlet and outlet temperatures were measured. The total heat transfer to the coolant at different engine pressures and engine speeds was calculated using the measurements as shown in Figure 2.10. In the model, the engine heat rejection data was inserted into a look-up table, where a known engine speed and pressure corresponded to a heat transfer rate from the engine to the coolant. The engine speed and engine pressure at each time instance during the simulation were the same as measured at each time instance during the experimental ATB and NEDC tests.

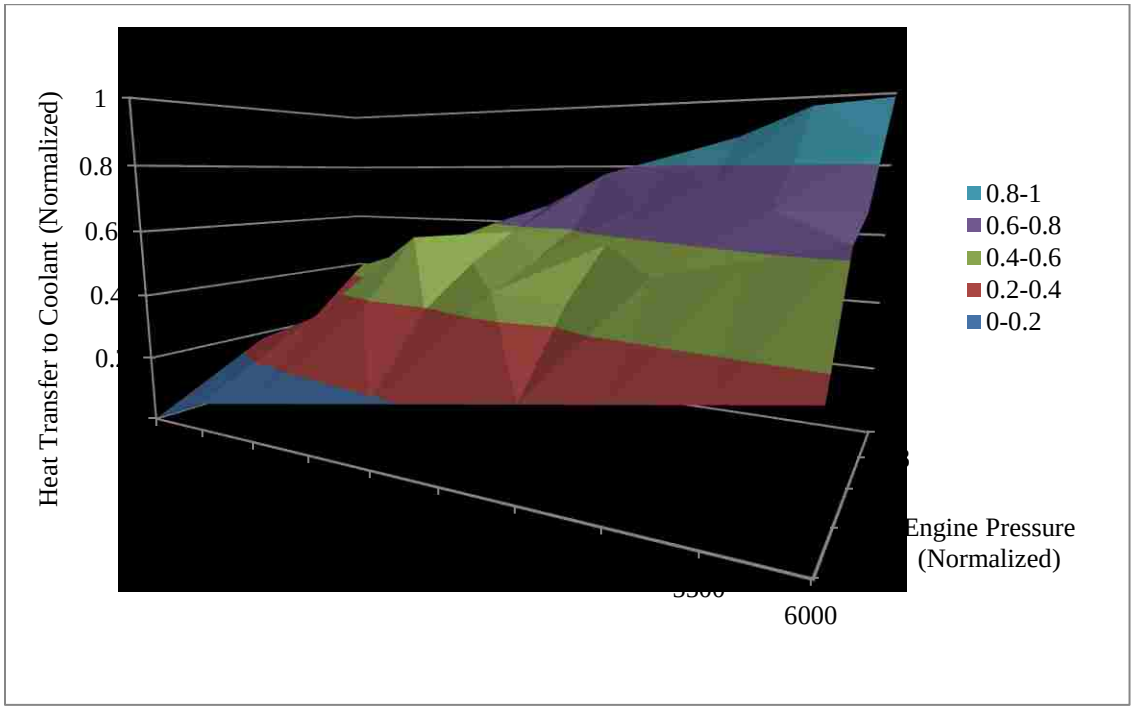

Figure 2.10: Engine Heat Rejection to Coolant (Normalized Engine Pressure and Heat Transfer to Coolant)

The HT loop coolant pump bench test data was inserted into a look-up table, where a known pump speed and total system resistance corresponded to a coolant flow

rate. The pump speed is equal to the engine speed because the pump is powered by the engine with a gear ratio of 1:1. The engine speed at each time instance during the simulation was the same as measured at each time instance during the experimental ATB and NEDC tests.

The total system resistance (pressure head across the pump) was determined in the model at each time instance using an iterative process of the coolant flow rate through the HT pump. A pressure head across the pump was assumed and used, along with the pump speed at each time instance, to determine the corresponding coolant flow rate from the look-up table as shown in Equation 2.11:

$$\dot{\forall}_{cool} = f\left(N_{pump,}\, \Delta p_{sys}\right) \tag{2.11}$$

The pressure drop of the coolant across all of the hoses and heat exchangers is a function of the coolant flow rate. The total system pressure drop is equal to the pressure drop of the coolant through all the hoses and heat exchangers. The coolant flow rate found from the look-up table was used to re-calculate the total pressure head using Equation 2.12:

$$\Delta p_{sys} = \sum \Delta p_{pipe} + \sum \Delta p_{hx} \tag{2.12}$$

If the difference between the assumed and calculated system pressure heads was within the specified allowable error, then the coolant flow rate was accurate. If the difference was greater than the allowable error, then a different system pressure head was assumed and the process was repeated. The simulation would continue to iterate until the difference between the assumed and calculated pressure heads was within the allowable error.

In both the HT and LT loops, there were some parallel coolant flow paths. If the coolant flow paths were in parallel with each other, the pressure drop through the parallel flow paths is equal as shown in Equation 2.13:

$$\Delta p_{flow1} = \Delta p_{flow2} \tag{2.13}$$

The total mass flow rate in the system is the mass flow rate of both parallel branches combined as shown in Equation 2.14:

$$\dot{m}_{tot} = \dot{m}_{flow1} + \dot{m}_{flow2} \tag{2.14}$$

The pressure drop through each branch was determined in the model at each time instance through an iterative process with the combined mass flow rate of the coolant through the parallel branches. The pressure drop through the branches was assumed and used to calculate the mass flow rate through each branch. The mass flow rate through each branch was used to determine the total mass flow rate. If the difference between the calculated total mass and the actual total mass flow rate was greater than the allowable error, then another pressure drop was assumed and the process was repeated.

The system resistance through all the heat exchangers in the model was known from the bench test data from the supplier. It was inserted into a look-up table at the respective heat exchanger, where a known coolant flow rate corresponded to a coolant pressure drop through the heat exchanger. The system resistances through the engine and pipes connecting all the components were determined through calibration using the experimental data.

The HT loop system resistance, total HT loop system flow rate and the flow rate of coolant through the HTR were greatly dependent on the TSTAT opening and closing

temperatures as well as its opening and closing hysteresis. The TSTAT is a valve that regulates the coolant flow through the HTR from the engine. As the engine coolant temperature exceeds the opening temperature, the TSTAT opens to allow coolant to flow through the radiator. As the coolant temperature continues to rise, the TSTAT will open wider allowing more coolant to flow through the HTR. The TSTAT's purpose is to maintain the engine at a constant temperature of approximately 82 ℃. The TSTAT opening and closing temperatures as well as the hysteresis were calibrated using the NEDC experimental data. The maximum opening area was calibrated using the ATB test data because during the ATB test, the TSTAT was forced to the completely open position.

In the LT loop, the LT loop coolant pump curves from the supplier bench test were inserted into a look-up table, where a known pump speed and total system resistance corresponded to a coolant flow rate. The LT loop coolant pump is driven by an electric motor instead of the engine because it does not require as much power as the HT loop coolant pump. The electric motor activation level corresponds to a pump speed. The electric motor activation level at each time instance during the simulation was the same as measured at each time instance during the experimental ATB and NEDC tests. The total system resistance and coolant flow rate of the LT loop was determined using the same iterative calculation procedures described previously for the HT loop coolant pump.

The CAC air inlet conditions and the condenser refrigerant inlet conditions at each time instance during the simulation were the same as measured at each time instance during the experimental ATB and NEDC tests. The CAC air inlet conditions in the model were the airflow rate and the inlet air temperature. The condenser refrigerant inlet

conditions in the model were the refrigerant mass flow rate, the inlet refrigerant pressure and inlet gas mass fraction.

A one-dimensional simulation model of the compressor was created in order to determine the mass flow rate and mass fraction of the refrigerant at the inlet of the condenser. The simulation model of the compressor was created using the supplier bench test data. The compressor is run directly from the engine with a known gear ratio of 1:1. When the A/C is activated, the compressor clutch is engaged to some degree depending on the activation signal from the expansion valve. The engine speed, and the compressor inlet and outlet pressures in the compressor model at each time instance during the simulation were the same as measured at each time instance during the experimental ATB and NEDC tests.

The underhood cooling airflow which flows through the LTR and the HTR was unknown for the dual loop setup. There was CFD data for the standard VTMS setup [27] which was used to create an underhood cooling airflow model. The underhood cooling airflow model was used to determine the airflow rate through the dual loop setup at different vehicle speeds and fan activation levels.

In the model, the dual loop setup airflow rate results from the underhood cooling airflow model were inserted into a look-up table, where a known fan activation level and vehicle speed corresponded to an airflow rate. The vehicle speed and fan activation level at each time instance during the simulation were the same as measured at each time instance during the experimental ATB and NEDC tests.

The airflow rate calculated from the underhood cooling airflow model did not take into account the effect of the bumper and front grill on the airflow path through the

heat exchangers. In the actual vehicle, the air flows non-uniformly over the heat exchangers due to the bumper and front grill, which lowers the amount of heat transfer. To compensate for this, it is standard within Chrysler and Fiat to use a 10% non-uniformity factor unless an in-vehicle heat exchanger bench test was conducted. The non-uniformity factor decreased the airflow rate through the heat exchangers by 10% in the simulation model.

2.8 Underhood Cooling Airflow Model

Once the system model was constructed, the underhood cooling airflow rate at various fan activation levels and vehicle speeds had to be determined. The underhood airflow rate was required in the simulation model to accurately predict the heat transfer of the heat exchangers.

The underhood airflow rate for the dual loop setup was unknown because no experimental testing or CFD data has been found. There was airflow data available for the standard setup which was used to construct and calibrate a one-dimensional underhood cooling airflow simulation model for the Fiat Punto. The model was then used to determine the dual loop airflow rates at various fan activation levels and vehicle speeds.

In an actual vehicle, the air flows into the underhood compartment through the front grill, where it experiences a pressure increase due to the ram air effect and a large decrease in velocity compared to the vehicle speed. The air will then flow through the heat exchangers in the underhood compartment and experience a pressure drop due to the airflow resistance of the heat exchangers. If the airflow resistance of the heat exchangers is lower, then the airflow rate will be greater. The total resistance of the heat exchangers

to airflow for the standard and dual loop VTMS setups in the Fiat Punto are shown in Figure 2.11. The system resistance was different for each arrangement because each setup used different heat exchangers and had a different number of heat exchangers at the front-end of the vehicle.

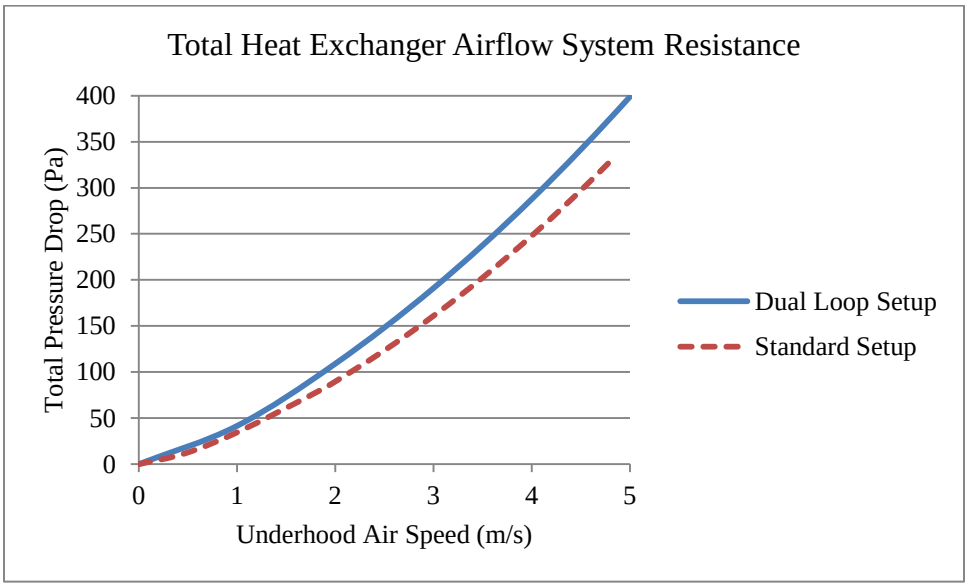

Figure 2.11: Total Heat Exchanger Airflow System Resistance

After flowing through the heat exchangers, the air flows through the cooling fan and increases in pressure. After the cooling fan, the air flows over the engine, where it experiences another pressure drop and eventually exits through the underside of the vehicle. The underhood air exits at the air pressure of the underbody of the vehicle's air stream. The airflow speed is limited by the pressure difference between the air pressure at the front grill and the underbody air pressure. The total pressure drop, the air experiences after flowing through the heat exchangers and over the engine, will be equal to the difference between them. The underbody air pressure is directly related to the vehicle

speed and the shape of the vehicle. The air path of the underhood airflow is shown in Figure 2.12 [29].

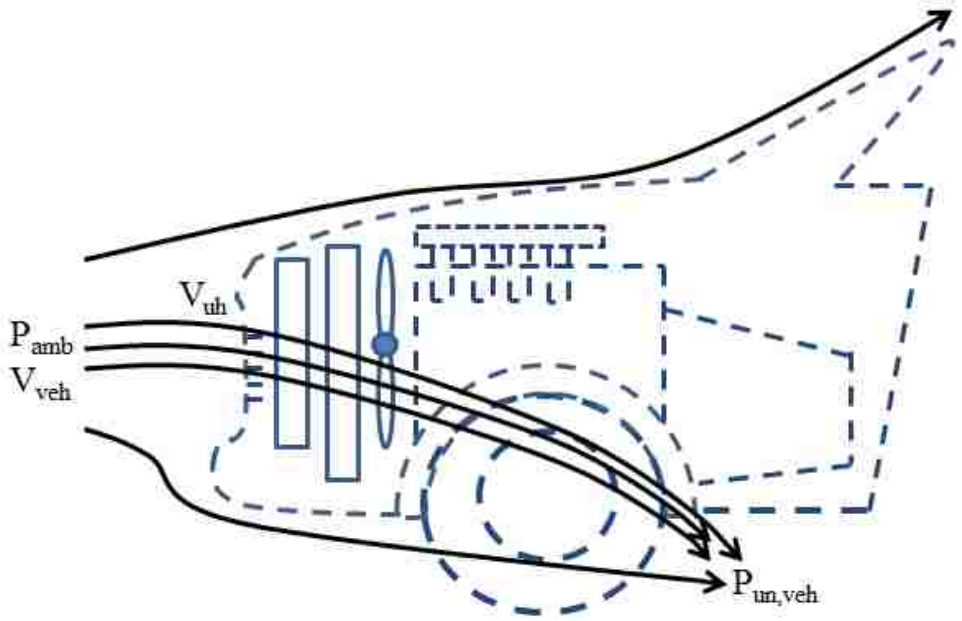

Figure 2.12: Underhood Airflow Path [29]

The CFD data for the standard VTMS setup included the mass airflow rate through the underhood compartment at various vehicle speeds and fan activation levels. The fan activation level is the amount of power supplied to the fan, which is directly proportional to the cooling fan speed. As the fan speed is increased, the underhood airflow rate increases which is shown by the fan performance curves in Figure 2.13. The standard setup airflow data was used to calibrate the underhood cooling airflow model once it was constructed and is shown in Figure 2.14.

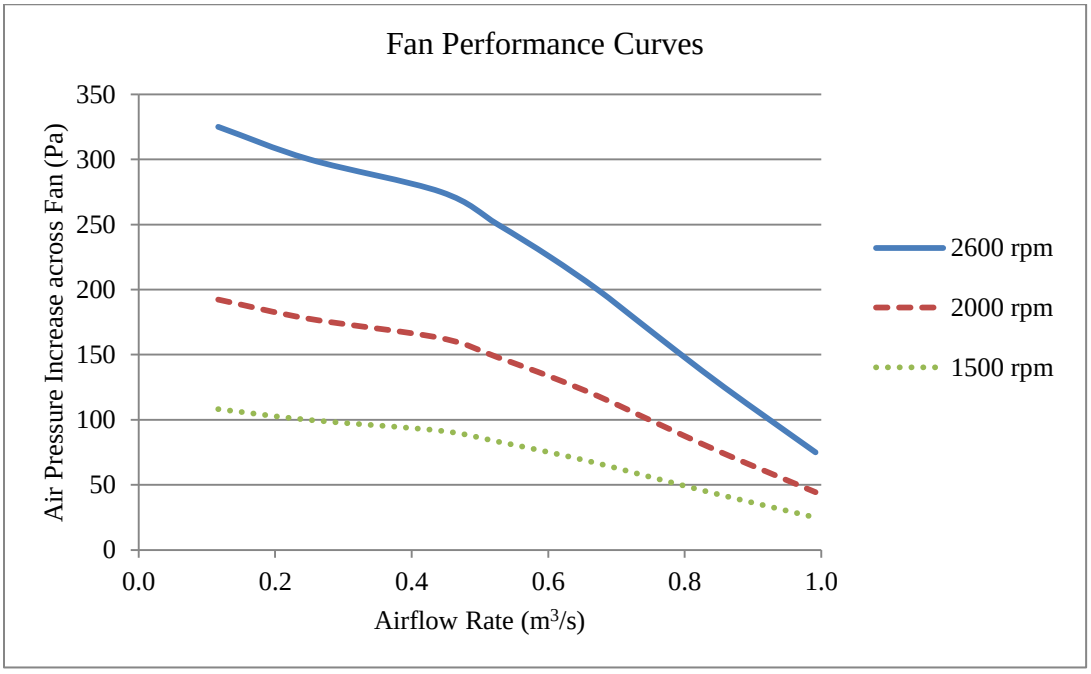

Figure 2.13: Cooling Fan Performance Curves

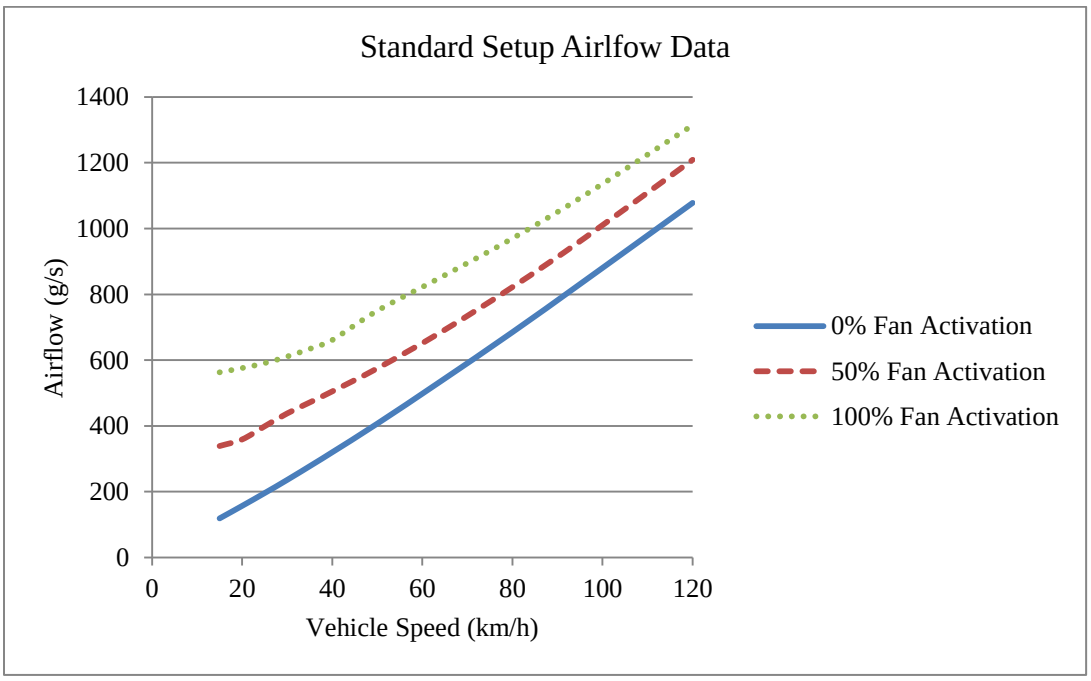

Figure 2.14: Standard Setup Airflow CFD Data

In the model, the airflow pressure data for each heat exchanger and the cooling fan came from the supplier bench tests. The heat exchanger pressure drop data was inserted into a look-up table, where the airflow rate through the heat exchanger corresponded to a pressure drop. The airflow pressure data for the fan was also inserted into a look-up table, where the airflow rate through the fan corresponded to a pressure increase. The fan bench test was only performed at the maximum fan speed. To predict the fan performance at different fan speeds the fan affinity laws were used in the model. The fan affinity law used a pressure coefficient, which was calculated using the bench test data. The fan pressure coefficient was calculated at each airflow rate in the bench test data using Equation 2.15 [25]:

$$C_{press} = \frac{dp_{fan}}{\rho_{air}[(N_{fan})(D_{fan})]^2} \tag{2.15}$$

The fan pressure coefficient was assumed to be constant at all fan speeds because the fan airflow data was only provided at the maximum fan speed. In actuality, the fan pressure coefficient would vary at different fan speeds because the efficiency of the fan changes at different fan speeds. Once the fan pressure coefficient was calculated using the supplier bench test data, Equation 2.19 was rearranged to calculate the change in pressure increase at any fan speed, as shown in Equation 2.16 [25]:

$$dp_{fan} = (C_{press})\rho_{air}[(N_{fan})(D_{fan})]^2 \tag{2.16}$$

The model unknowns were the engine and the front grill pressure coefficients. The standard setup airflow data was used to determine the engine and the front grill pressure coefficients through calibration. The pressure coefficients for the engine and front grill, determined for the standard setup, were then also used for the dual loop and

single module setup models because the Fiat Punto's front grill and engine compartment remained the same regardless of the heat exchanger arrangement. The equations for the overall pressure change when the air flows through the front grill and around the engine are shown in Equation 2.17 and Equation 2.18 respectively [29]:

$$\Delta p_{grill} = \frac{1}{2} K_{grill} \rho_{air} {V_{veh}}^2 \tag{2.17}$$

$$\Delta p_{eng} = \frac{1}{2} K_{eng} \rho_{air} {V_{uh}}^2 \tag{2.18}$$

The pressure coefficients for both the engine and front grill determined from the model calibration are shown in Table 2.8. The engine pressure coefficients were negative because it decreased the air pressure. The front grill pressure coefficients were positive because the air pressure increased. The reason that the front grill pressure coefficients are small, in comparison to the engine pressure coefficients, are because Equation 2.21 used the vehicle speed to calculate the pressure drop, whereas Equation 2.22 used the underhood air velocity, which was much lower than the vehicle speed.

Table 2.8: Grill and Engine Pressure Coefficient Calibration Results

Fan Activation	Grill Pressure Drop Coefficent	Engine Pressure Drop Coefficent
0%	0.141	-1.15
50%	0.145	-2.00
100%	0.148	-2.70

The calibration for each fan activation level was succesful with an average error below 5%, which was acceptable. The average error for each fan activation level is shown in Table 2.9. The complete results of the calibration are shown in Appendix B.

Table 2.9: External Flow Model Calibration Average Error

Fan Activation Level	Average Error
0%	2.5%
50%	2.3%
100%	1.7%

Once the model was calibrated, the dual loop underhood cooling air flow model was created. The front grill and engine pressure coefficients remained the same from the standard setup model. The model was then used to determine the airflow rates of the dual loop setup. The difference of the airflow path between the standard setup and dual loop setup is shown in Figure 2.15.

A comparison between the standard setup and dual loop setup, for the underhood airflow rates at various fan activation levels, are shown in Figure 2.16, Figure 2.17 and Figure 2.18. The dual loop setup airflow rates were lower than the standard setup airflow rates. This was expected because the system resistance of the heat exchangers in the dual loop setup was greater than the standard setup, as shown previously in Figure 2.11. The dual loop airflow rates were approximately 13% lower than the standard setup airflow rates.

The underhood cooling airflow model, developed to determine the dual loop setup airflow rates, was the same model used to determine the single module setup underhood

cooling airflow rates. The front grill and engine pressure coefficients remained the same from the calibration of the standard setup in the single module setup model.

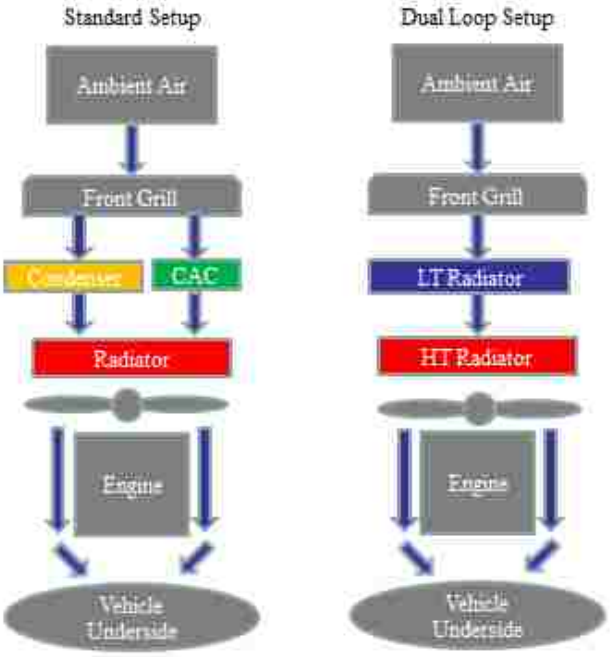

Figure 2.15: Standard Setup and Dual loop Setup Airflow Path

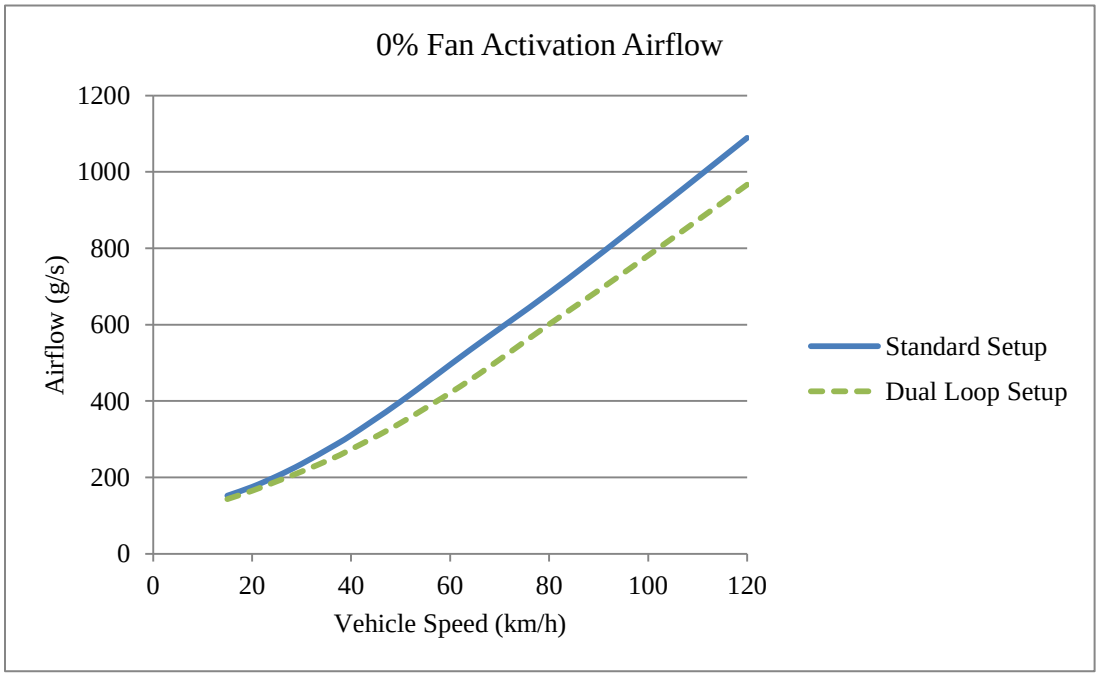

Figure 2.16: 0% Fan Activation Airflow Rate

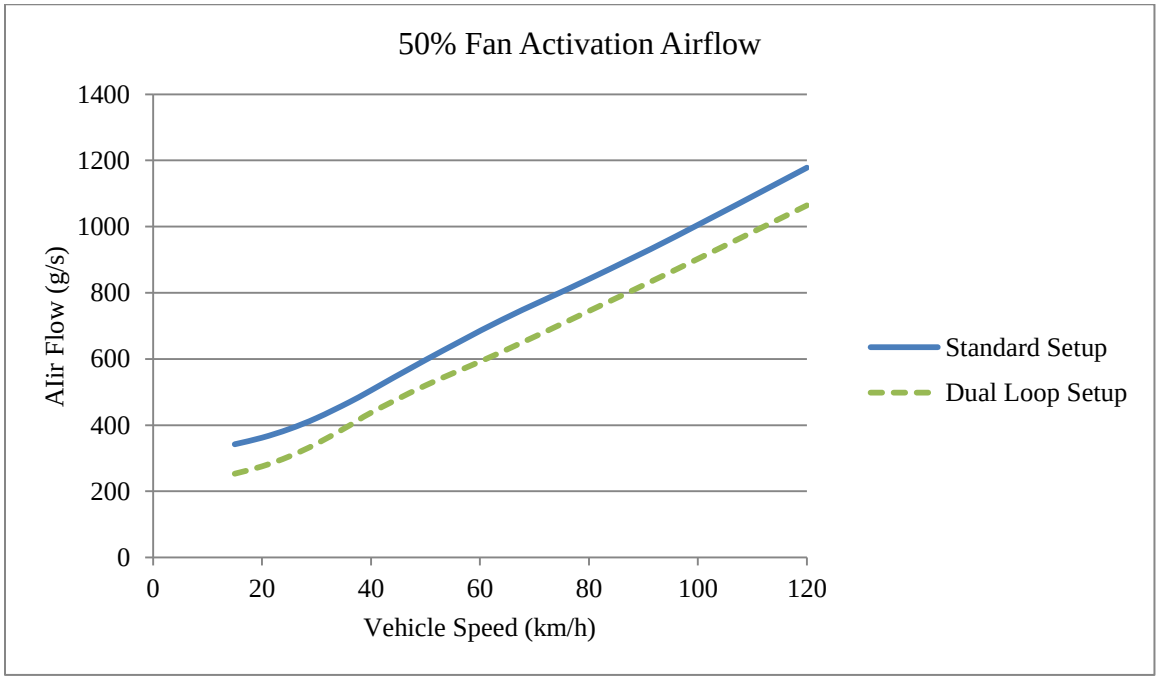

Figure 2.17: 50% Fan Activation Airflow Rate

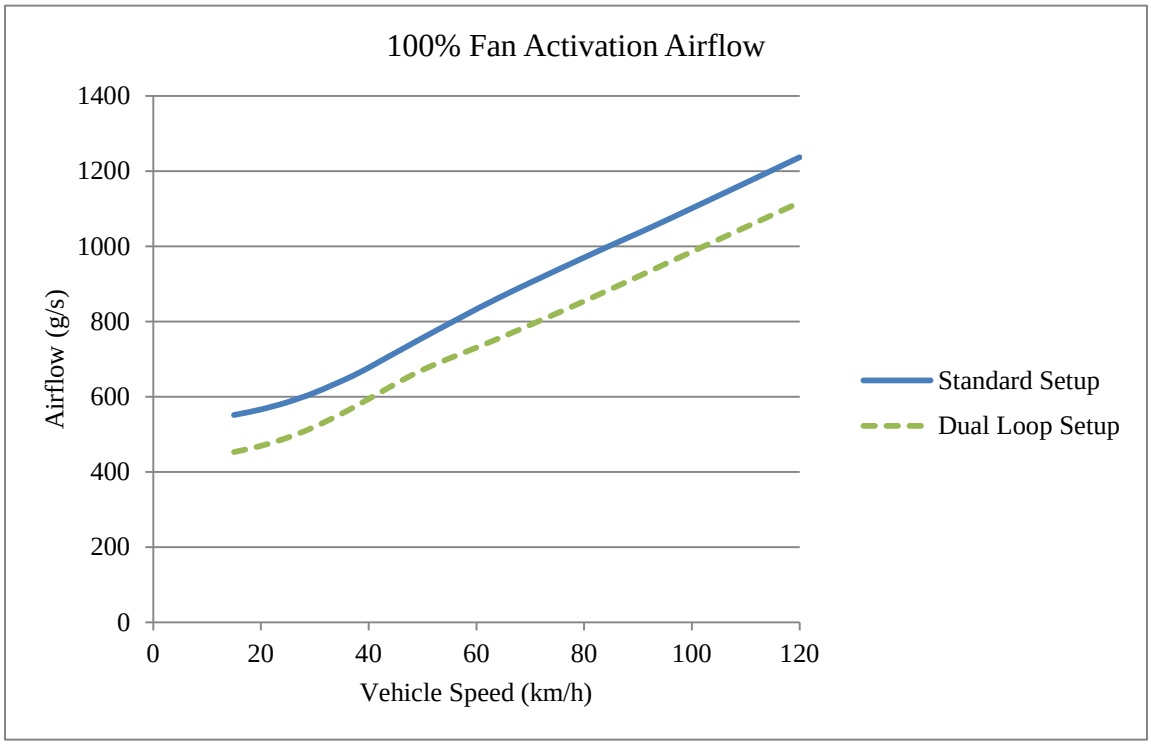

Figure 2.18: 100% Fan Activation Airflow

2.9 ATB and NEDC Dual Loop Setup Model Calibration

The complete model was calibrated using both the ATB and NEDC experimental test data for a dual loop setup on a Fiat Punto. The important calibration parameter from the ATB test data was the ATB temperature. The important calibration parameters from the NEDC test data were the inlet and outlet temperatures of the LTR and the HTR as well as the engine temperature. The calibration standard set by Chrysler and Fiat was that the simulation temperatures be within 3℃ of the experimental calibration parameters. The model parameters that were unknown and needed to be calibrated were the coolant system resistance of the hoses, which connect the components of the circuit together, and the TSTAT opening and closing temperatures.

When calibrating the TSTAT, the opening and closing temperatures as well as the TSTAT hysteresis curves from similar vehicles were modified to try to correlate the engine temperature and the HTR inlet and outlet temperatures to the NEDC test data. The TSTAT hysteresis determined from the calibration process is shown in Figure 2.19. The opening temperature and closing temperature are 84 ℃ and 82 ℃ respectively. These temperatures were reasonable because the engine operating temperature in an actual vehicle is around 83℃.

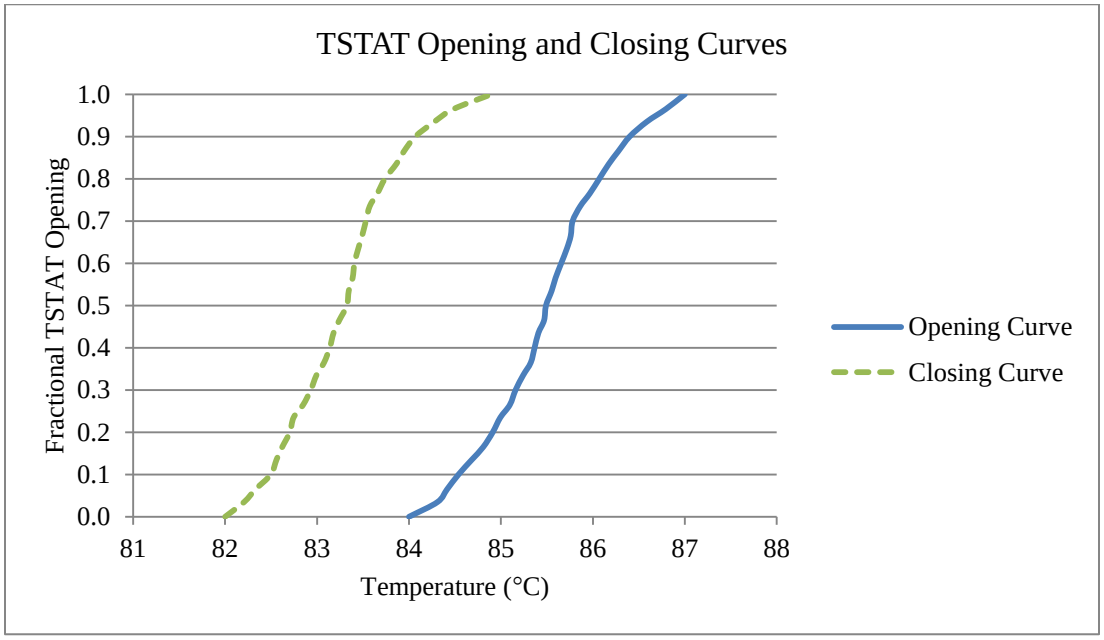

Figure 2.19: Thermostat Opening and Closing Hysteresis

After calibrating the TSTAT and the system resistance of the hoses, the final calibration results for the entire system were achieved. The calibration results for the ATB test are shown in Figure 2.20. The ATB simulation results were all within 3°C of the experimental results and had an error below 5%, except for test conditions 5 and 6. Test conditions 5 and 6 had an error of 7.6% and 8.6% respectively. The larger errors could be because test conditions 5 and 6 had a prescribed vehicle speed of 140 km/h. The underhood airflow rate at 140 km/h may not be accurately predicted because the airflow rate data used to create the underhood cooling airflow model had a maximum vehicle speed of 120 km/h.

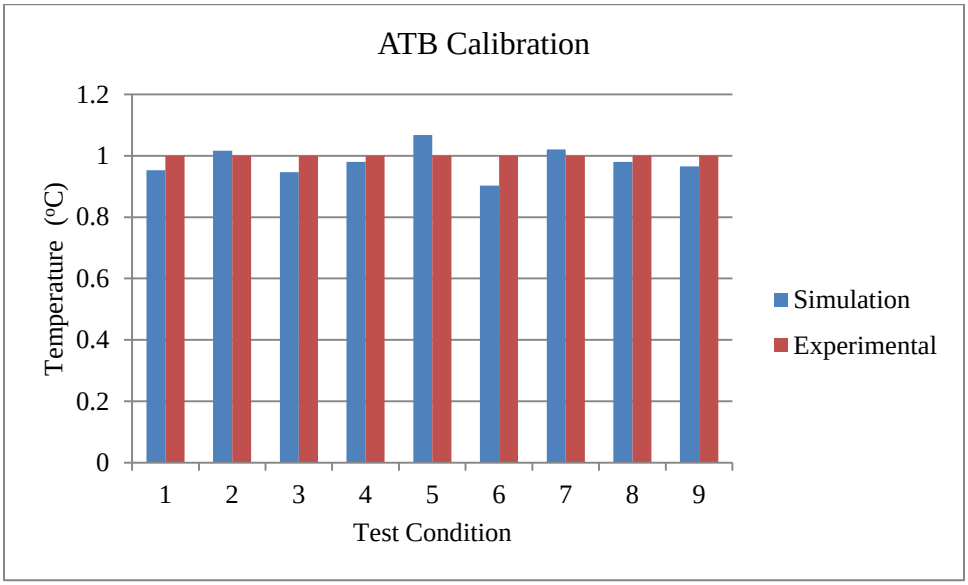

Figure 2.20: ATB Calibration Results

The NEDC test calibration results for the HTR outlet are shown in Figure 2.21. The HTR outlet temperature experimental data had large fluctuations of up to 5°C which were difficult to recreate in the simulation. The fluctuations may be due to the responsiveness of the TSTAT in the experimental vehicle, as the amount of area opening fluctuated. The fluctuations may also be caused by an instrumentation error when measuring the coolant temperature.

There was also a divergence between the experimental temperature and the simulation temperature, during the last 100s of the simulation, of up to 7°C. This could have been because the airflow rate at higher vehicle speeds was under predicted by the underhood cooling airflow model, or the amount of heat transfer from the LTR was over predicted causing the HTR incoming air temperature to be too high.

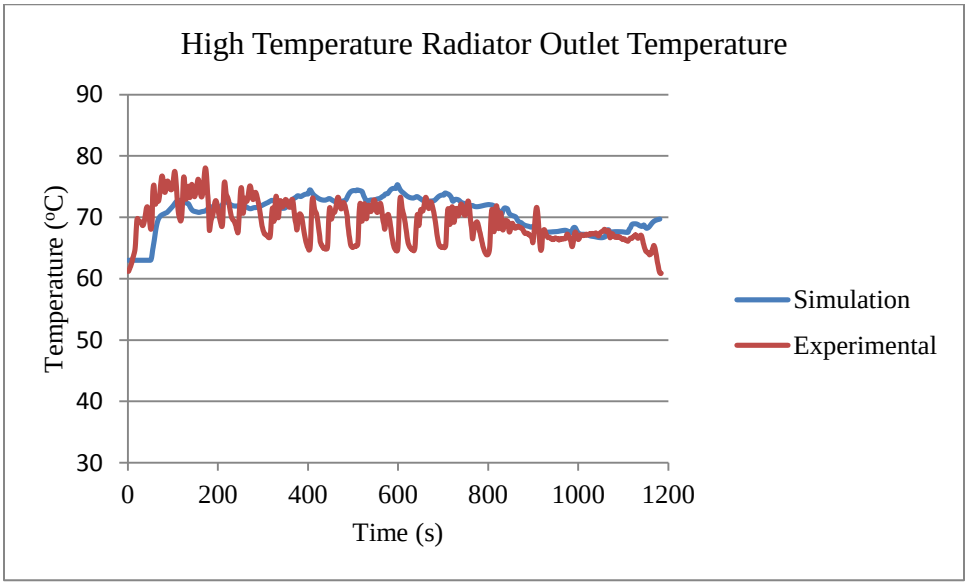

Figure 2.21: High Temperature Radiator Coolant Outlet Temperature

The results for the HTR inlet temperature are shown in Figure 2.22. There was a good correlation between the experimental and simulation results. The difference between the simulation and experimental temperatures never exceeded 3℃, until the last 100 seconds of the cycle. The last 100 seconds of the test was when there was a large variation in the HTR outlet temperature. If the simulation coolant outlet temperature was too high, then it could be expected that the inlet temperature of the coolant would be too high as well.

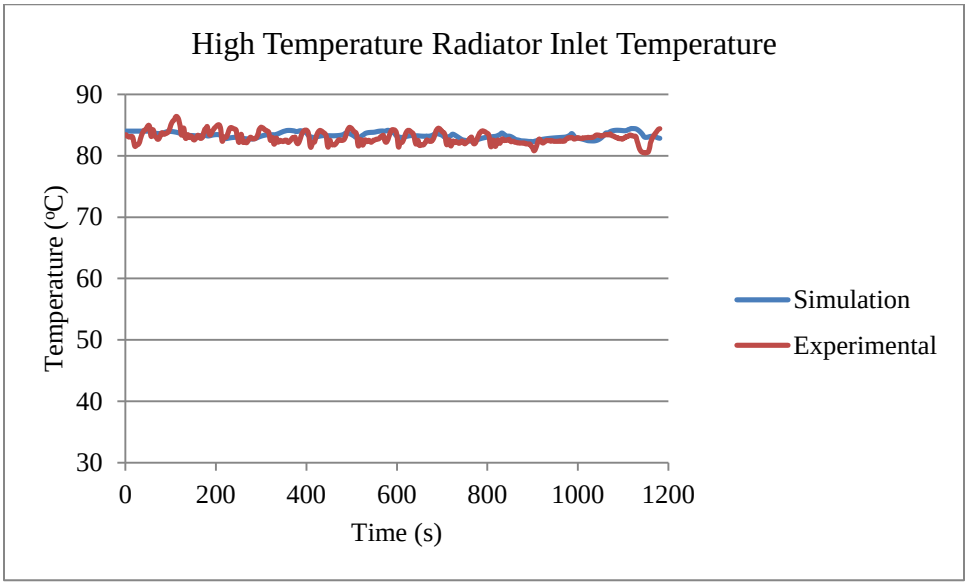

Figure 2.22: High Temperature Radiator Inlet Temperature

The LTR inlet temperature is shown in Figure 2.23. The temperature difference between the simulation and experimental results was below 3°C until the last 100 seconds of the cycle, where the simulation temperature is about 4°C lower than the experimental temperature. This could have been because the heat rejection from the LTR at higher vehicle speeds was over predicted.

The LTR outlet temperature is shown in Figure 2.24. The calibration was at a constant temperature difference of 4°C between the simulation and the experimental results. This was acceptable because the temperature difference was constant throughout the simulation. This was probably because the LTR bench test was performed at uniform airflow test conditions. The front grill and the bumper in the actual vehicle make the airflow non-uniform and decrease the heat exchange performance. The effect of the front grill and bumper on the LTR heat exchange may be greater than on the HTR because the LTR was closer to the front grill and bumper.

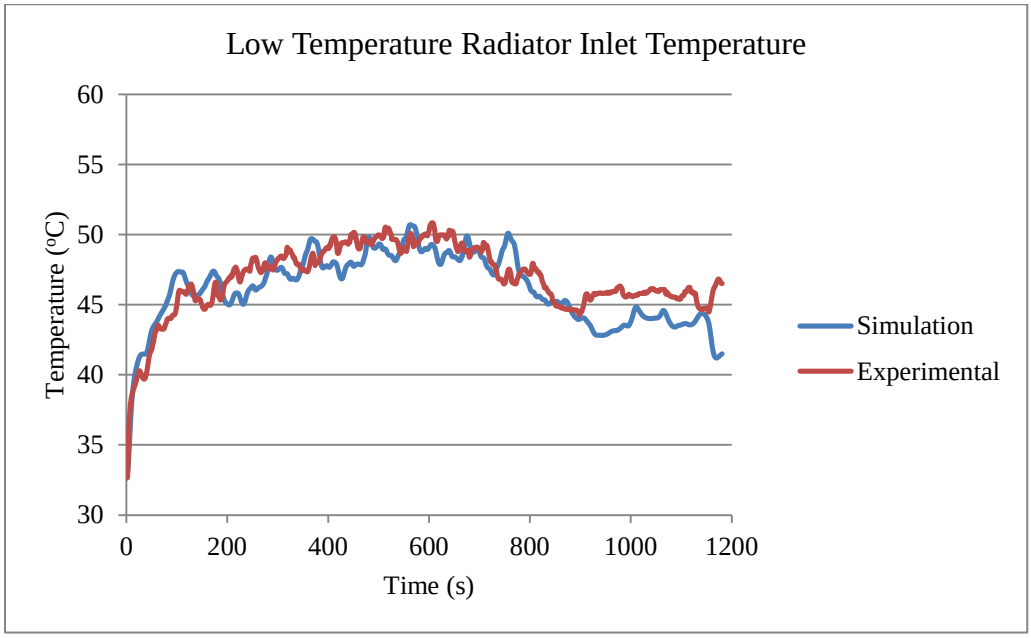

Figure 2.23: Low Temperature Radiator Inlet Temperature

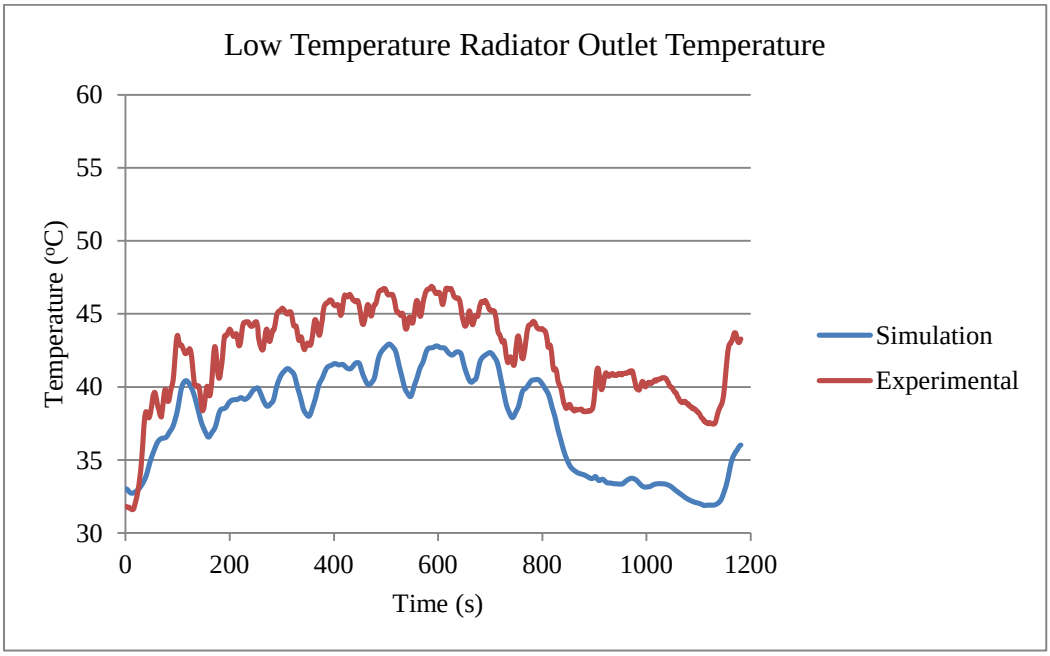

Figure 2.24: Low Temperature Radiator Outlet Temperature

2.10 Model Assumptions

In the construction and calibration of the model, several assumptions were made because experimental data was not available and to simplify the model.

1) The bench test data for the heat exchangers and the cooling fan were performed out of the vehicle, at ideal conditions with a constant and uniform airflow. In the actual vehicle, the airflow through the heat exchangers and cooling fan is non-uniform because the bumper and front grill geometry disrupt the airflow. The non-uniform airflow lowers the heat transfer capabilities of the heat exchangers compared to the heat transfer measured in the bench test. To compensate for the non-uniform flow, a non-uniformity factor of 10% was selected as is common practice within Fiat. In the simulation model, the non-uniformity factor decreased the airflow rate entering the vehicle by 10%, which reduced the heat transfer of the heat exchangers to match the in-vehicle performance.
2) The engine block and cylinder heads were assumed to be a single lumped mass with a constant temperature throughout the mass. In actuality, the engine block and cylinder head vary in temperature from each other however there was no experimental data on the engine temperature distribution. The coolant through the engine was also assumed to be a lumped volume with a constant temperature throughout the volume however the actual coolant temperature varies depending on where it is in the engine. Usually, the coolant flows around the engine block first, which is at a lower temperature, and then around the cylinder heads which are at a higher temperature. This coolant flow path through the engine promotes greater heat transfer to the coolant. Due to these assumptions, the transient

performance of the model was decreased because the temperature of the engine coolant was an average of the engine block and cylinder heads.

3) The engine and the oil cooler were assumed to be the same component and were represented as a single lumped mass in the model, with a constant temperature throughout the mass. The heat transfer from the engine to the coolant in the model represented the total heat transfer in the actual vehicle from both the oil cooler and the engine. The transient performance of the model was affected because the temperature of the lumped mass was the average between the engine and oil cooler which affects the heat transfer rate.
4) The underhood airflow recirculation through the heat exchangers was assumed to be negligible. The underhood recirculation is caused by air pressure buildup in the underhood compartment when the air is unable to exit. The effect is greater at lower vehicle speeds because the air pressure underneath the vehicle is higher which prevents the air from exiting underneath the vehicle. The effect is most common in larger vehicles such as trucks. The Fiat Punto is a passenger car, therefore it was assumed that the vehicle will have the proper seals and venting of underhood air to neglect the recirculation effect. These assumptions lead to greater heat transfer in the simulation because the recirculation air temperature was higher than the ambient air temperature because it had already travelled through the heat exchangers.
5) The fan bench test was only performed at the maximum fan operating speed. To predict the fan performance at lower fan operating speeds, the fan affinity laws were used and assumed to predict the fan performance at any operating speed.

6) The TSTAT hysteresis and pressure drop through the hoses were assumed from calibration by correlating experimental data with simulation data.
7) The engine pressure coefficient (K_{eng}) and the front grill pressure coefficient (K_{grill}) in the underhood cooling airflow model were assumed to remain constant when the front-end heat exchangers were changed. The front grill pressure coefficient would change with the system resistance because the air speed through the system would change. This was not taken into account in the model because the front grill coefficient was calculated using only the vehicle speed, which assumed the ram air pressure was the same for all the VTMS setups. The engine pressure coefficient would change depending on the VTMS setup because the distance between the engine and the heat exchangers changes.

2.11 Single Module Design

Once the dual loop setup model was properly calibrated, the calibrated model was used to design the single module setup model. To create the model, the HTR and LTR radiators were changed to a single module radiator. The system layout of the coolant side remained the same as it was in the dual loop setup, as shown previously in Figure 2.1. The airflow path changed in the single module setup as shown in Figure 2.25. The change to a single module radiator affected the airflow rate through the underhood compartment because the airflow system resistance changed. The airflow rates at different fan activation levels and vehicle speeds were determined using the underhood cooling airflow model that was used to determine the dual loop airflow rates. The coolant flow was also affected because each radiator had a smaller coolant volume than it did in the

dual loop setup, which changes the pressure drop of the coolant as it flows through the radiators.

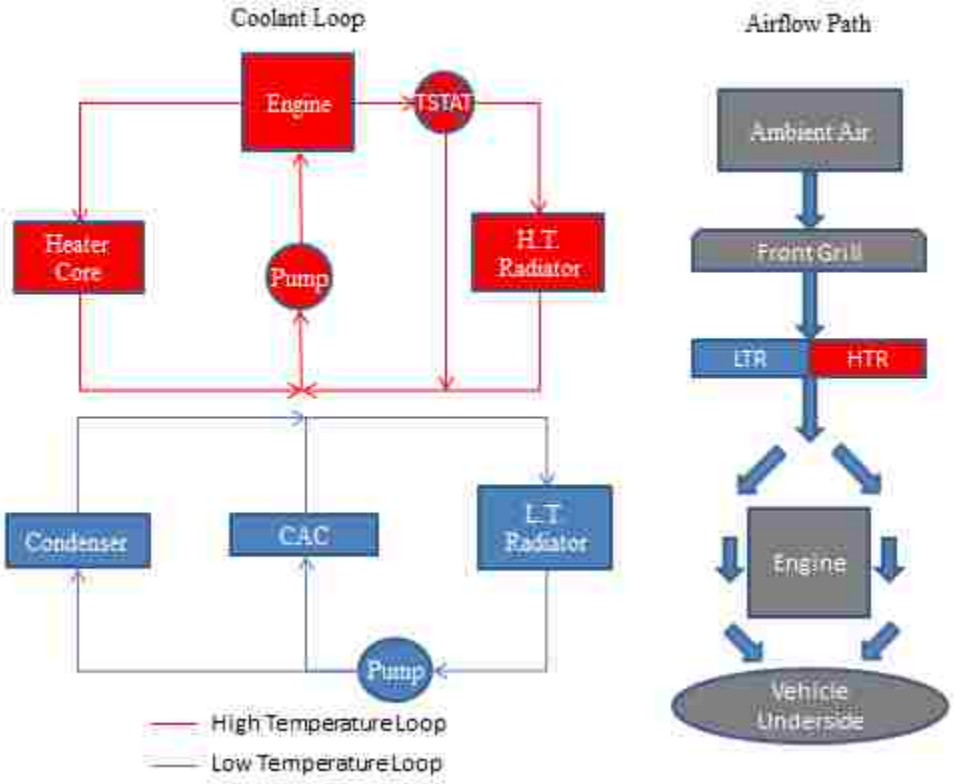

Figure 2.25: Single Module Model Basic System Layout

The single module's frontal area was divided between the HTR and the LTR and was arranged as shown in Figure 2.26. The HTR portion was placed above the LTR portion to prevent the bumper from completely blocking the HTR in an actual vehicle. The coolant flow arrangement remained horizontal. It was assumed there was negligible heat transfer through the connection between the HT and LT radiators occurs.

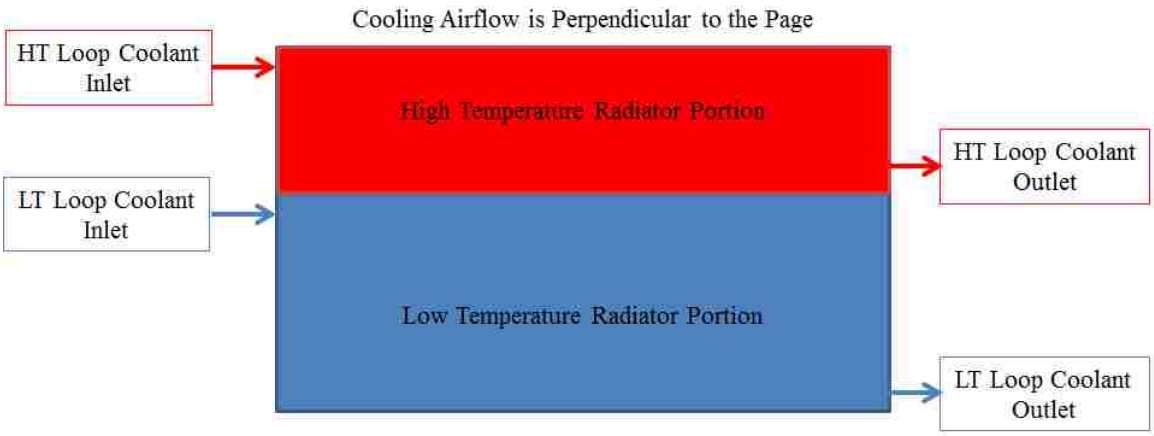

Figure 2.26: Single Module Radiator Arrangement

The size of the single module was constrained by the vehicle front-end geometry. The height was constrained by the hood profile and the width was constrained by the vehicle width. The maximum total possible frontal area of a front-end heat exchanger in the Fiat Punto was 400 mm x 720 mm. The single module radiator frontal area was made as large as possible (400 mm x 720 mm) in order to maximize the heat transfer capacity. The frontal areas of the LTR and HTR were both 395 mm x 620 mm in the dual loop setup, which combined was 489800 mm^2. The frontal area in the single module setup was 288000 mm^2, which is 41% less frontal area than in the dual loop setup. The frontal area of the single module radiator was divided between the LTR and HTR to give the best overall performance between the radiators. The best overall performance was determined by comparing the radiator outlet temperatures determined from simulation of the dual loop setup and the single module setup.

There was no prototype of the single module radiator available however the single module radiator in the simulation model had the same design as the LTR. The LTR bench test data was used to calibrate the heat transfer coefficients of the single module radiator.

The heat transfer measured in the LTR bench test data was modified to include the increase in frontal area of the single module. The thickness of the single module radiator was the same as the LTR. The difference in heat transfer between the LTR and single module radiator was only a function of the frontal area of each heat exchanger. The heat transfer data was assumed to be scalable to account for the change in frontal area using Equation 2.19:

$$\dot{Q}_{SM} = \dot{Q}_{LTR}\left(\frac{A_{SM}}{A_{LTR}}\right) \tag{2.19}$$

The single module system requirement was to match the performance of the dual loop system while using less power to operate the fan and the compressor. The single module system performance parameters that had to be the same as the dual loop setup throughout the NEDC test include the engine temperature and the heat transfer from the HTR, LTR and condenser.

The engine temperature had to be maintained around 83^{o}C. The engine temperature should not be lower in order to maintain a lower oil viscosity to decrease the mechanical loss due to friction. The engine temperature should not be greater than 83^{o}C to maintain ideal conditions for combustion and reduce the thermal wear on the engine. The condenser heat transfer must be maintained in order to maintain the performance of the A/C system. To maintain the engine temperature the HTR heat transfer to the cooling air must be maintained from the dual loop setup. To maintain the condenser heat transfer performance the heat transfer from the LTR must be the same as it was in the dual loop setup.

The single module radiator had to also have enough cooling capacity to meet or exceed the ATB test performance standards. The average heat exchange demand from the HTR and LTR throughout the NEDC test and the average engine temperature are shown in Table 2.10.

Table 2.10: Average Heat Exchanger Demand During NEDC Test

Heat Exchanger	Average NEDC Test Results
High Temperature Radiator	6930 W
Low Temperature Radiator	4680 W
Engine Temperature	83.2 ^{o}C

2.12 Simulation Runs

The following simulations were performed in order to determine the amount of vehicle power that was saved by switching the VTMS setup to a single module radiator setup in a Fiat Punto with a 1.4L 4 cylinder spark ignition engine.

1) An underhood cooling airflow model simulation for the single module radiator setup was needed to have accurate airflow data for the single module model. The simulation results showed the improvement in airflow rate over the dual loop setup by switching to a single module radiator.
2) Several simulations with different area divisions of the single module between the HTR and the LTR were needed to determine the best area division. The ATB and NEDC simulations were performed with the different radiators shown in Table 2.11. The results from the simulations of the different radiators were compared to

each other to determine which single module radiator had the best overall performance.

Table 2.11: Single Module Radiator Division

Name	Division	LTR Area (mm^2)	HTR Area (mm^2)
Radiator A	50 % LT 50% HT	144000	144000
Radiator B	60 % LT 40% HT	172800	115200
Radiator C	70 % LT 30% HT	201600	86400
Radiator D	80% LT 20% HT	230400	57600

3) Once the best single module radiator was chosen for the system, the NEDC test simulation was performed at a lower fan activation level. The fan activation is the amount of power supplied to the fan. It is measured as a percentage of the maximum power that can be supplied to the fan, which determines the rotational speed of the fan. The relationship between the fan activation level and the fan rotational speed is shown in Figure 2.27.

   The fan activation was lowered to determine the potential fan power which can be saved. The fan activation was lowered to match the single module simulation performance results to the dual loop model. The fan activation results from the dual loop prototype NEDC experimental test are shown in Figure 2.28. The average fan power consumption in the dual loop setup for the NEDC experimental test was 341W.

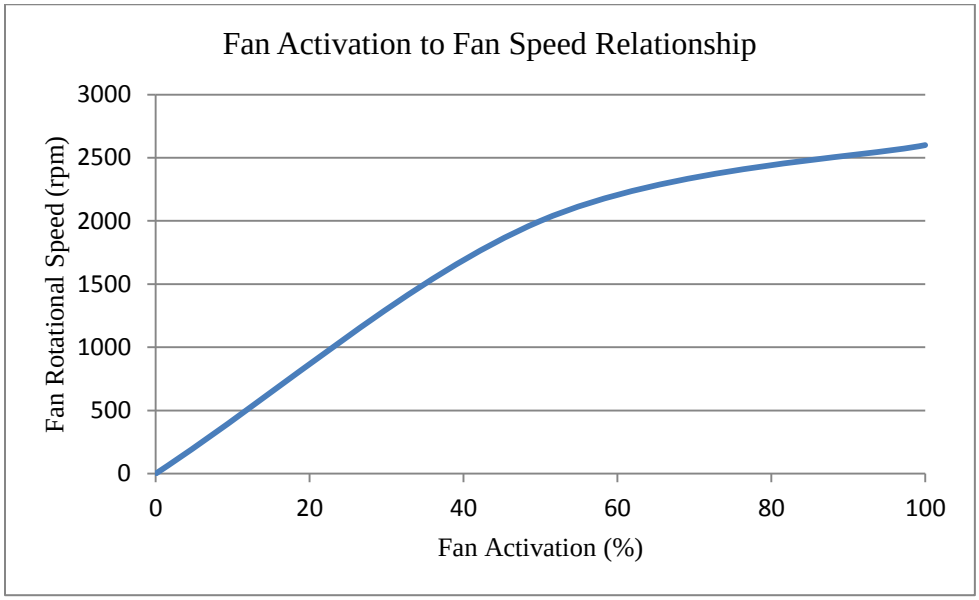

Figure 2.27: Relationship between Fan Activation and Fan Speed

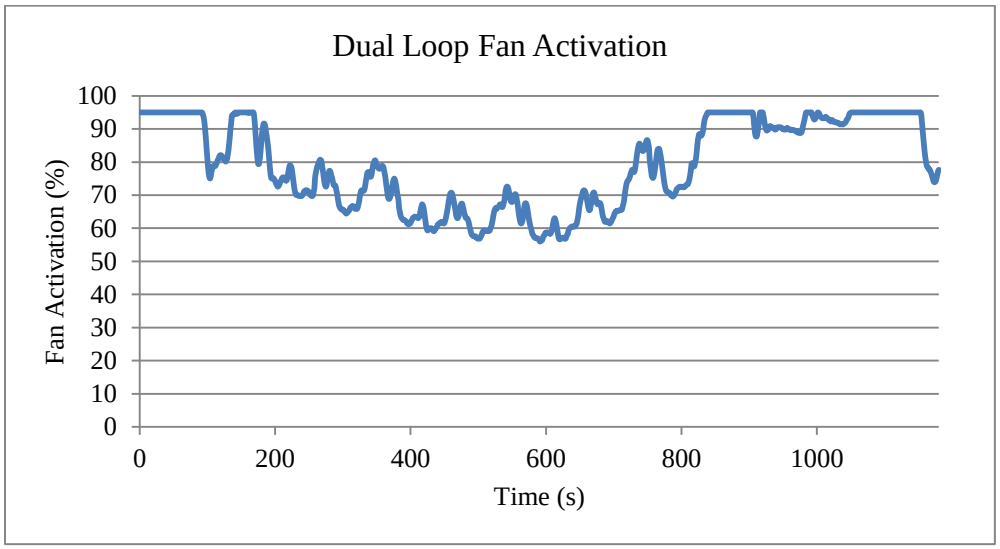

Figure 2.28: NEDC Dual Loop Fan Activation Results

4) The NEDC test was again performed on the single module radiator setup to determine the power savings of lowering the condenser inlet pressure of the condenser refrigerant side while maintaining the dual loop setup fan activation and system performance. The compressor model was used to determine the power consumed by the compressor to provide the lower refrigerant pressure.

5) The final simulation was to determine the combinations of compressor and fan activation that provided the greatest power saving.

CHAPTER 3: ANALYSIS OF RESULTS

3.1 Single Module Underhood Airflow Results

The underhood cooling airflow model for the single module radiator was constructed using the same model setup as the underhood airflow model used to find the dual loop setup flow rates. The cooling fan, the engine pressure coefficient and front grill pressure coefficient were the same for the single module setup. The single module setup had an improved system resistance compared to the dual loop setup, as shown in Figure 3.1. The system resistance was decreased by an average of 35% across all the airflow speeds. The decrease in the system resistance was caused by the removal of a heat exchanger.

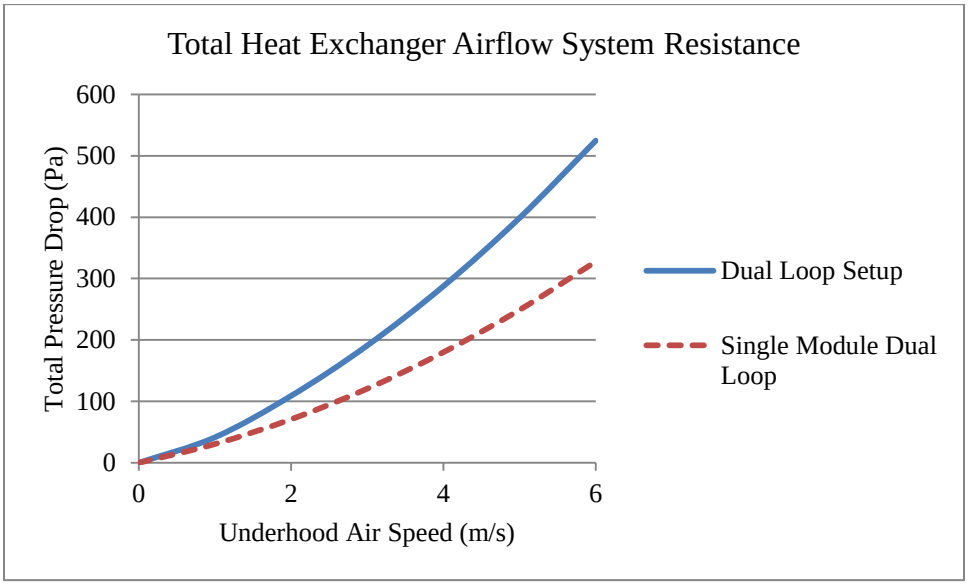

Figure 3.1: Airflow System Resistance Comparison

The underhood airflow rate results for the single module setup were greater than the dual loop setup, which is shown in Figure 3.2, 3.3 and 3.4. The underhood airflow rate for the single module setup was on average 64% greater than the dual loop setup and 42% greater than the standard setup airflow rates.

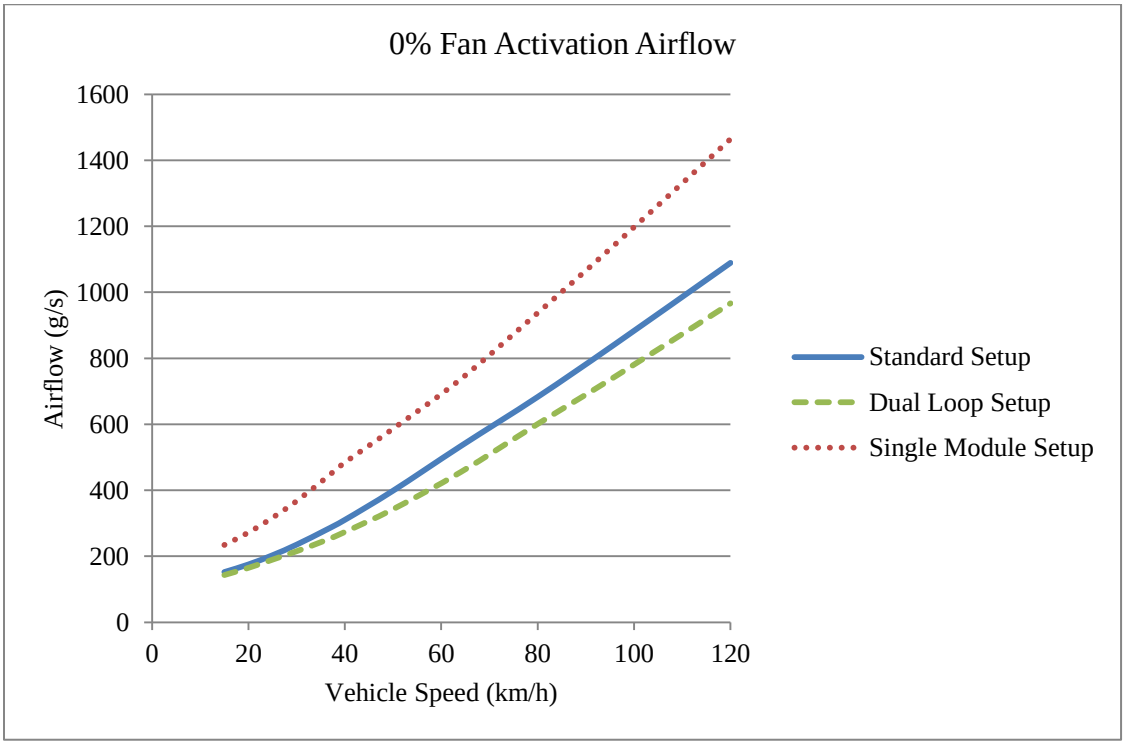

Figure 3.2: 0% Fan Activation Airflow Comparison

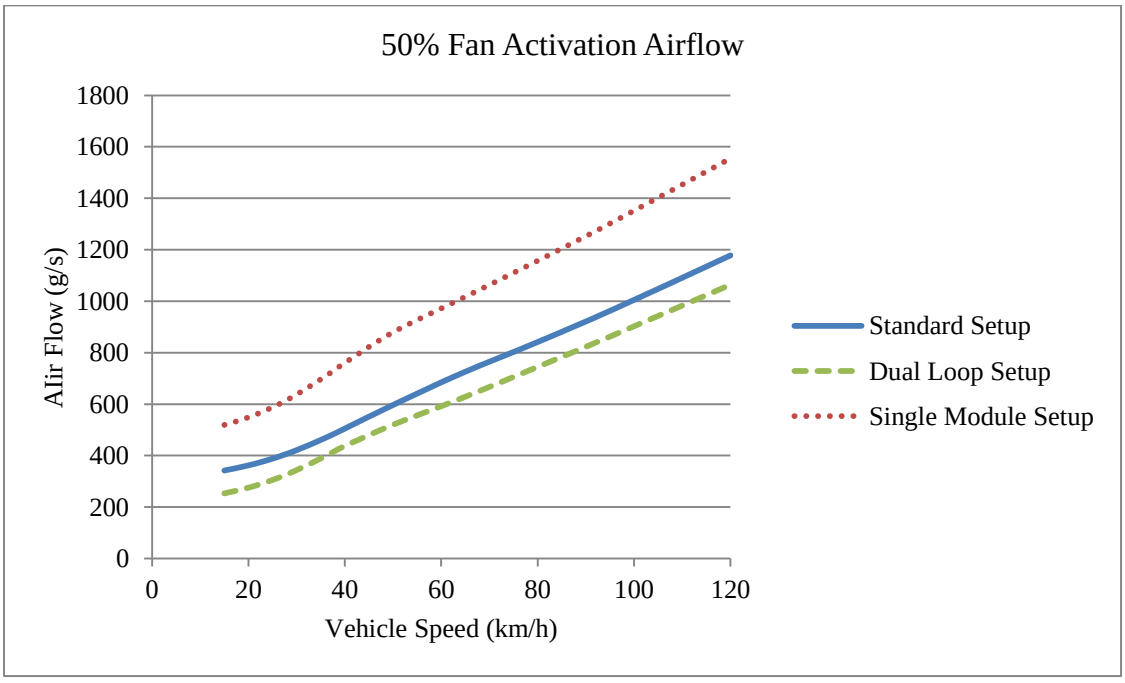

Figure 3.3: 50% Fan Activation Airflow Comparison

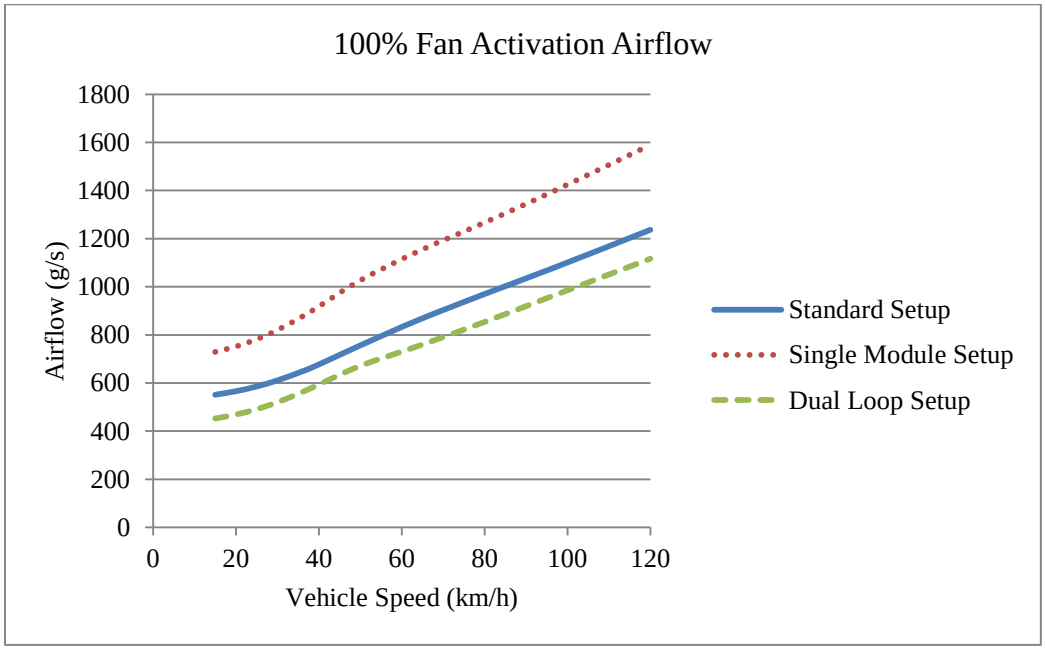

Figure 3.4: 100% Fan Activation Comparison

The airflow rate increases because the system resistance was decreased by switching to the single module setup. At the same vehicle speed and fan activation level, both the dual loop and single module setups operate between the same pressure difference because the inlet and outlet pressures were independent of the VTMS setup. The inlet pressure would change slightly when the underhood arrangement was changed but was assumed to be constant, and the outlet pressure was the pressure of the air under the vehicle, which was a function of the vehicle shape only. From Figure 3.1, the single module setup achieved larger airflow rates at the same pressure difference as the dual loop setup.

3.2 Area Division of Single Module

The frontal area of the single module was divided between the LTR and HTR to give equal performance based on the outlet temperatures of the radiators. The outlet temperatures of the radiators in the dual loop setup were compared to the single module

outlet radiator temperatures to determine what area division gave the best overall performance. The single module radiator designs listed in Table 2.12 were simulated using the NEDC test to determine their performance in the system. The fan activation level was not changed for these simulations.

The results of the LTR and HTR performance for Radiator A, which had a LTR occupying 50% and a HTR occupying 50% of the total frontal area are shown in Figure 3.5 and Figure 3.6 respectively. The Radiator A LTR outlet temperature was on average about 2^{o}C greater than the LTR in the dual loop setup simulation results. The fan activation level would have had to be increased to increase the airflow rate in order to decrease the Radiator A LTR outlet temperature. The LTR radiator frontal area had to be increased to prevent the need for increasing the fan activation level because this would increases the power consumption. The Radiator A HTR had an outlet temperature on average 10^{o}C below the dual loop HTR, indicating it had a larger cooling capacity than needed. The HTR area was reduced in order to increase the area of the LTR.

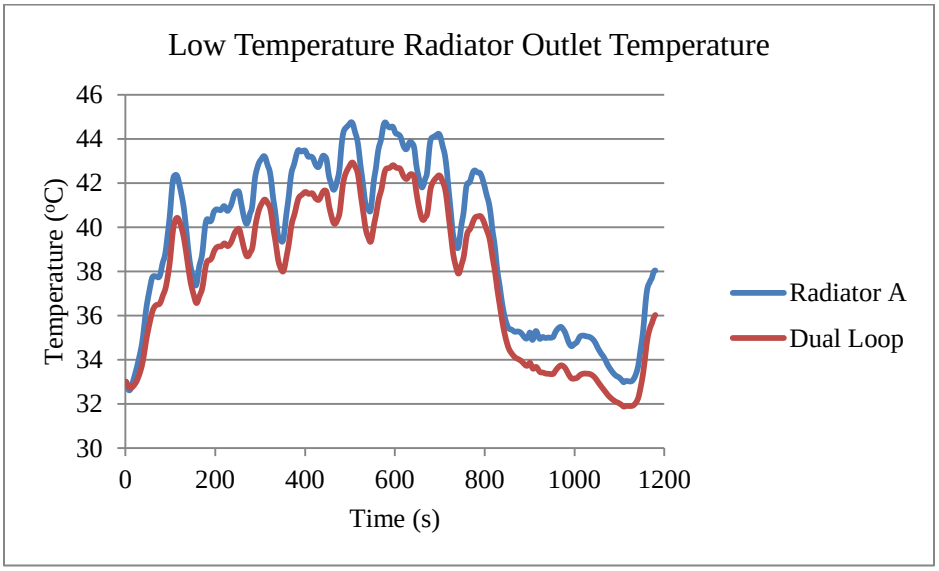

Figure 3.5: Radiator A LTR Temperature Outlet Comparison

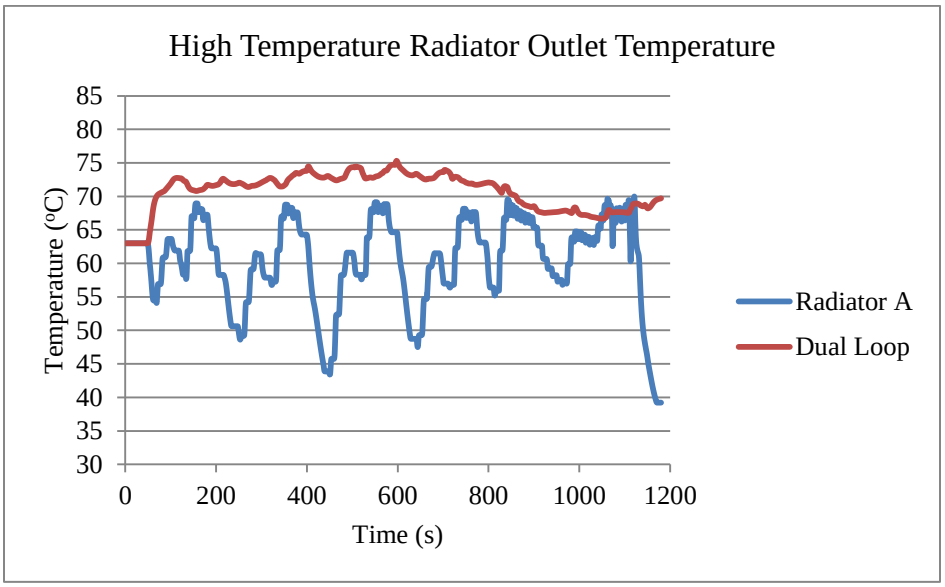

Figure 3.6: Radiator A HTR Temperature Outlet Comparison

The Radiator B LTR frontal area percentage was 60%, which was an increase compared to Radiator A. The LTR outlet and HTR outlet temperature results for Radiator B were shown in Figure 3.7 and Figure 3.8 respectively. The LTR outlet temperature of Radiator B was higher than the dual loop simulation LTR outlet temperature by 0.5°C. The Radiator B HTR was still over performing with an average temperature difference of 15°C compared to the dual loop setup. This was a larger temperature difference than the Radiator A HTR because the TSTAT was open more frequently in the Radiator B setup due to its lower cooling capacity. The HTR frontal area could be reduced and the area of the LTR increased in order to decrease the fan activation level.

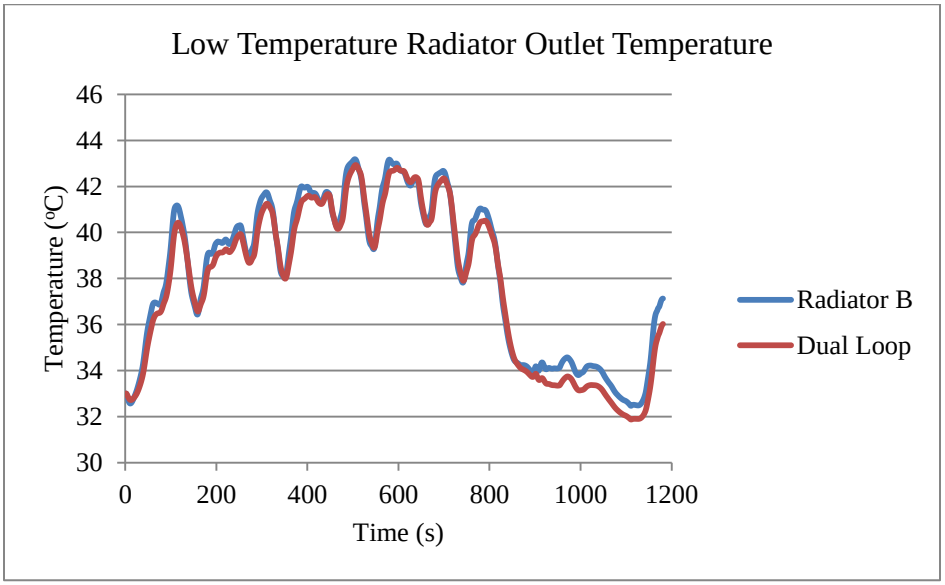

Figure 3.7: Radiator B LTR Outlet Temperature Comparison

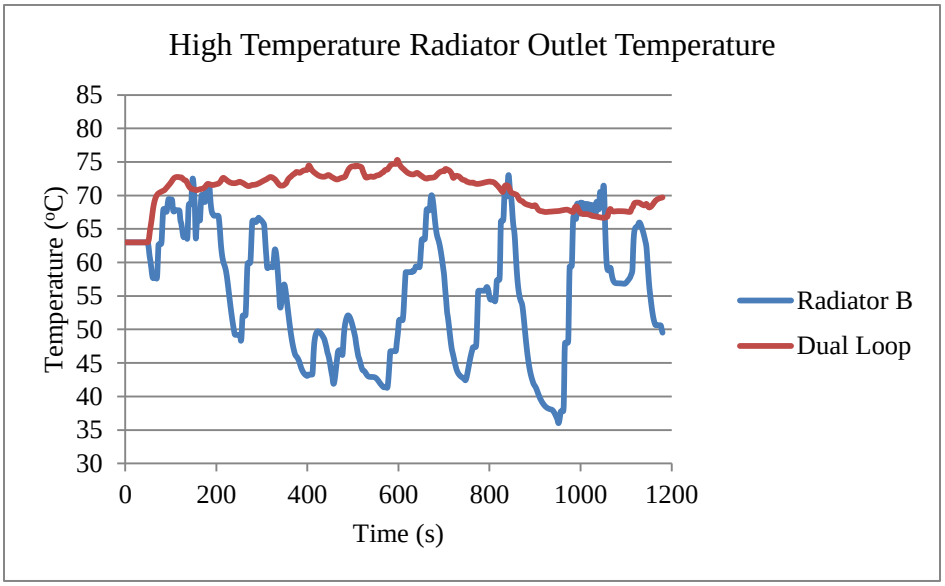

Figure 3.8: Radiator B HTR Outlet Temperature Comparison

The Radiator C area of the LTR was increased to 70% of the frontal area and the HTR decreased to 30%. The results of the simulation were shown in Figure 3.9 and 3.10. The Radiator C HTR outperformed the dual loop setup HTR, with an outlet temperature

lower than the dual loop setup by 11°C on average. However, at some instances during the simulation, the outlet temperature of the Radiator C HTR was greater than the dual loop setup. This was because of TSTAT cycling which did not occur in the dual loop simulation. There were parts of the simulation where the Radiator C HTR outlet temperature was lower than the Radiator B HTR outlet temperature because of TSTAT cycling. Radiator C did not cool the coolant down past the TSTAT closing temperature of 82°C as often as Radiator B, which maintained a constant coolant flow rate through the radiator. The LTR performance was better than the dual loop setup LTR, with an average temperature of 1.5°C below the dual loop setup temperature, which would allow for a decrease in fan activation.

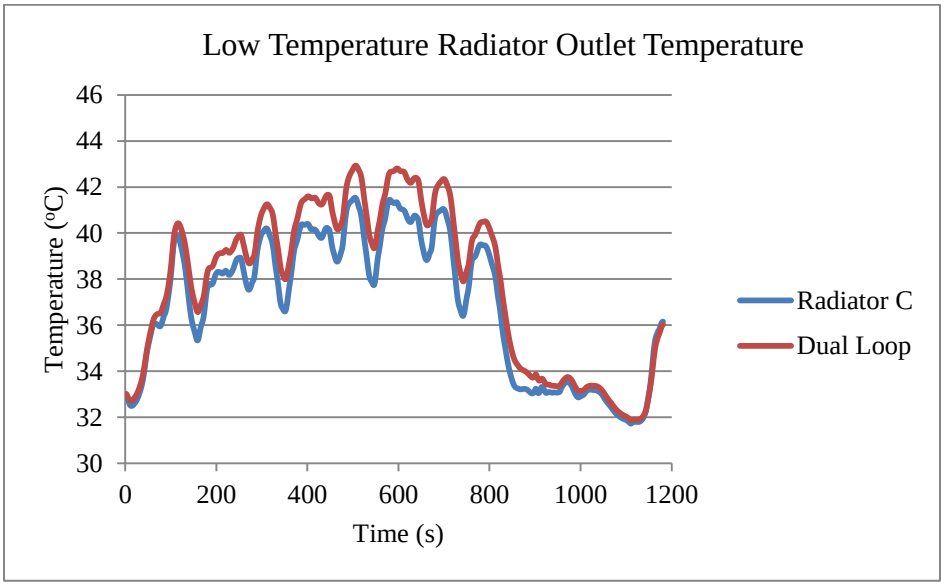

Figure 3.9: Radiator C LTR Outlet Temperature Comparison

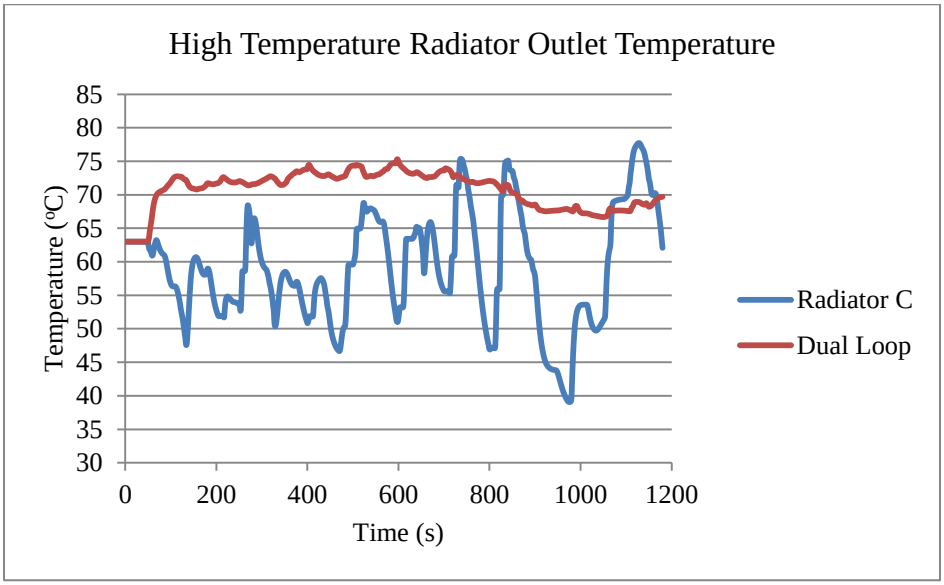

Figure 3.10: Radiator C HTR Outlet Temperature Comparison

The Radiator D HTR frontal area percentage was reduced to 20%. The Radiator D LTR and HTR outlet temperatures are shown in Figure 3.11 and Figure 3.12 respectively. The Radiator D HTR was undersized and did not outperform the dual loop HTR. It had an average outlet temperature of 3°C higher than the dual loop HTR. The HTR could not be smaller than 20% of the frontal area or it would not be able to transfer enough heat to meet the NEDC test system demands and reduce the fan activation level.

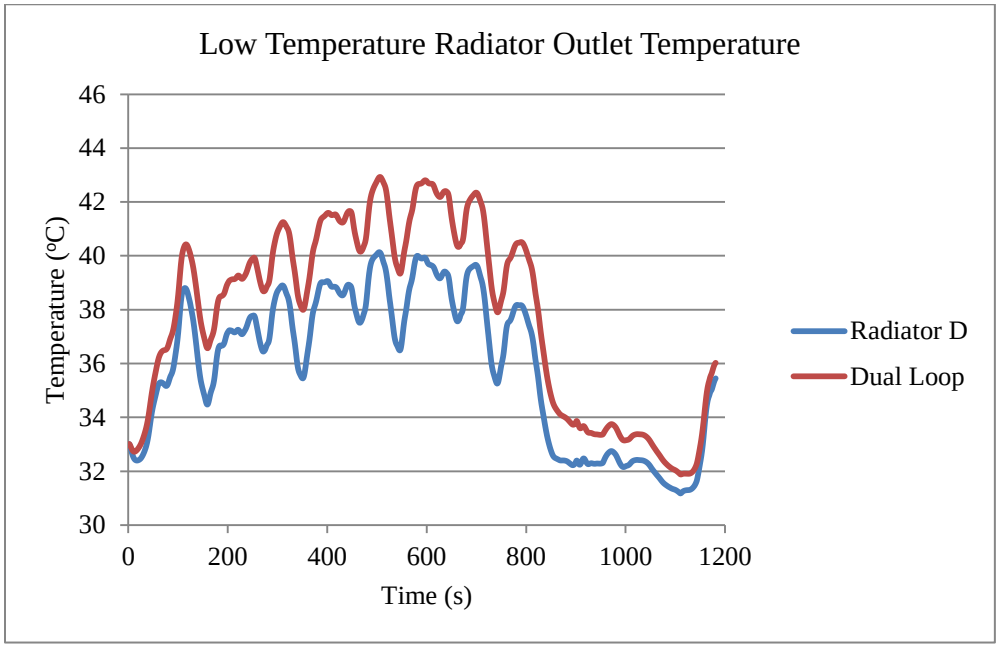

Figure 3.11: Radiator D LTR Outlet Temperature Comparison

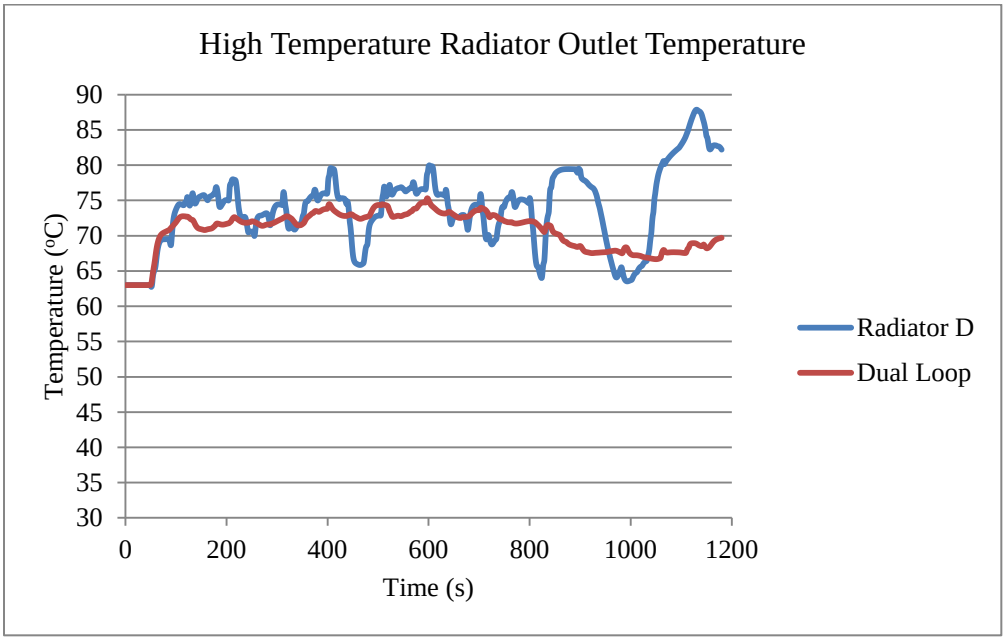

Figure 3.12: Radiator D HTR Outlet Temperature Comparison

The radiator selected for the system was Radiator C. The Radiator C LTR gave the largest outlet temperature difference compared to the dual loop setup while

maintaining the HTR outlet temperature at a level which would allow for a decrease in fan activation. To ensure that the Radiator C HTR had enough cooling capacity, at the operating conditions which put the greatest demand on the system, the ATB test was simulated on Radiator C. The results of the ATB test simulation compared to the standard dual loop ATB test simulation results are shown in Figure 3.13. The HTR portion of Radiator C had a lower cooling capacity than the standard dual loop setup HTR. However, the Radiator C ATB temperature at each test condition was above the ATB temperature limit of 50^{o}C, which indicates acceptable performance.

A single module radiator with an LTR occupying 75% of the frontal area and an HTR occupying 25% was also simulated. The HTR did not have a large enough capacity to meet the ATB test standards. This indicates that the HTR must be at least 30% of the frontal area to have a large enough cooling capacity.

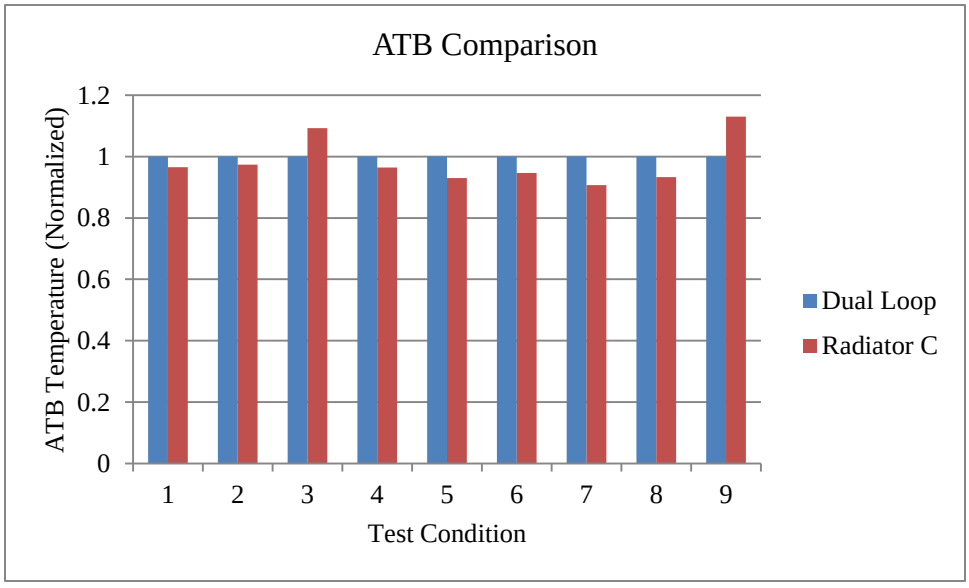

Figure 3.13: ATB Comparison of Single Module

3.3 Fan Activation

The fan activation for the Radiator C single module setup was reduced in order to match the system performance of the dual loop setup, in terms of global heat transfer and outlet temperature of the HTR, LTR and condenser. The compressor power in the refrigeration loop remains unchanged from the dual loop setup.

The improvement in incoming air temperature for the HTR is shown in Figure 3.14. The incoming air temperature into the HTR was on average about 10°C less in the single module setup for the NEDC test. The decrease in the inlet air temperature was because the air was no longer heated by the LTR before entering the HTR. The lower air temperature allowed for the fan activation to be decreased because the heat transfer increases with an increase in the temperature difference rather than requiring a greater airflow rate.

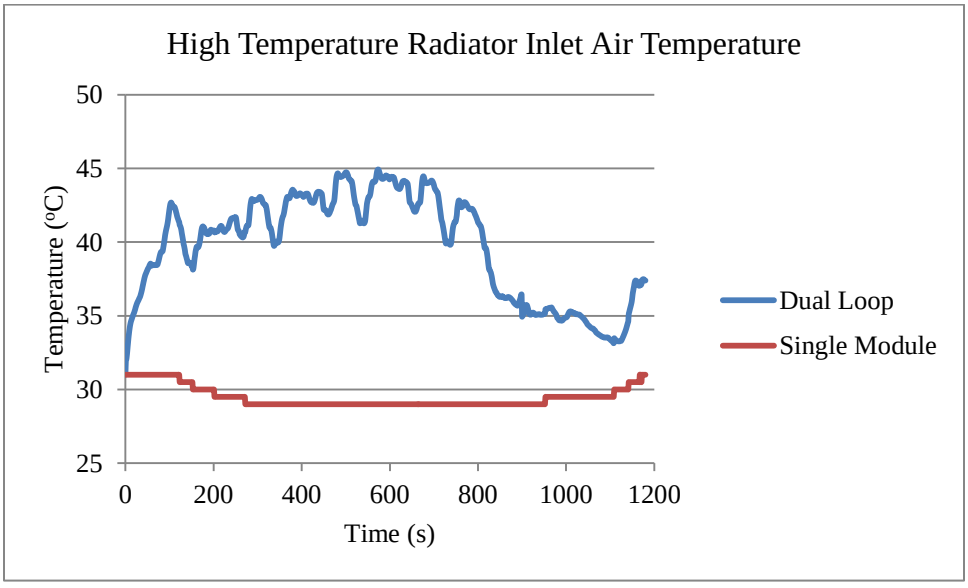

Figure 3.14: High Temperature Radiator Inlet Air Temperature

A comparison between the fan activation for the dual loop setup and the single module setup is shown in Figure 3.15. The single module setup has a lower level of fan

activation because its system resistance was lower and its initial HTR temperature difference was lower than the dual loop setup. The lower system resistance provides a greater airflow rate at the same vehicle speed and fan activation allowing for fan activation to be decreased. The single module setup decreased fan activation by 31%. The average power consumed by the fan in the single module setup was 233.85W compared to 341.1W for the dual loop setup for a total power savings of 107.3W. Fiat recommended assuming a constant alternator efficiency of 60%. If the alternator efficiency was taken into account, then the total power savings were 178.8W.

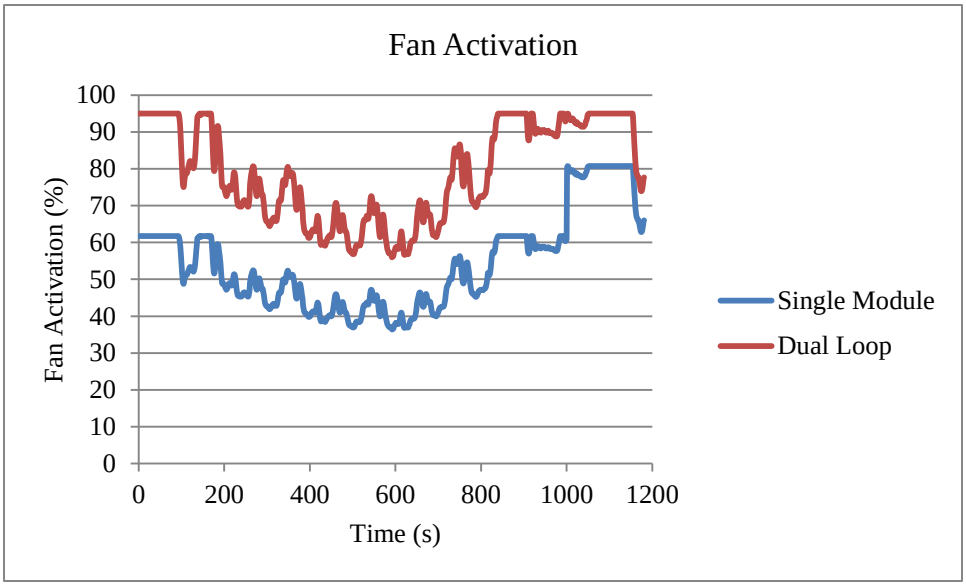

Figure 3.15: Fan Activation Comparison between Single Module and Dual Loop Setup

Despite the lower fan activation, the single module setup had a larger airflow rate during the NEDC test. The comparison between the airflow rates is shown in Figure 3.16. The larger airflow rate was due to the lower system resistance of the single module setup compared to the dual loop setup. To compensate for the reduction in frontal area, the airflow rate must be greater than the dual loop setup to provide the same heat exchange

because of the reduction of frontal area for both radiators. The average airflow rate of the single module setup was about 50% greater than the airflow rate of the dual loop setup.

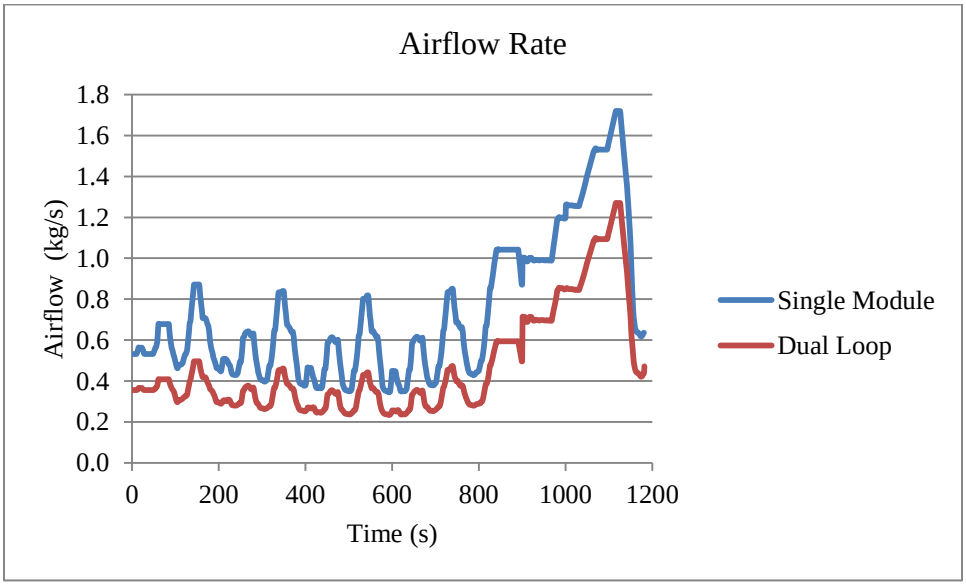

Figure 3.16: Airflow Rate through Heat Exchangers

The performance of the HTR in the single module setup was matched to the dual loop setup using the fan activation shown previously in Figure 3.15. The global heat exchange throughout the entire NEDC test was identical to the dual loop setup despite the 65% reduction of the frontal area of the single module HTR. The increase in initial temperature difference between the air and coolant and the increase in airflow rate allows for equivalent performance. The comparison of the heat transfer between the dual loop and single module HTR performance is shown in Figure 3.17.

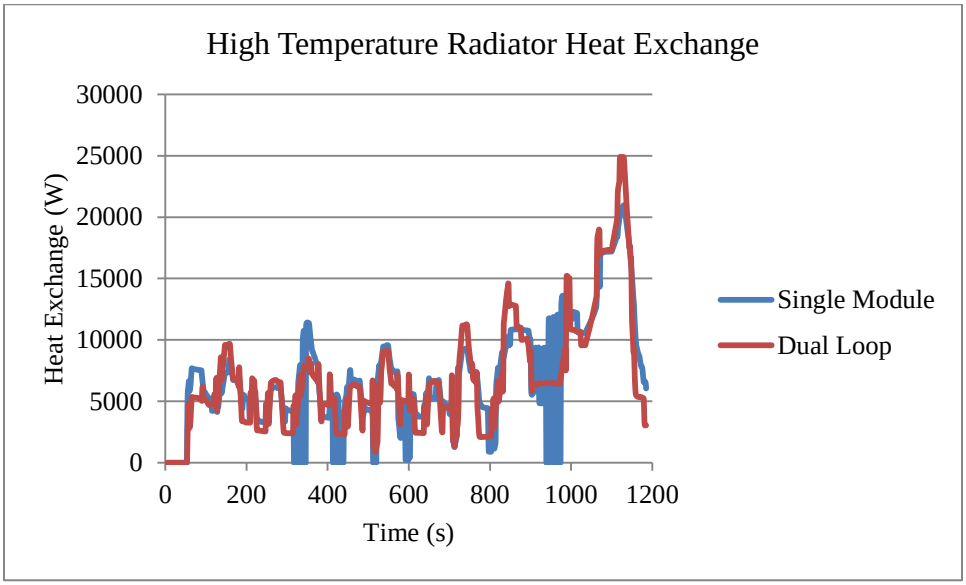

Figure 3.17: HTR Heat Exchange Comparison

The outlet radiator temperature was important to determine if the coolant was at an acceptable temperature. The outlet temperature of the HTR is shown in Figure 3.18. The outlet radiator temperature drops well below that of the dual loop setup because of TSTAT cycling. The TSTAT cycling is evident in Figure 3.19 which shows the coolant flow rate through the HTR of the dual loop and single module setups. The coolant flow rate of the single module setup had large peaks at 343s, 970s and 1120s which corresponded to the outlet temperature peaks.

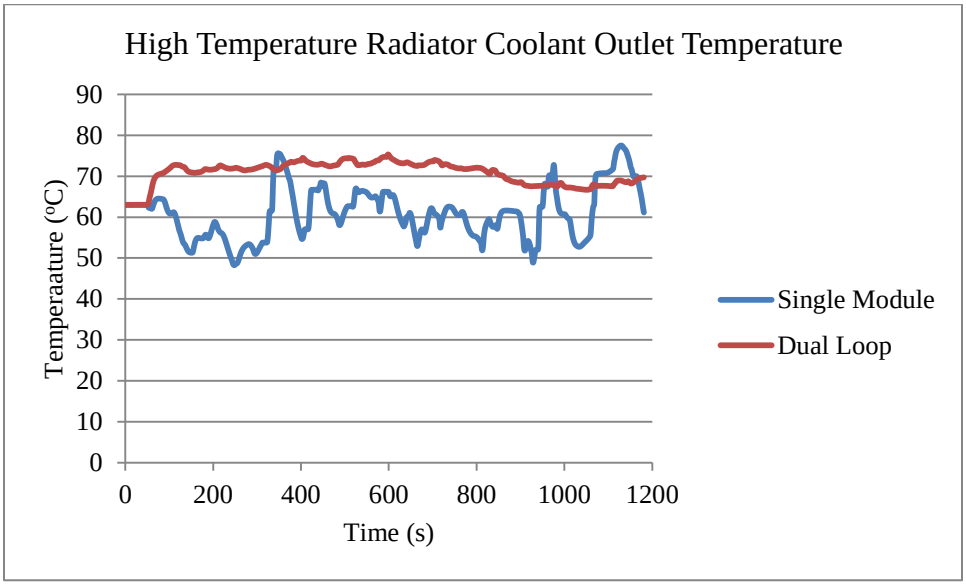

Figure 3.18: High Temperature Radiator Outlet Temperature

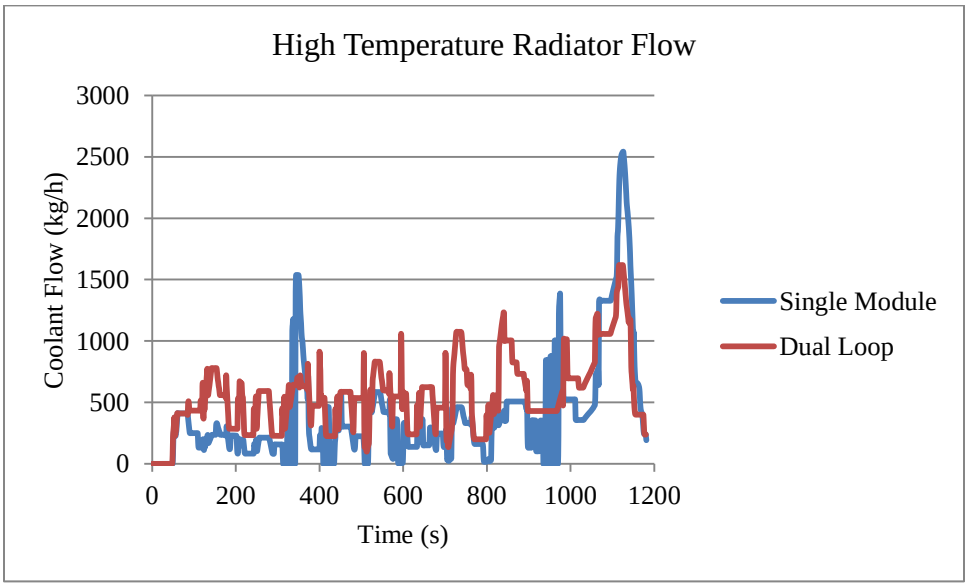

Figure 3.19: HTR Coolant Flow Rate

The engine temperature had to be maintained at a similar temperature to that of the dual loop arrangement for the most efficient performance. The engine outlet temperature is shown in Figure 3.20. The engine temperature of the single module was similar to the engine temperature of the dual loop setup and was only a few degrees

greater than the dual loop setup in the last 100s of the NEDC test. This was still in an acceptable range for the engine temperature.

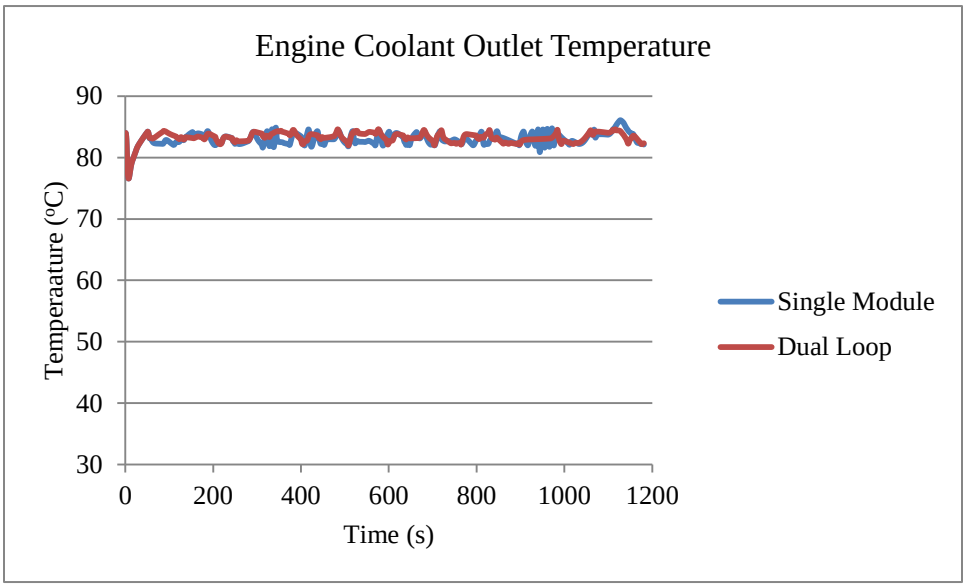

Figure 3.20: Engine Outlet Temperature Comparison

The LTR heat transfer, at the lower fan activation was the same as the dual loop setup, shown in Figure 3.21. The LTR outlet temperature was at the same level as the dual loop setup, shown in Figure 3.22. This indicated that the fan activation level could not be lowered any further without increasing the temperature in the LT loop, which would decrease the condenser heat transfer. The condenser heat transfer, shown in Figure 3.23, could not be lowered any further because it was at the average dual loop condenser heat transfer rate of 3630 W, which was required to maintain the A/C performance.

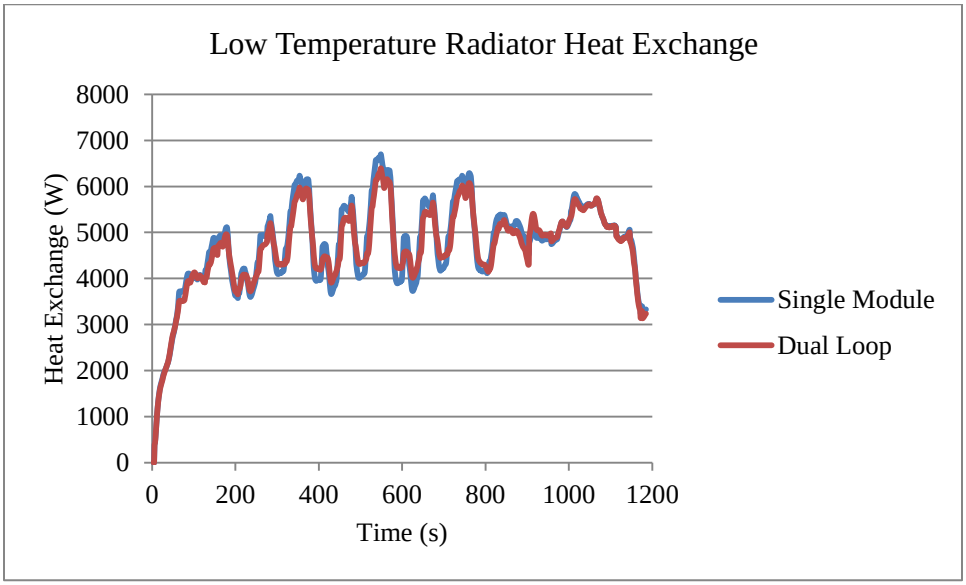

Figure 3.21: LTR Heat Exchange

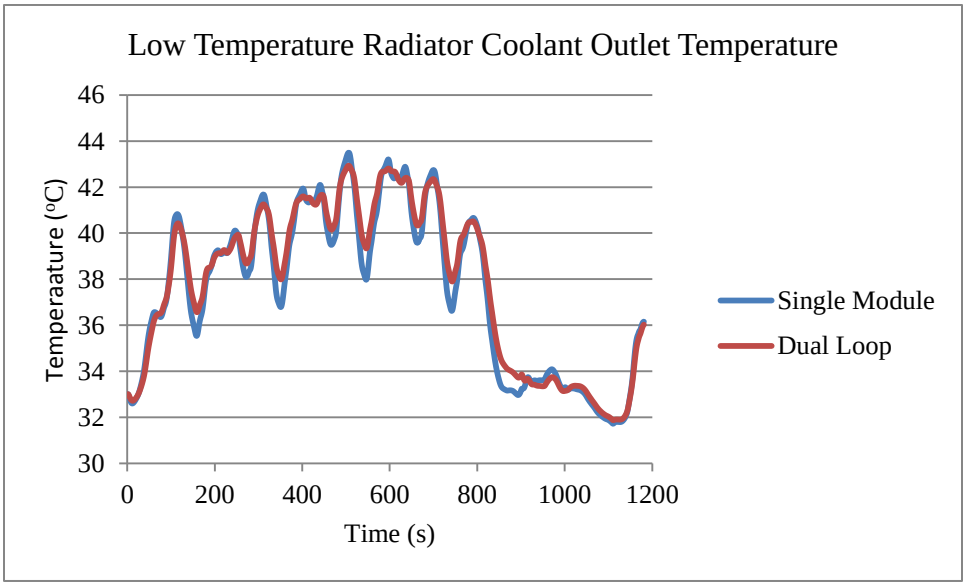

Figure 3.22: LTR Coolant Outlet Temperature

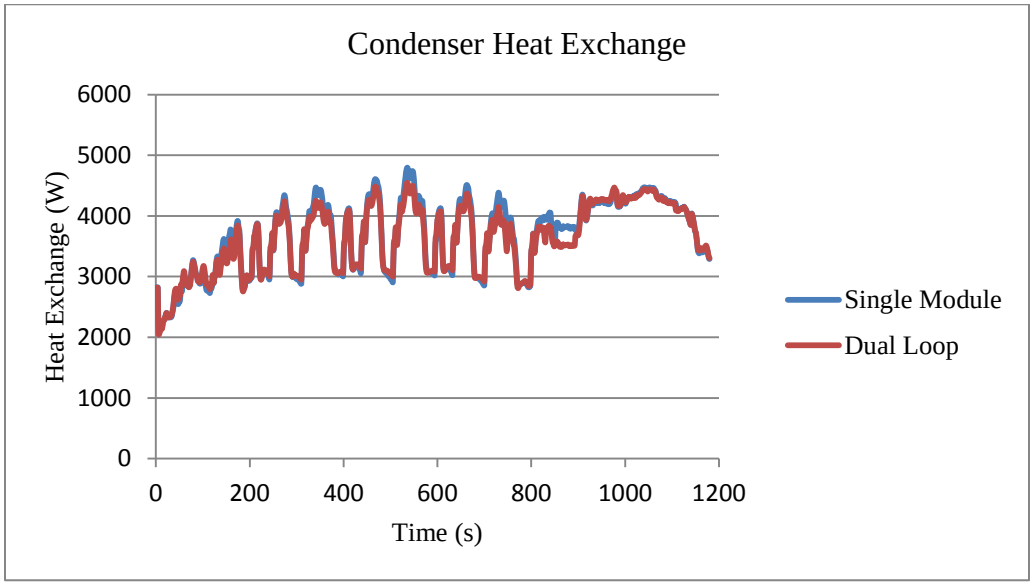

Figure 3.23: Condenser Heat Exchange

3.4 Compressor Power

If the fan activation was maintained at the same level as it was in the dual loop model, then the condenser heat transfer would be greater than in the dual loop model. The condenser heat transfer increases because the LTR outlet temperature will be lower, resulting in a larger temperature difference between the air conditioning refrigerant and the coolant. The increase in condenser heat transfer by maintaining the fan activation is shown in Figure 3.24.

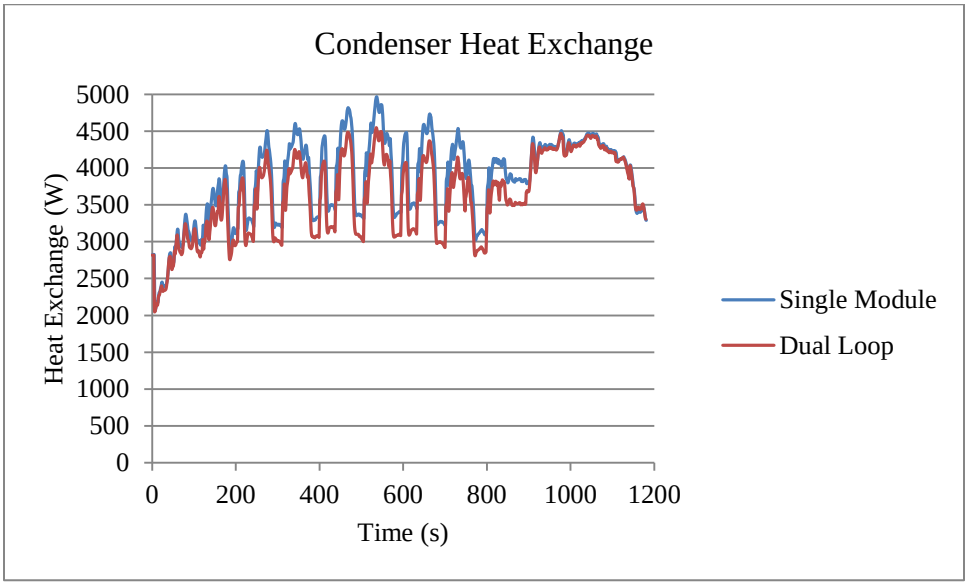

Figure 3.24: Condenser Heat Transfer

There was 6% more condenser heat transfer in the single module setup than in the dual loop setup. The refrigerant inlet temperature of the condenser can be reduced to reduce the amount of heat transfer to the same level as the dual loop setup. The condenser inlet temperature was reduced by reducing the outlet pressure of the compressor, which reduced the power consumed by the compressor.

The condenser heat transfer was reduced to the same level as the dual loop setup by decreasing the compressor outlet pressure by 5%. This decrease in outlet pressure decreased the compressor power by 1.9%, this was found using the compressor simulation model. The average compressor power in the NEDC dual loop test was 2761W, which amounts to a total compressor power savings of 61W. This is the maximum amount of power that the compressor will save by switching to the single loop setup. The decrease in outlet pressure with the compressor power consumption is shown in Figure 3.25.

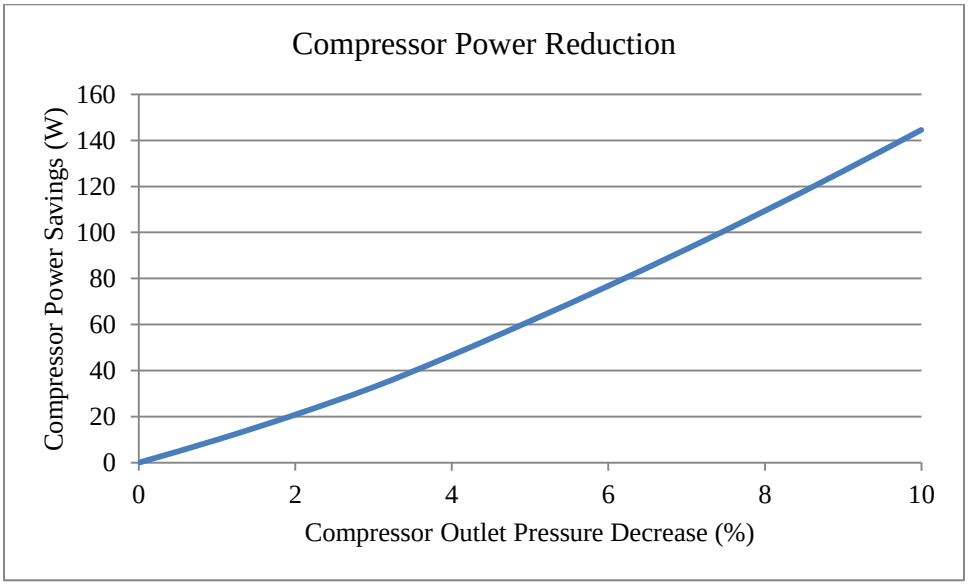

Figure 3.25: Compressor Power Reduction with Decreasing Outlet Pressure

The power saved by decreasing the fan activation to its maximum potential was greater than the power saved by decreasing the compressor power. The fan power consumption and the compressor power consumption were inversely proportional. The greater the fan power consumption, the smaller the power consumption of the compressor. The least amount of vehicle power was consumed when the compressor power was at the same level as it was in the dual loop setup but the fan activation was decreased as much as possible, as shown in Figure 3.26.

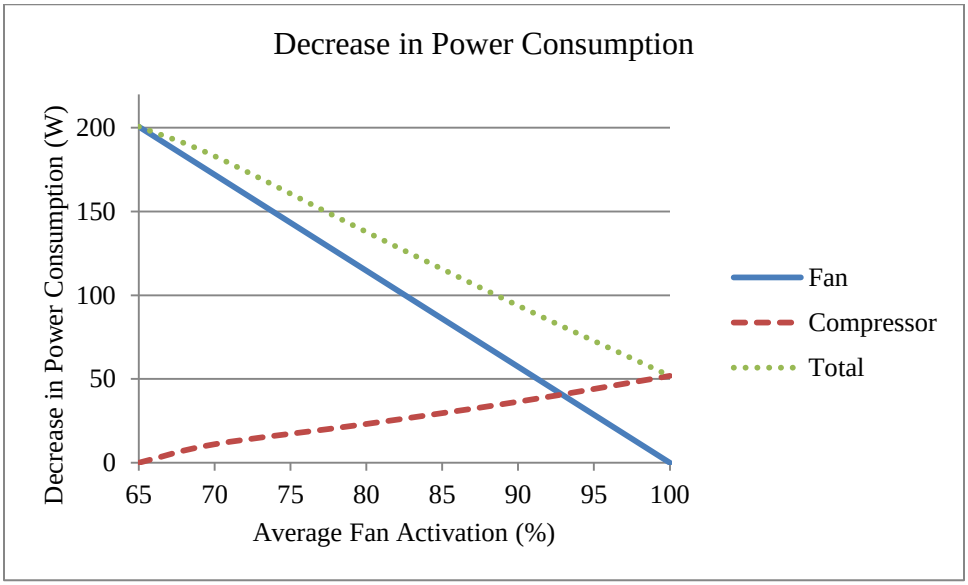

Figure 3.26: Decrease in Power Consumption Using Single Module Setup

3.5 Total Power Savings and Vehicle Fuel Economy Improvement

The total fan power consumption of the single module VTMS setup compared to the dual loop VTMS setup in the NEDC test with the A/C operating is shown in Table 3.1 [7]. The alternator efficiency was assumed to have a constant power conversion efficiency of 60% as recommended by Fiat. The alternator efficiency in the actual vehicle varies with the engine speed however no alternator efficiency data with engine speed was available so a constant value was selected.

Table 3.1: Fan Power Consumption Comparison

	Urban Driving	Extra-Urban Driving	Total
Dual Loop	528W	647W	569W
Single Module	343W	481W	390W
% Fan Power Savings	35%	26%	31%

The total vehicle power consumption improvement was estimated based on the simulation results and the data provided by Fiat of the vehicle power consumption for a Fiat Punto with a standard VTMS setup. The single module setup improved the vehicle power consumption over the dual loop setup by 3%. The total vehicle power consumption of the single module setup was 7% lower compared to the standard setup when the A/C was operating. These power consumption improvements did not take into account the potential vehicle power saved from aerodynamic improvements.

3.6 Size Reduction

The dual loop setup contains two front-end heat exchangers, as opposed to the single module which contains one. The single module setup reduced the total underhood volume and depth occupied by the VTMS by 49% and 58% respectively compared to the dual loop setup. The depth and volume occupied by both the dual loop setup and single module setup are shown in Table 3.2.

Table 3.2: VTMS Size Comparison

	Dual Loop Setup (Normalized)	Single Module Setup (Normalized)
Depth	1	0.42
Volume	1	0.51

The additional underhood space saved can be used to arrange the underhood compartment in a way that will achieve a better airflow path. This would reduce the underhood airflow drag on the vehicle which would also have an effect on the vehicle power consumption. The underhood space could also be used to increase the size of the bumper back into the underhood compartment without having to greatly modify the

external vehicle shape. This would make it easier to comply with new safety standards that will come into effect in Europe which will require an increase in the size of the front bumper [30].

CHAPTER 4: CONCLUSION AND RECOMENDATIONS

4.1 Conclusion

A single module radiator within a dual loop VTMS setup was investigated as a method for reducing the power consumption of the cooling fan and air conditioning compressor of a Fiat Punto when the A/C system was operating. The single module radiator VTMS setup was investigated by performing simulations of the NEDC test in a one-dimensional model of the system using the commercial software AMESim. The simulation results led to the following conclusions:

- The single module setup decreased the total vehicle power consumption of the Fiat Punto when the A/C was operating
- The single module setup provided a 3% power consumption reduction compared to the dual loop setup and a 7% reduction compared to the standard setup
- The fan power consumption was decreased by an average of 31 % compared to the dual loop setup
- The compressor power consumption remained the same compared to the dual loop setup

The reduction of the fan power consumption in the single module setup was due to the effects on the cooling airflow. The following changes to the cooling airflow compared to the dual loop setup were observed:

- The system resistance to the cooling air flow was reduced by 35%
- The airflow rate through the system was increased by 64%
- The inlet air temperature of the HTR was reduced by an average of 10^{o}C

4.2 Recommendations

The simulations in this thesis were preliminary and the results found should be verified by further simulations and experimental testing. The following simulations and tests should be performed in order to improve and confirm the simulation models:

- A bench test on a prototype of the single module radiator to determine the air pressure drop and the heat transfer
- CFD simulations or experimental testing to determine the underhood airflow rate, to validate the underhood cooling airflow model
- One-dimensional simulations of the full system with the air conditioning turned off, to determine the overall vehicle power consumption
- An experimental NEDC test on a full vehicle prototype, to determine the actual decrease in power consumption

The single module radiator system performance can be improved by re-designing certain components to function more efficiently at the new operating points of the single module radiator. The following components should be re-designed:

- The fan should be resized to have the maximum efficiency operating point at a lower fan speed due to the lower fan activation level
- The TSTAT hysteresis should be modified to allow a steadier flow through the HTR

APPENDIX A: COMPONENT BENCH TEST DATA AND CALIBRATION

The complete bench test data for the HT loop and LT loop coolant pumps are shown in Figure A.1 and Figure A.2 respectively. The bench test data of each pump was inserted into a look-up table within the model where a known pump speed and pressure head determined the flow rate.

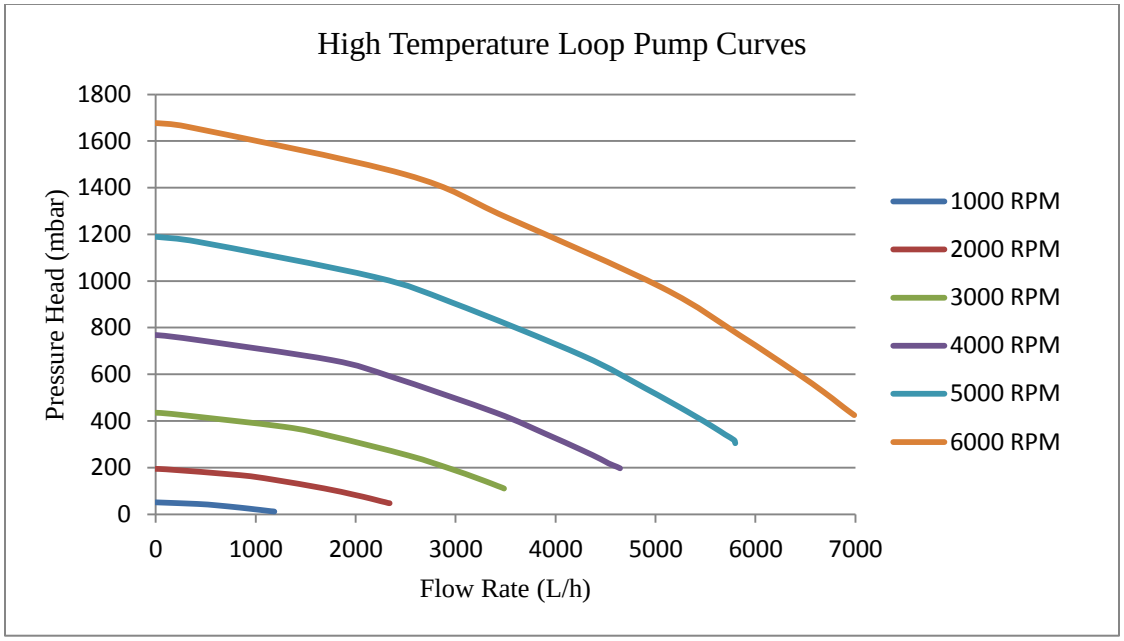

Figure A.1: HT Loop Pump Curves

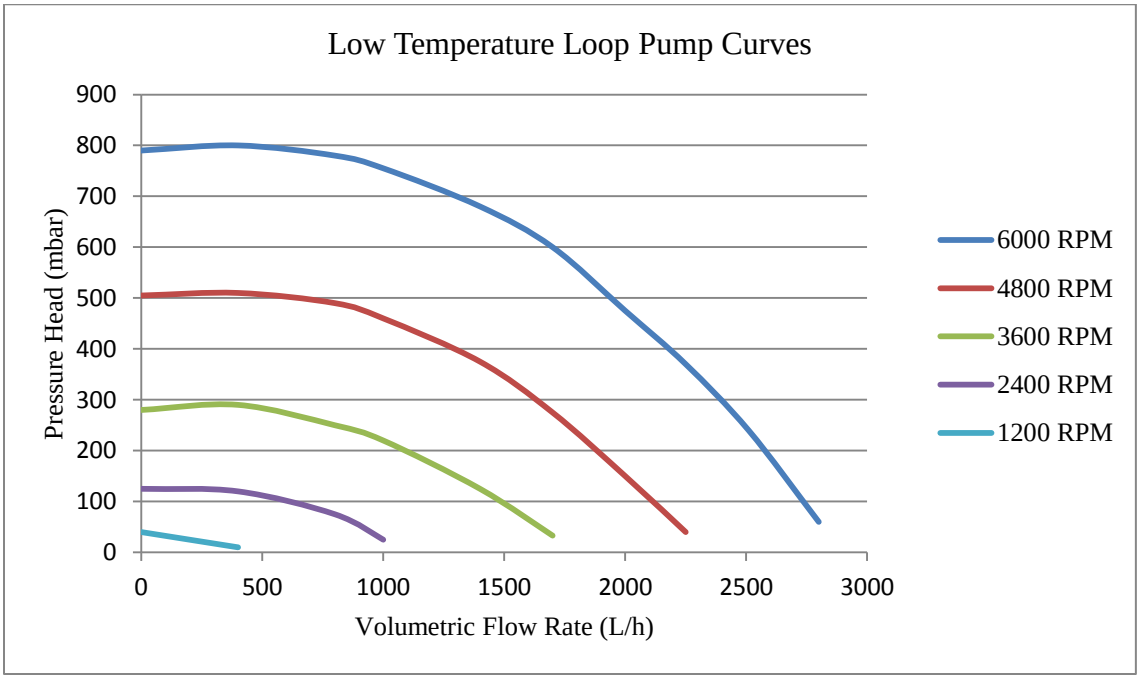

Figure A.2: LT Loop Pump Curves

The bench test data and calibrations for the HTR, the LTR, the heater core and the CAC are shown in Figure A3, Figure A4, Figure A5 and Figure A6 respectively. The calibration results were all within 5% at each coolant flow rate tested in the bench tests.

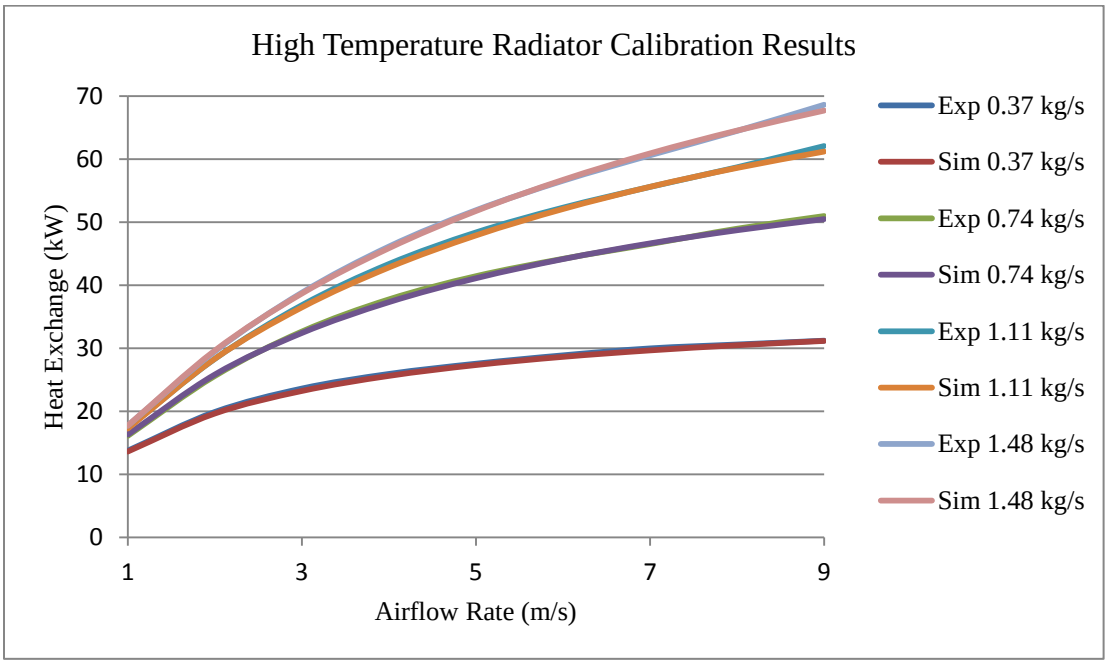

Figure A.3: High Temperature Radiator Calibration Results

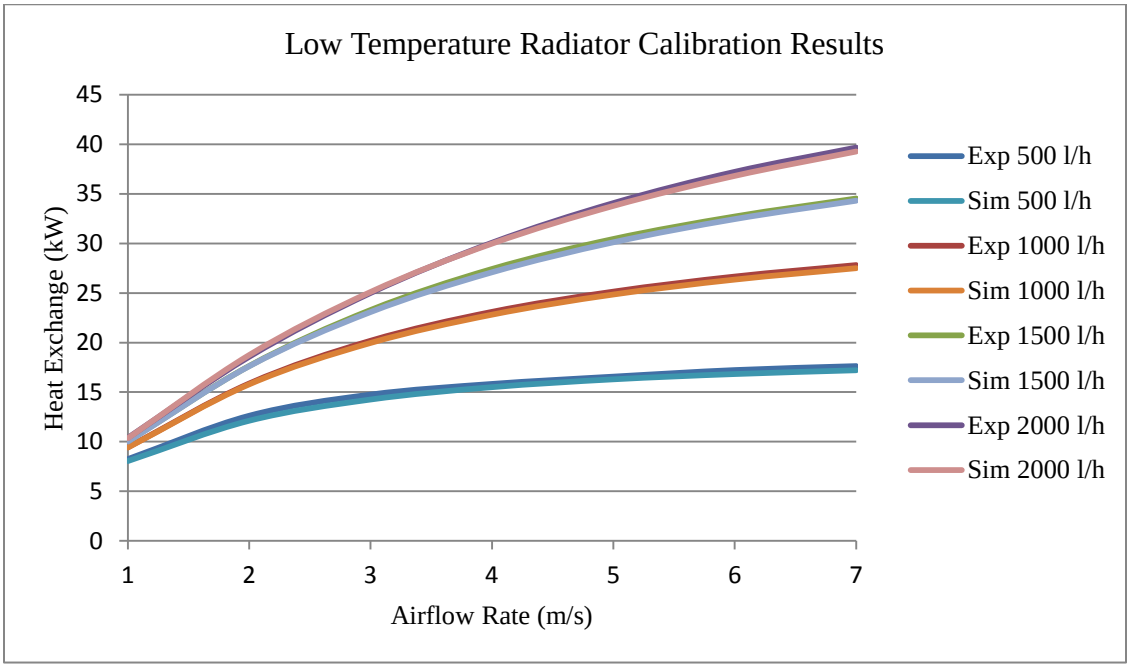

Figure A.4: Low Temperature Radiator Calibration Results

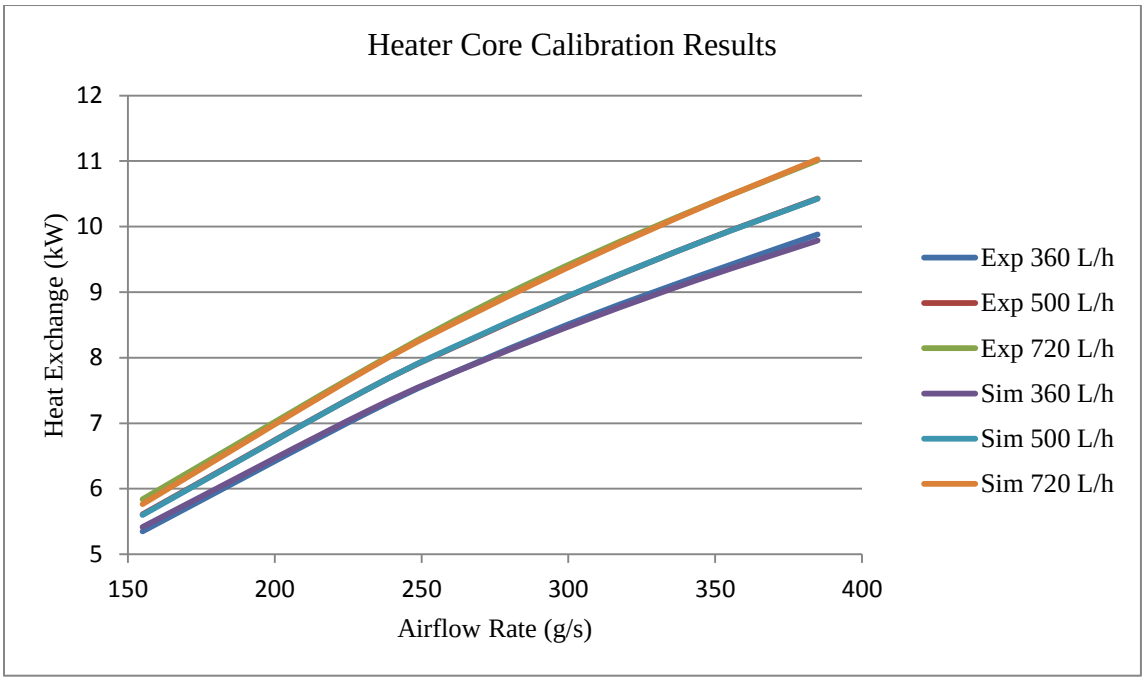

Figure A.5: Heater Core Calibration Results

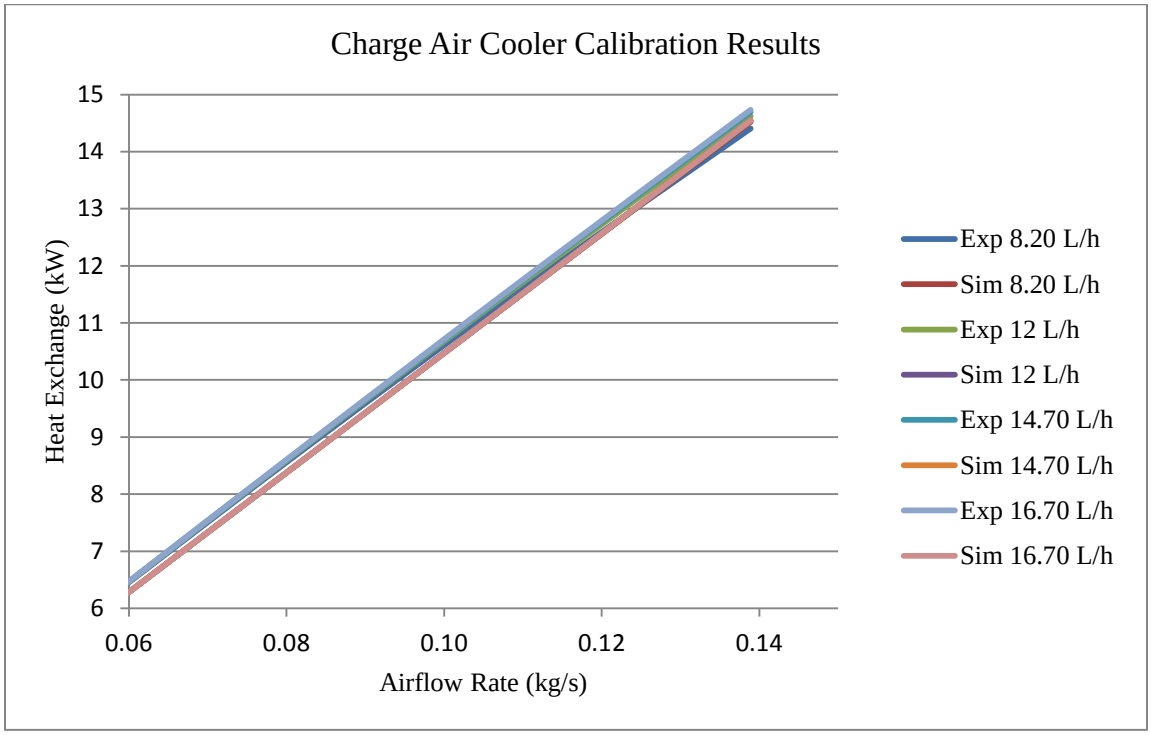

Figure A.6: Charge Air Cooler Calibration Results

APPENDIX B: UNDERHOOD AIRFLOW MODEL CALIBRATION

The calibration results of the underhood cooling airflow model are shown in Figure B.1. The engine pressure coefficient and the front grill pressure coefficient were calibrated using the airflow data for the standard setup. The error between the simulation and experimental results was less than 5% at each fan activation level.

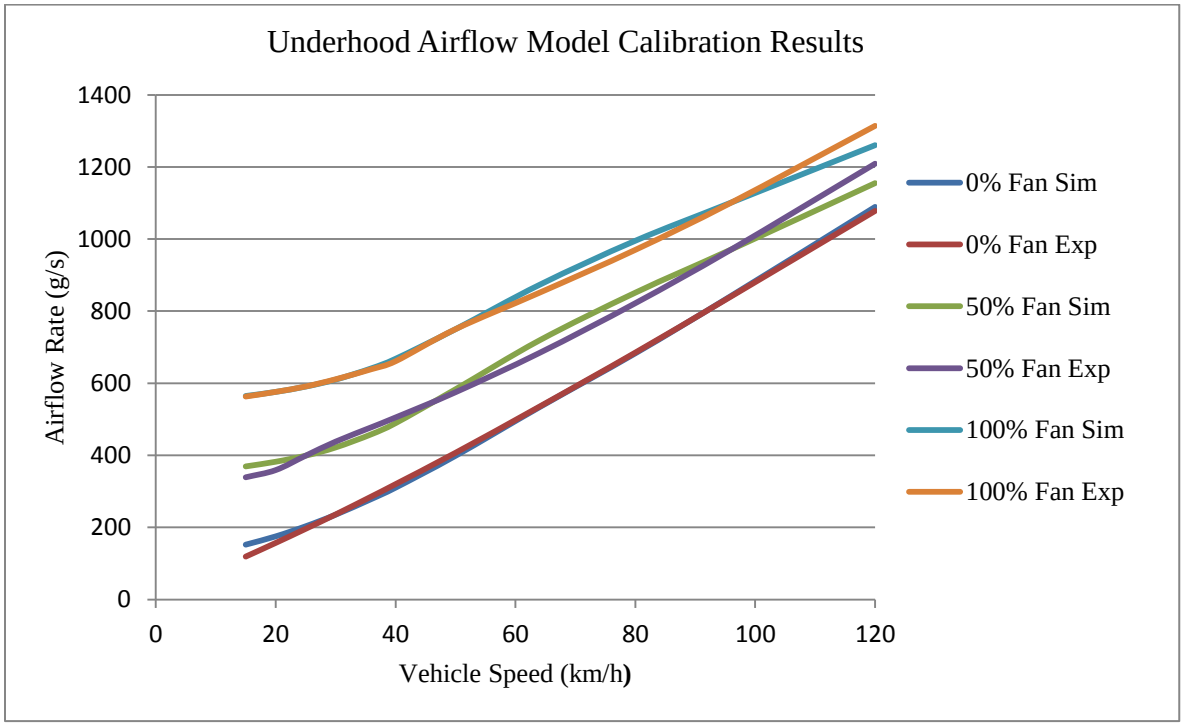

Figure B.1: Underhood Airflow Model Calibration Results

REFERENCES

1. National Highway Traffic Safety Administration , 2012, “Obama Administration Finalizes Historic 54.5 mpg Fuel Efficiency Standards,” Retrieved from http://www.nhtsa.gov/About+NHTSA/Press+Releases/2012/Obama+Administration+Finalizes+Historic+54.5+mpg+Fuel+Efficiency+Standards, Accessed July 2013.
2. Department of Transportation, 2009, “Average Fuel Economy Standards,” NHTSA Report No. NHTSA-2009-0062.
3. European Parliament and Council of the European Union, 2009, “Regulation (EC) No 443/2009 of the European Parliament and of the Council,” European Council Regulation No. 445/2009.
4. Global Fuel Economy Initiative, 2012, “Auto Fuel Economy,” Retrieved from http://www.unep.org/transport/gfei/autotool/understanding_the_problem/About_Fuel_Economy.asp, Accessed July 2013.
5. Lukas H., Saperstein Z.P., Rogers C.J., 1995, “Vehicular Cooling System and Liquid Cooled Condenser,” United States Patent No. 5,408,843.
6. Ap N., 2007, “UltimateCooling™System Application for R134a and R744 Refrigerant,” SAE International Congress, Scottsdale, Arizona.
7. Malvicino C., Di Sciullo F., Ferraris W., 2012, “Advanced Dual Level Vehicle Heat Rejection System for Passenger Cars,” SAE Paper No. 2012-01-1204.
8. Rostagno M. and Mattiello F., 2013, “High Efficiency Heat Rejection Systems,” Fiat Internal Document No. 2011-50I-RP-005, Centro Ricerche Fiat, Turin, Italy.

9. U.S. Department of Energy, 2013, “Many Factors Affect Fuel Economy,” Retrieved from http://www.fueleconomy.gov/feg/factors.shtml, Accessed July 2013.
10. Fiat Automotive Group, 2013, NEDC Experimental Data, Centro Ricerche Fiat, Turin, Italy.
11. Borgnakke C., Sonntag R., 2009, Fundamentals of Thermodynamics 7th Edition, John Wiley & Sons, Hoboken, New Jersey, Chap.8.
12. Kargilis A., 2008, Design and Development of Automotive Cooling Systems, Aklar Engineering Company, Southfield, Michigan, pp 95-99.
13. Baeder D., Indinger T., Adams N., Unterlechner P., Wickern G., 2011, “Interference Effects of Cooling Air-Flows with External Aerodynamics,” International Journal of Automotive Engineering Paper No. 20114635.
14. D’Hondt M., Gillieron P. and Devinant P., 2011, “Flow in the Engine Compartment: Analysis and Optimization,” International Journal of Aerodynamics Paper No. 10.1504/IJAD.2011.038852.
15. Muto S., Sugimoto T., Utikawa A. and Yamamoto M., 2001, “Development of a Cooling Module Containing a Radiator and a Condenser Part 1: Product Design,” SAE Paper No. 2001-01-1018.
16. Peuvrier O., Iwasaki M., Hara J. and Meguriya Y., 2011, “Development of Compact Cooling System (SLIM),” SAE Paper No. C1305/074/2011.
17. D’Hondt M., Gillieron P. and Devinant P., 2011, “Flow in the Engine Compartment: Analysis and Optimization,” International Journal of Aerodynamics Paper No. 10.1504/IJAD.2011.038852.

18. Kargilis A., 2008, Design and Development of Automotive Cooling Systems, Aklar Engineering Company, Southfield, Michigan, pp. 100-103.
19. Fiat Automotive Group, 2013, Fiat Punto VTMS Component Data, Centro Ricerche Fiat, Turin, Italy.
20. Cengal Y., Cimbala J., 2006, Fluid Mechanics: Fundamentals and Applications 3rd Edition, McGraw-Hill Higher Education, New York, New York, pp.738-740.
21. Global Fuel Economy Initiative , 2012, "International Test Cycles for Emissions and Fuel Economy," Retrieved from http://www.unep.org/transport/gfei/autotool/approaches/information/test_cycles.asp, Accessed July 2013.
22. Mock P., German J., Bandivadekar A., Riemersma I., 2012, "Discrepancies between type approval and "real-world" fuel consumption and CO_2 values," International Council on Clean Transportation Paper No. 2012-2.
23. SAE Surface Vehicle Standard, 1995, "Engine Cooling System Field Test" SAE Standard Paper No. REAF NOV 95.
24. Fiat Automotive Group, "Air-to-Boil Test for Vehicles in Climatic Tunnel," Fiat Internal Document No. 7.T0010, Centro Ricerche Fiat, Turin, Italy.
25. AMESim User's Guide, 2011, "Heat Library Rev 11," LMS Imagine S.A., Leuven, Belgium.
26. AMESim User's Guide, 2011, "Two Phase Flow Library Rev 11," LMS Imagine S.A., Leuven, Belgium.
27. AMESim User's Guide, 2011, "Thermal Hydraulic Library Rev 11," LMS Imagine S.A., Leuven, Belgium.

28. Fiat Automotive Group, 2013, Underhood Airflow CFD Test Data, Centro Ricerche Fiat, Turin, Italy.
29. KULI User's Guide, 2002, "Theory: Cooling Airflow," Magna Powertrain, Toronto, Ontario.
30. European Parliament and Council of the European Union, 2009, "Regulation (EC) No 78/2009 of the European Parliament and of the Council," European Council Regulation No. 78/2009.
31. Cengal Y., 2007, Heat and Mass Transfer: A Practical Approach 3rd Edition, McGraw-Hill Higher Education, New York, New York, Chap. 11.

VITA AUCTORIS

Timothy Reaburn was born in Windsor, Ontario, Canada in 1989. He received his Bachelor's Degree of Applied Science at the University of Windsor in 2011. He is currently a candidate for the Master's Degree at the University of Windsor.